AD NUMBER

AD463558

NEW LIMITATION CHANGE

TO

Approved for public release, distribution unlimited

FROM

Distribution authorized to U.S. Gov't. agencies and their contractors; Administrative/Operational Use; JAN 1965. Other requests shall be referred to Air Force Materials Lab., Wright-Patterson AFB, OH 45433.

AUTHORITY

AFML ltr, 22 Aug 1968

AFML-TR-65-2
Part I, Vol I

TERNARY PHASE EQUILIBRIA IN TRANSITION METAL-BORON-CARBON-SILICON SYSTEMS

Part I. Related Binary Systems

Volume I. Mo-C System

E. Rudy
St. Windisch
Y. A. Chang

Aerojet-General Corporation

TECHNICAL REPORT NO. AFML-TR-65-2, Part I, Volume I

January 1965

Air Force Materials Laboratory
Research and Technology Division
Air Force Systems Command
Wright-Patterson Air Force Base, Ohio

NOTICES

When Government drawings, specifications, or other data are used for any purpose other than in connection with a definitely related Government procurement operation, the United States Government thereby incurs no responsibility nor any obligation whatsoever; and the fact that the Government may have formulated, furnished, or in any way supplied the said drawings, specifications, or other data, is not to be regarded by implication or otherwise as in any manner licensing the holder or any other person or corporation, or conveying any rights or permission to manufacture, use, or sell any patented invention that may in any way be related thereto.

Copies of this report should not be returned to the Research and Technology Division unless return is required by security considerations, contractual obligations, or notice on a specific document.

AFML-TR-65-2-Pt.I-Vol.II
Part I, Vol I

TERNARY PHASE EQUILIBRIA IN TRANSITION METAL-BORON-CARBON-SILICON SYSTEMS

Part I. Related Binary Systems (U)

Volume I. Mo-C System

Erwin [redacted] Rudy,
Stefan [redacted] Windisch and
Austin Y. [redacted] Chang

[redacted] Materials Research Laboratory
Aerojet-General Corporation,
Sacramento, California

Approved by:

A. S. Ginsburgh, Manager
Propulsion R&D Division
Solid Rocket Operation

FOREWORD

This report was prepared by the Materials Research Laboratory, Aerojet-General Corporation, Sacramento, California under USAF Contract No. AF 33(615)-1249. The contract was initiated under Project No. 7350, Task No. 735001. The work was administered under the direction of the Air Force Materials Laboratory, Research and Technology Division, with Captain R. A. Peterson acting as Project Engineer, and Dr. E. Rudy, Aerojet-General Corporation, as Principal Investigator.

The project which includes the experimental and theoretical investigation of selected ternary systems in the system classes Me_1-Me_2-C, Me-B-C, Me_1-Me_2-B, Me-Si-B, and Me-Si-C, was initiated on 1 January 1964. The system class report on carbides covers part of the experimental effort during the time period from 1 January 1964 to 15 December 1964.

The phase-diagram work was performed by E. Rudy and St. Windisch. Assisting in the experimental investigations were: J. Pomodoro (preparation of sample material), H. Heetderks (DTA-runs), J. Hoffman (metallographic preparations), and R. Cobb (X-ray exposures). The thermodynamic model of the Me_2C phases was developed by E. Rudy. Y. A. Chang performed the numerical (computer) evaluation of the equations and made the literature compilation of the thermodynamic data on molybdenum carbides.

The authors wish to acknowledge the help received from the members of the Analytical Chemistry Laboratory and the Computing Sciences Division. We also express our thanks to Dr. A. J. Stosick, Senior Scientist, who

proofread the manuscript and made many helpful suggestions, and to Prof. Dr. H. Nowotny, University of Vienna, who served as consultant to the project.

The manuscript of this report was released by the authors December 1964 for publication as an RTD Technical Report.

This technical report has been reviewed and is approved.

W. G. RAMKE
Chief, Ceramics and Graphite Branch
Metals and Ceramics Division
Air Force Materials Laboratory

ABSTRACT

A complete phase diagram of the system molybdenum-carbon is presented. A thermodynamic model for the description of the phase separation of the Me_2C phases in transition metal-carbon systems has been developed and was semiquantitatively applied to Mo_2C. Literature data on thermodynamic properties of molybdenum carbides have been critically evaluated and data were selected.

Apparative techniques for the precise study of phase reactions at high temperatures are described.

TABLE OF CONTENTS

TABLE OF CONTENTS (continued)

ILLUSTRATIONS

ILLUSTRATIONS (continued)

ILLUSTRATIONS (continued)

ILLUSTRATIONS (continued)

ILLUSTRATIONS (continued)

TABLES

TABLES (continued)

I. INTRODUCTION AND SUMMARY

A. INTRODUCTION

In view of their refractoriness and thermal stability, carbides and carbide alloys have attracted considerable interest during the past few years as a material source for very high temperature applications.

Their extreme brittleness in the lower temperature region, leading to failures due to thermal stresses, necessitates the consideration of composite structures, a development which depends to a large degree on the knowledge of the phase reactions occurring in the particular system or group of systems.

A program was therefore initiated under AF 33(615)-1249, with the objective, to determine and to interpret the high temperature phase-equilibria occurring in ternary systems Me_1-Me_2-C, Me-B-C, Me_1-Me_2-B, Me-Si-B, and Me-Si-C, where Me stands for a refractory transition metal.

As a result of the high temperatures involved in the investigations of these system classes, it is not surprising that older investigations —— due to the lack of adequate high temperature facilities —— are often shown to be incomplete and are superseded by more detailed, more accurate, and even new information as the methods of investigation improve[1].

It should be mentioned, however, that often the reverse is also true, i.e. that older findings are sometimes rejected on a somewhat arbitrary basis in modern reinvestigations. This applies especially to the carbide systems, where more than 30 years ago, the existence of polymorphic modifications of W_2C[2, 3] and Ta_2C[4] at high temperatures had been deduced from careful metallographic and X-ray studies on these

compounds. Although the existence of these high temperature polymorphs has been denied in a number of recent works, extensive investigations on the binary carbide systems carried out in this laboratory under this program revealed their definite existence. These studies showed the reaction type to be common to nearly all subcarbide phases (Mo_2C, W_2C[5], Nb_2C, and Ta_2C[6]), having its origin in the temperature-activated disordering of the carbon sublattice in these compounds. In view of the very close structural relationships of the phases coexisting in the transformation process, the term "phase separation" may be better suited for the description of this type of transformation, and will be used throughout the report.

Although at present, conclusive data are available for carbide systems only, there are indications from preliminary investigations in other system classes, that this reaction type may be a quite common phenomenon for interstitial compounds. In particular, this reaction type can be expected with such phases, where at the stoichiometric composition a substantial fraction of the totally available interstitial lattice sites, i.e. sites which from size or other considerations have to be regarded as potential for occupation with the respective interstitial atom, is still unoccupied (e.g. diborides). Filling of such energetically less favored lattice sites by foreign interstitial atoms of suitable size should therefore lead to interesting combinations.

The present report is one of a series of documentary reports on the high temperature phase-equilibria in refractory binary and ternary carbide systems. The bulk of the experimental effort was devoted to the establishment of the general equilibria, i.e. the gross interaction of the various phases of the boundary systems. Although of minor influence on the overall appearance of the phase equilibria in the ternary phase field, the

limitations, which solid state transformations could impose on the technical applicability of these compounds, —— apart from the theoretical interest —— seemed to justify a more extended study of these phenomena.

B. SUMMARY

Using X-ray, metallographical, and differential-thermo-analytical (DTA) methods, which were supported by chemical analysis, the binary system molybdenum-carbon was investigated and a complete phase diagram was established (Figure 1 and Table 1).

Four congruently melting intermediate phases (α-Mo_2C, β-Mo_2C, η-MoC_{1-x}, and α-MoC_{1-x}), from which only one (α-Mo_2C) is stable below 1400°C, occur in the system. These are:

1. α-Dimolybdenum Carbide

The α-Mo_2C phase, with a hexagonal close-packed arrangement of metal atoms, extends at 2000°C from 30 At% C (a = 2.990 Å, c = 4.728 Å) to 32.8 At% C (a = 3.006 Å, c = 4.734 Å), and at the eutectic temperature (2200°C) from 26 to 32.5 At% C. The phase melts congruently at 2486 ± 5°C at a composition of 31.5 At% C. α-Mo_2C forms a eutectic with the α-molybdenum phase at 2200 ± 5°C at a carbon concentration of 17 atomic percent.

2. β-Dimolybdenum Carbide

This phase, not previously reported in this form in the literature, exists between 1475° and 2520°C, and has a hexagonal close-packed arrangement of metal atoms, with a = 3.007 Å, c = 4.778 Å at 33 atomic percent carbon. The β-Mo_2C-phase results from a phase separation of the Mo_2C-phase above 1475°C, caused by disordering effects in the carbon sublattice. Its range of homogeneity extends from 33 to 34 At% at 2000°C and reaches a maximum of 36 At% C at the eutectic temperature of

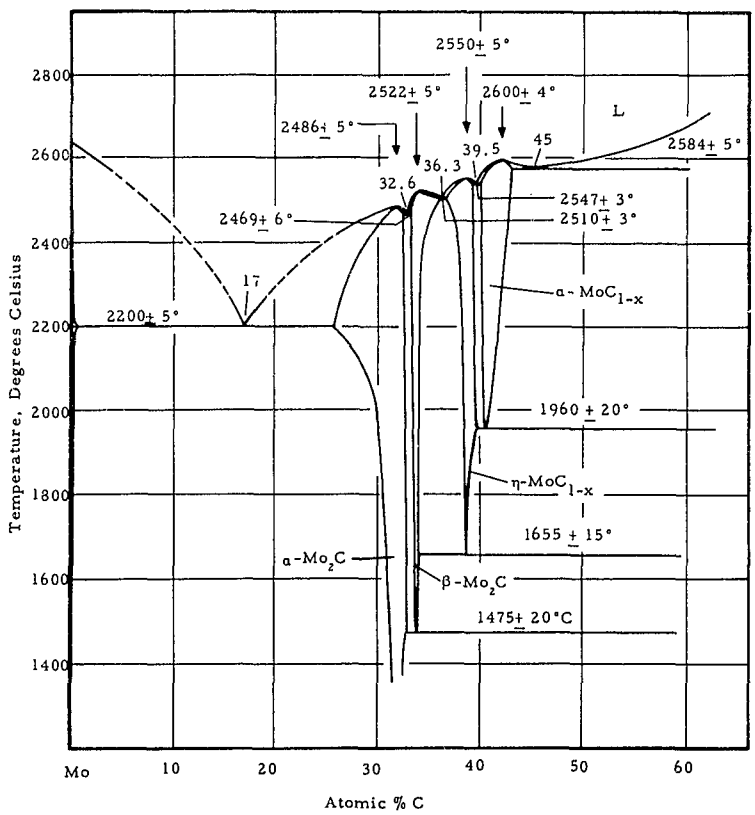

Figure 1. The Phase Diagram of the System Molybdenum-Carbon

(The uncertainties attached to the temperature figures resemble the accuracy of the measurements and do not include the error in the pyrometer calibration)

Table 1. Isothermal Reactions in the System Molybdenum-Carbon

Temperature °C	Reaction	Compositions of the Equilibrium Phases At% C			Type of Reaction
2600 ± 5	$L \rightleftarrows \alpha\text{-}MoC_{1-x}$	42	42	-	Congruent Transformation
2584 ± 5	$L \rightleftarrows \alpha\text{-}MoC_{1-x} + C_{(gr)}$	45	43	~100	Eutectic Reaction
2550 ± 5	$L \rightleftarrows \eta\text{-}MoC_{1-x}$	38.6	38.6	-	Congruent Transformation
2547 ± 3	$L \rightleftarrows \eta\text{-}MoC_{1-x} + \alpha\text{-}MoC_{1-x}$	39.5	39.3	39.9	Eutectic Reaction
2522 ± 5	$L \rightleftarrows \beta\text{-}Mo_2C$	34.0	34.0	-	Congruent Transformation
2510 ± 3	$L \rightleftarrows \beta\text{-}Mo_2C + \eta\text{-}MoC_{1-x}$	36.3	36.1	36.7	Eutectic Reaction
2486 ± 5	$L \rightleftarrows \alpha\text{-}Mo_2C$	31.8	31.8	-	Congruent Transformation
2469 ± 6	$L \rightleftarrows \alpha\text{-}Mo_2C + \beta\text{-}Mo_2C$	32.6	32.3	32.8	Eutectic Reaction
2200 ± 5	$L \rightleftarrows \alpha\text{-}Mo + \alpha\text{-}Mo_2C$	17	~0.15	26	Eutectic Reaction
1960 ± 20	$\alpha\text{-}MoC_{1-x} \rightleftarrows \eta\text{-}MoC_{1-x} + C_{(gr)}$	40.4	39.6	~100	Eutectoid Reaction
1655 ± 15	$\eta\text{-}MoC_{1-x} \rightleftarrows \beta\text{-}Mo_2C + C_{(gr)}$	39.0	33.6	~100	Eutectoid Reaction
1475 ±20	$\beta\text{-}Mo_2C \rightleftarrows \alpha\text{-}Mo_2C + C_{(gr)}$	33.8	32.8	~100	Eutectoid Reaction

of the equilibrium β-Mo_2C-η-MoC_{1-x}. β-Mo_2C melts congruently at 2522 $\pm$ 5°C at a composition of 34 At% C and forms eutectic equilibria with α-Mo_2C (2469 $\pm$ 6°C, 32.6 At% C) and the hexagonal η-MoC_{1-x}-phase (2510 $\pm$ 3°C, 36.3 At% C). The phase decomposes in a eutectoid reaction at 1475 $\pm$ 20°C into α-Mo_2C and graphite.

3. η-MoC_{1-x}

η-MoC_{1-x} has a hexagonal (pseudocubic) lattice (D_{6h}^4- type) with a = 3.013 Å, and c = 14.65 Å. It melts congruently at 2552°C at a composition of 39 At% C and decomposes in a eutectoid reaction at 1655 $\pm$ 15°C into β-Mo_2C and graphite.

4. α-MoC_{1-x}

α-MoC_{1-x} has a sodium chloride (B1) type of structure with a = 4.265 Å (41 At% C), and melts congruently at 42 At% C at 2600 $\pm$ 4°C. Its range of homogeneity extends from 39.7 At% C (a = 4.266 Å) to 42 At% C (a - 4.274 Å) at 2300°C, and up to 43 At% C (a = 4.281 Å) at 2580°C.

α-MoC_{1-x} decomposes in a eutectoid reaction at 1960 $\pm$ 20°C into the hexagonal η-phase and graphite. It forms eutectics with the η-phase (39.5 At% C, 2547 $\pm$ 3°C) and graphite (45 At% C, 2584 $\pm$ 5°C).

The liquidus line of the equilibrium $(Mo, C)_{melt}$——graphite has been experimentally determined up to 3200°C.

The α-β——Me_2C phase separation is interpreted on the basis of two energetically different interstitial lattice sites. The equilibrium conditions have been derived and are discussed. A semiquantitative application of the Mo_2C-phase yielded $\Delta G \simeq 8500$ cal per mole Mo_2C_y ($y \sim 1$) as the free energy difference between the two kinds of interstitial lattice sites.

This energy results from the volume changes associated with the disordering reaction and can therefore be interpreted as strain energy. While the degree of disorder can be quite high at high temperature (25% of the carbon atoms on lattice sites of the second kind at 2200°K) the calculations indicate that at room temperature Mo_2C is an essentially ordered compound. Analogous types of phase reactions have been found for Nb_2C (~2500°C), Ta_2C (~2000°C) and W_2C (~2450°C). The analysis identifies the observed phase separations as secondary effects of the disordering reaction in the carbon sublattice.

The literature data on thermodynamic properties of molybdenum carbides have been critically evaluated and data were selected.

II. LITERATURE REVIEW

The currently accepted phase diagram of the system molybdenum-carbon, based mainly on the work by H. Nowotny, et.al.[7] and available literature information up to 1961 has been presented by R. Kieffer and F. Benesovsky[8] (Figure 3).

The existence of at least three intermetallic phases, of which two are stable at high temperatures only, has been ascertained and their structures have been established. There is general agreement among the various investigators, that the solubility of carbon in molybdenum is very small ($\leq$ 0.15 At%).

Mo_2C has a hexagonal close-packed arrangement of metal atoms[8,9], with a = 3.007 Å, and c = 5.778 Å. Based on room temperature neutron diffraction experiments, which revealed an essentially ordered carbon sublattice, E. Parthé and V. Sadagopan[10] conclude, that Mo_2C is only pseudo-hexagonal and crystallizes orthorhombically (space group D_{2h}^{14} - Pbcn), with

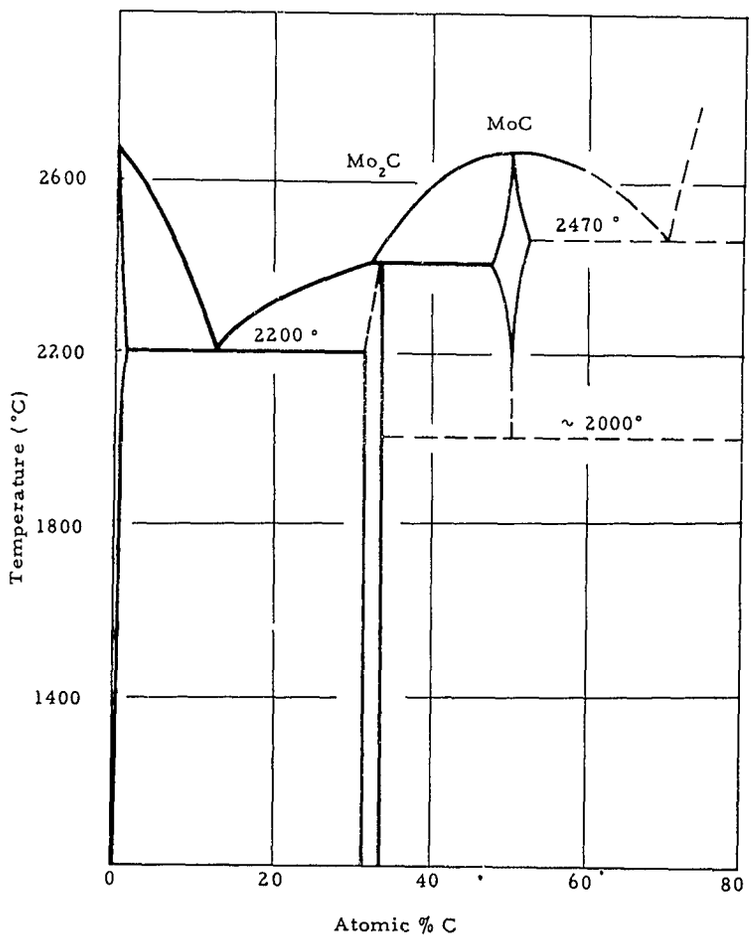

Figure 2. Molybdenum-Carbon Phase Diagram
(After R. Kieffer and F. Benesovsky, 1963)

$a_o = 7.24_4$ Å, $b_o = 6.00_4$ Å, and $c_o = 5.19_9$ Å. The orthorhombic axes are related to the hexagonal dimensions by $a_o = c_H$, $b_o = 2a_H$, $c_o = a_H \sqrt{3}$.

η-MoC, later shown to exist in the composition range from 38-40 At% C[11,12,13], has a hexagonal (D_{6h}^4- type) structure with a = 3.006 Å, and c = 14.61 Å[7]. The structure of η-MoC is closely related to the cubic B1-type[7]. The phase is stable only at high temperatures[7] decomposing into Mo_2C and graphite at 1450 ± 100°C[13].

α-MoC[7,14], occurring at a carbon concentration of approximately 40 atomic percent[13,14], has a face-centered cubic (B1) unit cell, with a ≃ 4.27 Å[12,14]. The phase is unstable below 2000°C[12].

A compilation of recent lattice parameter measurements of molybdenum carbide phases together with data from the present investigations are presented in Table 2.

The solubility of carbon in molybdenum has been investigated by T. Takei[15], W. P. Sykes, et.al.[16], and W. E. Few and G.K. Manning[17]. The latter authors give the solubility limits of 0.005-0.009 Wt% C at 1650°C, 0.012 Wt% C at 1925°C, and approximately 0.018 Wt% C at 2200°C. The lattice parameter of molybdenum increases slightly upon incorporation of carbon atoms[18].

Mo_2C was first prepared by H. Moissan[19] by reduction of molybdenum dioxide with carbon and calcium carbide; it was also isolated by H. Moissan and M. K. Hoffman[20] from molten mixtures of molybdenum with aluminum and petroleum coke. J. N. Pring and W. Fielding[21] observed the formation of Mo_2C upon decomposition of molybdenum chloride on graphite rods heated above 1300°C. Other preparation techniques[8] included the gas-phase carburization of molybdenum[22,23], the direct combination of the elements at high temperatures[9,16,24,25], the electrolytic deposition from salt melts[26,27] and the decomposition of molybdenum carbonyls[28,29,30].

Table 2 Structure and Lattice Parameters of Molybdenum Carbides

Phase	Structure	Lattice Parameters, Å	
		Literature Values	This Investigation
Mo_2C		a=3.000-3.012 c=4.732-4.735 (23, 50) a=2.997-3.012 c=4.727-4.736 (12)	T = 2000°C (Quenched Alloys)
	hex., L'3-type	a=3.0028 ± 0.0001 c=4.7288 ± 0.0001 at $MoC_{0.48}$ (51)	a=2.990 c=4.728 α-Mo_2C at 30 At% C
			a=3.006 c=4.734 α-Mo_2C at 32.8 At% C
	orthorh. D_{2h}^{14}	a_o=7.24$_4$; b_o=6.00$_4$; c_o=5.19$_9$ (10)*	a=3.007 c=4.778 β-Mo_2C at 33.5 At% C
			a=3.010 b=4.780 β-Mo_2C at 34 At% C
η-MoC_{1-x}	hex., D_{6h}^4-type	a=3.006 (7) c=14.61 a=3.013 c=14.64 at $MoC_{\sim 2/3}$ (12)	a 3.008 c 14.63 at ~38 At% C; 3.012 14.65 at ~39 At% C
α-MoC_{1-x}	cub., B1-type	a=4.27 (Subcell) (7) a=4.27 (14) a=4.281$_o$ (12)	a=4.267 at 41 At% C; a=4.281 at 43 At% C
γ-MoC**	hex. WC-type	a=2.898 (38) c=2.809 a=2.901 (39) c=2.786	Not Confirmed
γ'-MoC**	hex.	a=2.932 c=10.97 (38)	Not Confirmed

* Orthorhombic Setting: $a_o = c_{hex}$; $b_o = 2a_{hex}$,; $c_o = a_{hex} \cdot \sqrt{3}$

**Probably oxygen - stabilized carbide phases

T. Takei[15] gives its range of existence between 5.5 and 6 Wt% (31.7 - 33.8 At%) carbon, which is in good agreement with later determinations by W. P. Sykes, et.al.[16]. A. Westgren and G. Phragmen[9] report the metal-rich limit at 31 At% carbon.

According to W. P. Sykes et.al.[16], the Mo_2C phase forms in a peritectic reaction at approximately 2400°C. E. Friedrich and L. Sittig[24] measured 2230 to 2330°C. Agte and H. Alterthum[25] report 2690 ± 50°C. In a recent investigation, M. R. Nadler and C. P. Kempter[31] measured a melting temperature of 2410 ± 15°C, which is in good agreement with the measurements by G. A. Geach and F. O. Jones[32], and by T. C. Wallace, et.al.[13], reporting a melting temperature of 2440 ± 30°C at a composition of 34 At% carbon (Table 3).

J. L. Lander and L. H. Germer[29] claimed to have found a cubic Mo_2C in the decomposition products of molybdenum carbonyl-steam mixtures. The original doubts of R. Kieffer and Benesovsky[8], which attributed the appearance of this phase to oxygen stabilization, have been confirmed in recent investigations by I. F. Ferguson, et.al.[30]. The existence and structure of higher molybdenum carbides were a matter of extensive controversy[8,33].

Using arc-quenched alloys, H. Nowotny and R. Kieffer[34] stabilized a monocarbide and first assigned a cubic subcell to a compound MoC. In later investigations by H. Nowotny and coworkers[7], the phase was successfully indexed on the basis of a hexagonal unit cell (Table 2), which is closely related to the B 1-type. The phase melts congruently at approximately 2650°C and decomposes into Mo_2C and graphite at temperatures below 2000°C[7]. According to E. Friedrich and L. Sittig[24] MoC melts at 2570°C. C. Agte and H. Alterthum[25] report 2695 ± 50°C, and J. L. Engelke, et.al.[35]

measured 2870°C. Recent redeterminations of the melting temperatures by T. C. Wallace, et.al.[13] at the Los Alamos Laboratory, however, shed some doubts on the previous measurements, as has been pointed out by K. Storms in a recent critical review of carbide data[36]. The melting point data obtained by T. C. Wallace, et.al.[13] are listed in Table 3. The peritectoid decomposition temperature of η-MoC, reported by the same authors, is 1450° ± 100°C. According to A. E. Kovalskii and S. V. Semenovskaja[37], application of pressure favored the formation of η-MoC at 1750°C.

Table 3. Melting Temperatures of Molybdenum-Carbon Alloys (T.C. Wallace, C.D. Guitierrez, and P.L. Stone[13]).

Composition (At% C)	Melting Temperatures (°C)	Presence of Free Carbon
34	2440 ± 30	No
37	2460 ± 30	No
38	2590 ± 30	No
41	2580 ± 30	Yes
43	2570 ± 30	Yes
45	2580 ± 30	Yes
51	2575 ± 30	Yes

H. Tutiya[23] and K. Kuo and G. Hägg[38] report a monocarbide with a simple hexagonal WC-type unit cell (γ-MoC, a = 2.898 Å, c = 2.809 Å). In addition to the γ-phase, the latter authors found another carbide (γ-MoC, a = 2.932 Å, c = 10.97 Å, space group P 6_3/mmc), which had formed in the low temperature carburization of molybdenum. In equilibrium measurements,

L. C. Browning and P. H. Emmett[39] observed the γ-MoC-phase in the reaction products of carbon monoxide with molybdenum, and they report a lower temperature stability limit of approximately 700°C. The occurrence of γ-MoC was also noted in high pressure experiments by L. Kaufman and E. V. Clougherty[40]. In neither case was the composition of the alloys well defined, which applies also to earlier claims for the preparation of a molybdenum monocarbide[16, 20, 22, 23, 24, 27, 41, 42].

E. V. Clougherty, et.al.[14] reported the high pressure stabilization of a cubic MoC(α-MoC_{1-x}, a = 4.27 Å) at temperatures above 2000°C. The same phase was also prepared in pure form by rapid quench of molybdenum-carbon melts by E. Rudy et.al.[12], and shown to exist at a composition of approximately 40 At% C. Based on thermochemical considerations[11, 12], the lower temperature stability limit of the cubic α-MoC_{1-x} was estimated to be 2000°C, but T. C. Wallace, et.al.[13], did not find the solid solution $(Zr, Mo)C_{1-x}$ to extend to the binary system Mo-C at 2100°C.

On the metal-rich side, a eutectic is reported at 2200°C[16, 31] and 1.8 Wt% (12.8 At%) carbon[16]. T. Takei[15] places the eutectic composition at 4 Wt% (25 At%) carbon.

H. Nowotny, et.al.[7] measured the approximate melting points of molybdenum carbon alloys in the range from 40 to 75 At% C and located the carbon-rich eutectic at $\sim$ 70 At% C and a temperature of approximately 2400°C. The measurements of T. C. Wallace, et.al.[13] (Table 3) indicate the eutectic line at 2575 $\pm$ 30°C.

III. EXPERIMENTAL PROGRAM

A. EXPERIMENTAL TECHNIQUES

1. Starting Materials

The elemental powders served as the starting materials for the preparation of the experimental alloy material.

Molybdenum, with an average grain size of 2.02 μ, was purchased from Wah Chang Corporation, Albany, Oregon, and had the following analysis (Table 4):

Table 4. Chemical Analysis of the Molybdenum Powder

Impurity Element	Impurities (Contents in ppm) Suppliers Analysis	Our Analysis	Method
Aℓ	20	100	Spec
C	24	136	Comb
Co	<10	50	Spec
Cr	25	<50	Spec
Cu	<10	100	Spec
Fe	30	<20	Spec
Mg	<10	n.d.	-
Mn	10	n.d.	-
Ni	20	40	Spec
O_2	640	1120	Gas F
Pb	<10	<100	Spec
Si	100	<200	Spec
Sn	80	n.d.	-
W	200	n.d.	-
Ti	n.d.	50	Spec
non volatile matter	100	n.d.	-

Legend to Table 4: Spec - Spectrographic Analysis
Comb - Determined by combustion in a micro carbon analyzer.
Gas F - Value obtained from gas-fusion analysis
n.d. - Not determined

In general, our analysis of the molybdenum powder indicated slightly higher impurity levels than the analysis submitted by the vendor. No second phase impurities could be detected in strongly overexposed powder patterns on low background X-ray film (Laue, Agfa Wolfen). The lattice parameter of the molybdenum powder was determined to be $a = 3.147_3$ Å.

The spectrographic grade graphite powder was purchased from Union Carbide Corporation, Carbon Products Division and had the following analysis (Table 5):

Table 5. Chemical Analysis of the Graphite Powder

Impurity Element	Impurities (Contents in ppm) Supplier's Analysis	Our Analysis*	Method
Aℓ	0.3	<10	Spec
Cu	0.1	<10	Spec
Mg	0.1	<10	Spec
Si	0.2	<10	Spec
Fe	0.2	<10	Spec
Ash(1)	n.d.	0.05	Grav
H_2O(2)	n.d.	0.00	Grav
volatile matter(3)	n.d.	0.01	Grav

Legend to Table 5: (1) 1 hr at 1950°C
(2) 16 hrs at 105°C
(3) 7 min at 600°C
Spec - Spectrographic Analysis
Grav - Gravimetric Analysis
n.d. - Not Determined

*In most cases the impurity contents were below the accuracy limit of our spectrograph.

No second phase impurities were detected in strongly overexposed X-ray powder patterns. The lattice parameters obtained from an exposure with Cu-K_α-radiation was a = 2.463 Å, and c = 6.729 Å which is in good agreement with the reported literature values of a = 2.461 Å, and c = 6.708 Å [43].

2. Sample Preparation

The alloy material for the investigation in this system was exclusively prepared by a short-duration hot-pressing process applied to the well-blended mixtures of the elemental powders in graphite dies.

In this method, originally developed by Metallwerk Plansee, Reutte, Tirol, the powder mixtures are filled into a graphite cup and closed with a graphite piston. The filled die is then inserted into a graphite heater, which is clamped between two graphite holders, which also serve as the current connections to the water-cooled copper electrodes. The specimen is then heated and compacted while under pressure ($\leq$ 750 Atm.). The graphite components of the hot-press are shown in Figure 3.

In contrast to other current designs, this hot-press allows very fast heating and cooling rates and in this way keeps the reaction between the sample material and the graphite sleeves to a minimum. In general, one hot-pressing cycle lasts from two to five minutes and results in practically completely dense sample material, if required (Figure 4). After hot-pressing, the surface reaction zone, which in most cases is 0.1 to 0.4 mm thick, is removed by grinding and the alloys are subjected to further homogenization treatments.

Prior to the preparation of the bulk of the experimental alloy material, test runs were made to determine the maximum carbon pick-up during the hot-pressing. For these tests, molybdenum powder

with known analysis was filled into the graphite sleeves and compacted for 2, 5, 10, and 20 minutes at 1900°C and 380 atmospheres.

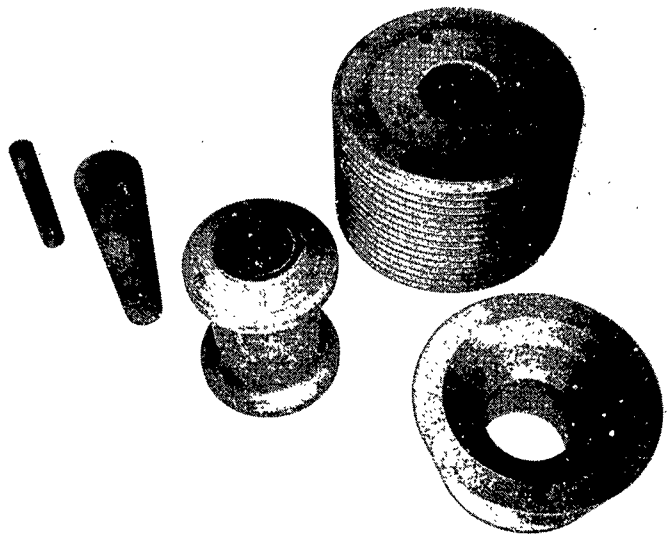

Figure 3. Graphite Components for Hot-Pressing

The observed reaction zones after hot-pressing were approximately 0.2, 0.2, 0.4 and 0.6 mm and consisted of Mo_2C and η-MoC_{1-x}. The chemical analysis of the surface cleaned samples showed carbon contents of 85, 127, 123, and 120 ppm. These lower carbon contents after the hot-pressing as compared to the starting material (136 ppm) are attributed to the partial removal of the originally present oxygen by reaction with carbon. This was confirmed by chemical analysis, which showed after the hot-pressing an average oxygen content of only 360 ppm in contrast

to the 1120 ppm present in the original powder. These tests, as well as the results of the chemical analysis on the experimental alloy material reported in a later section, show the hot-pressing route —— with proper design of the apparatus —— to be a very effective and reliable method for the preparation of carbidic alloy material.

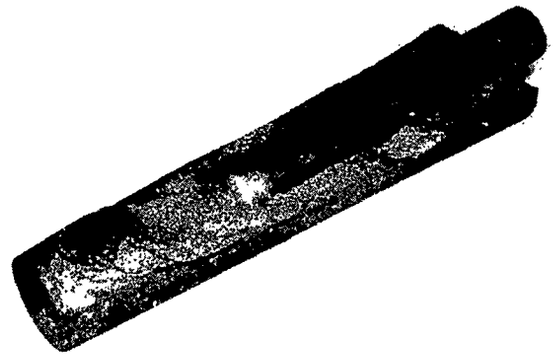

Figure 4. Graphite Die with Sample After Hot-Pressing

3. Heat-Treatments

The homogenization treatments of the alloy material were performed in a high vacuum tungsten-mesh element furnace manufactured by the Brew Company. The surface-cleaned hot-pressed compacts were placed in tantalum containers, which were then inserted into tantalum cans resting on a tungsten support table inside the heating element. The

temperature was measured pyrometrically (Section 7c) through a quartz window in the furnace wall and a small hole in the radiation shields and the top lid of the sample container. Corrections to the readings were only applied for the quartz window (Section II-7), since the small observation hole resembled nearly perfect black body conditions.

The equilibration treatments were carried out at 1800°C and 1550°C under a vacuum of 5×10^{-5} Torr. Prior heat treatments at temperatures of 2100° and 2200°C resulted in substantial carbon losses due to vaporization and therefore the lower temperature was chosen. One piece of each alloy was also arc melted. These prehomogenized alloys were analyzed and used as stock-material for the further studies.

4. Quenching Studies

From the X-ray evaluation of the initial heat-treatments it became obvious that the high temperature equilibrium states could not be frozen in by the comparatively slow cooling rates in the vacuum furnace mentioned above, and that rapid quenching of the alloys was required. These quenching experiments were conducted in the following manner:

A flat piece of the alloy to be studied was prepared by hot-pressing, surface-cleaned, and then inserted into a device as shown in Figure 5. The sample was brought to equilibrium temperature by direct resistance heating of the graphite heater around the specimen holder and held at temperature until equilibrium was attained. With the aid of a hydraulic piston, mounted on top of the sample holder, the sample was then ejected into a preheated tin bath (300°C) by breaking the thin diaphragm beneath the sample (Figure 5). The skin of tin adhering to the sample surface was removed by leaching in 3n HCl and the alloys subjected to X-ray, metallographic, and chemical analysis.

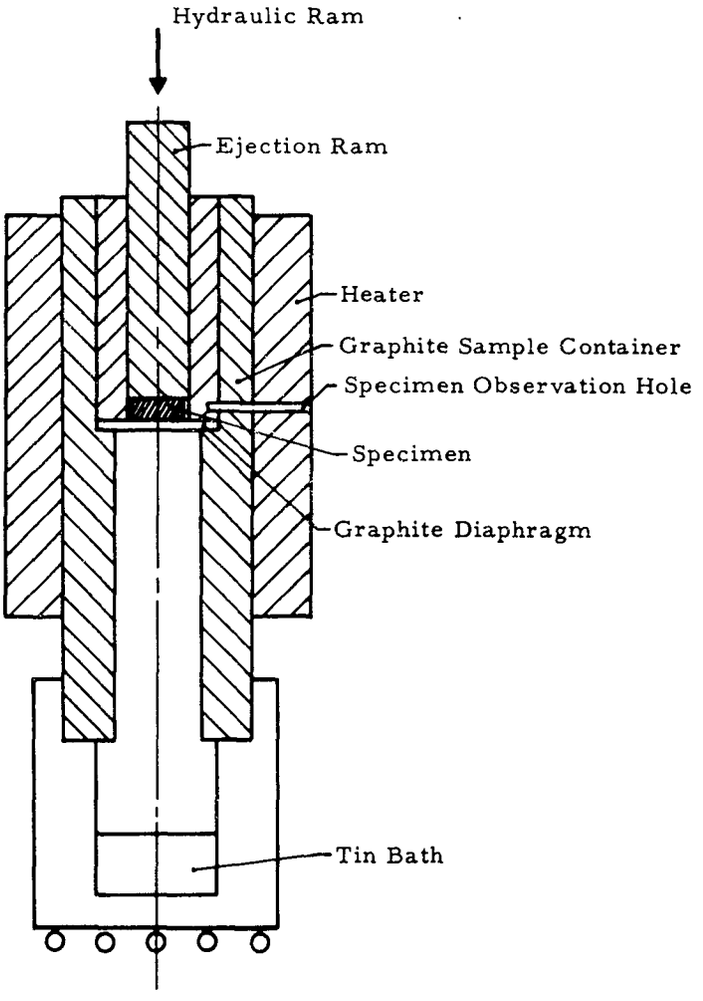

Figure 5. Experimental Setup for Rapid Quenching Studies on Carbides.

5. High Temperature Equilibration Experiments With Graphite

Since the liquidus line of the equilibrium Mo-C_{melt}—graphite could not be determined accurately by differential-thermoanalytical methods (Section III-6) or by melting point determinations (Section III-7), the direct route, i.e. chemical analysis of molybdenum-carbon melts, which had been equilibrated with carbon, was chosen.

A cylindrical piece of the alloy is placed into a graphite container, a graphite platelet placed on top of the sample, and the whole arrangement heated inside a graphite cylinder to equilibrium temperature. Once the alloy is molten, the pick-up of carbon from the container walls as well as from the graphite platelet on top of the sample up to the equilibrium concentration is fast. Experiments carried out over varying lengths of time showed that complete equilibrium was reached within ten minutes at temperatures 50°C higher than the corresponding lowest solidus temperatures. After attainment of equilibrium, the melt is cooled down fast to room temperature (approximately 200°C/sec in the critical range of solidification) in order to prevent segregation of the melt from the lighter graphite, the outer surfaces are removed by grinding and the sample analyzed chemically for the total carbon content.

6. Differential Thermal Analysis

a. Principle of Operation

A piece of sample material, along with a similar piece of material known to undergo no phase changes are heated at a controlled rate in a high temperature furnace. If at some temperature, say T_o, the sample undergoes an isothermal reaction which involves an

enthalpy change, the temperature of the sample will tend to remain at T_o, while the temperature of the inert sample continues to rise. Thus, an isothermal reaction generates a difference in temperature between the sample and the reference body. The difference is detected and recorded. After the reaction is completed, the sample temperature tends to approach the environmental temperature (i.e. the temperature of the inert sample). A typical plot of sample temperature (T) versus difference in temperature (ΔT) is shown in Figure 6, where both a heating and cooling curve are shown.

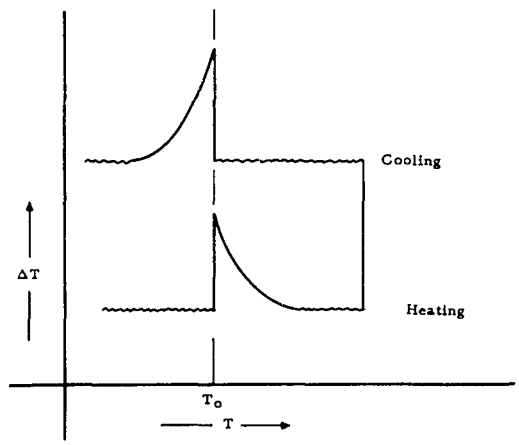

Figure 6. Differential Heating and Cooling Curves Indicating Thermal Arrest at T_o

b. Physical Setup

The sample is a small cylinder (9/16" dia x 5/8" high) with a concentric black body hole (5/32" dia x 3/8" deep) at one end. A piece of graphite or other material, known to undergo no phase changes in the specific temperature range, is used as a reference sample.

The samples are heated inside a container (Figure 7) which is made as symmetrical as possible in order to keep base-time drifting effects caused by uneven heating to a minimum. The sample

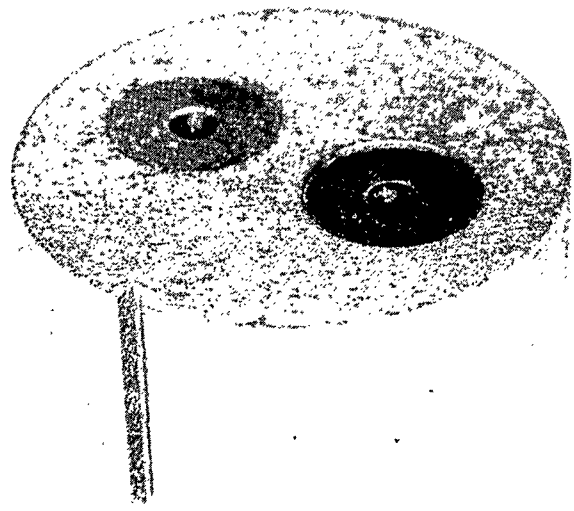

Figure 7. Reference and Test Sample Loaded in Graphite Container for DTA-Measurements

container is heated inside a cylindrical graphite heater, which is clamped between two water-cooled copper electrodes. The heating assembly is connected to a saturable reactor controlled power supply, which at full power delivers 15,000 amperes at 10 volts to the heater. An exploded view of the heating assembly of the DTA-apparatus is shown in Figure 8. The furnace assembly is enclosed in a chamber, which can be operated either in vacuum or in inert gas of up to six atmospheres.

The apparatus is further equipped with an automatic temperature control system. A variable speed motor-driven potentiometer produces a controlled variable set-point, which is compared with the output of the temperature sensor to produce an error signal.

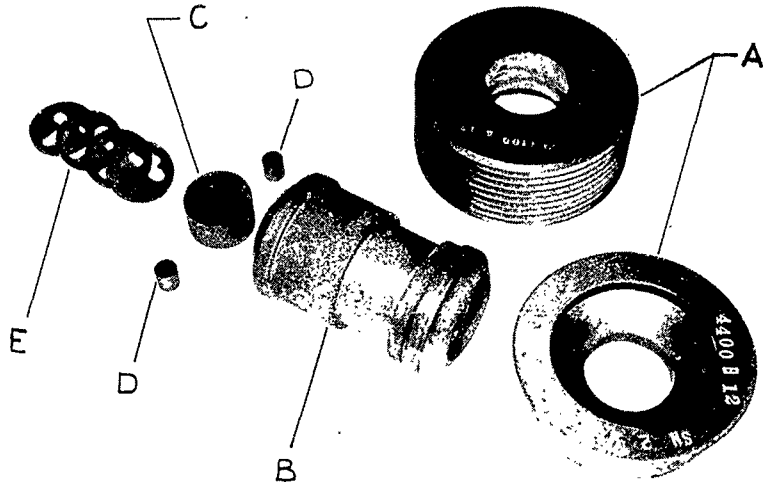

Figure 8. Exploded View of the Heating Assembly of the DTA-Apparatus

A - Graphite Electrodes
B - Heater
C - Sample Container
D - Reference Test Sample
E - Radiation Shields

This signal is amplified and controls a magnetic amplifier/silicon controlled rectifier system, which drives the saturable core reactor and which ultimately controls the power delivered to the heater. Both heating and cooling rates are adjustable to fractions of a degree per second. The maximum

heating rate obtainable is approximately 20°C per second, the maximum controllable cooling rate approximately 16°C per second.

c. Signal Path and Radiation Detection System

Situated above and outside the furnace assembly is an optical-electronic system, which produces two DC-voltages, one is a function of the sample temperature, the other is a function of the temperature difference between the sample and the reference body.

The temperature signal takes the following path: Radiation from the black-body hole in the sample passes through a quartz window and is reflected from a gold first-surface mirror to a commercial infrared radiation thermometer (Thermodot Model TD-6BT-70). This instrument produces a 0-10 millivolt output, which is a known function of temperature. The radiation thermometer was calibrated against an optical micropyrometer, which viewed the sample directly, and the temperatures during the runs were counterchecked pyrometrically.

The temperature-difference detection system operates on a radiation comparison principle. Radiation from the sample, after passing through a quartz window, is focussed by a lens with adjustable aperture onto a photocell (Figures 9, 10). A mirror directs the path through a rotating semicircular sector which interrupts the radiation. Radiation from the inert sample's black body hole falls on the same photocell. The rotating semicircle is so situated, that the photocell alternately views the sample's black body hole and then the inert sample's black body hole.

By using this system[44] instead of two opposite radiation detectors, we were able to eliminate completely the problem resulting from the change of the matching characteristics of the radiation sensors with temperature, which causes excessive base line drifting[45].

The sector rotates at 5400 rpm, so that the photocell views the sample for 1/180th of a second, then the inert sample for 1/180th second, then the sample . . . . . etc.

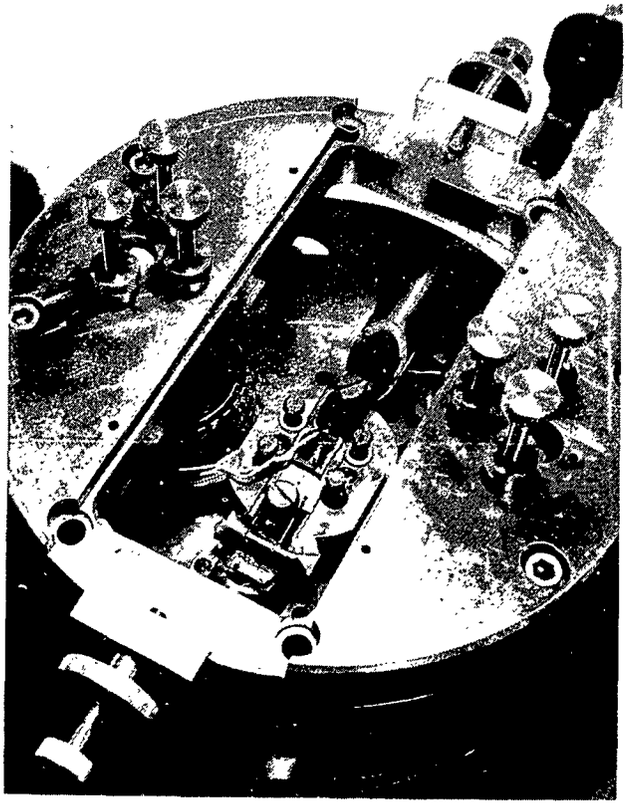

Figure 9. Optical and Radiation Detection System in the DTA Apparatus

A temperature difference of the sample produces a square wave from the photocell, with the amplitude of the wave increasing with increasing temperature difference. This square wave is applied to the input of a differential amplifier, with a bandpass of three cycles per second,

tuned to 90 cycles per second. The output of the amplifier is rectified and filtered, producing a DC-output, which is recorded. The DC-voltages from the temperature difference sensor are plotted by an X-Y recorder (Varian model F-80).

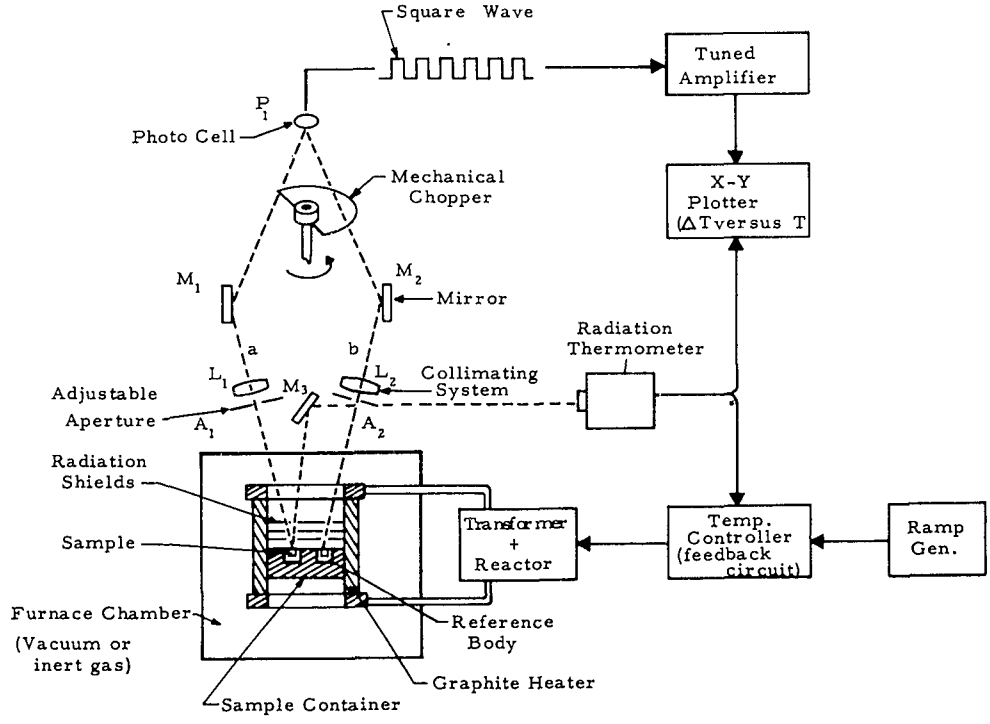

Figure 10. Experimental Setup for DTA-Measurements at High Temperatures

For adjusting and monitoring purposes, the square wave is simultaneously displayed on the screen of an oscilloscope during the experiment.

d. Capabilities and Limitations

The temperature limitations of the furnace itself are imposed by the sublimation of graphite. Although the diffusion of carbon vapor can be slowed down by the application of higher inert gas pressures, the lifetime of the heating element is limited to seconds at a temperature of 3800°C. The maximum safe operation temperature, giving reproducible results, is approximately 3600°C.

A problem, which in many cases limits the temperature range of investigation, is the interaction of the sample with the container material, and special precautions (change of container material, linings on the sample hole walls, etc.) have to be taken to prevent errors in the interpretation of the results.

Another important characteristic of a DTA-device is its sensitivity, i.e. the minimum heat-quantity which produces a reproducible and distinguishable signal. Obviously, this quantity is a function of many parameters, such as temperature, heating rates, heating geometries, the thermophysical properties of sample and container material, etc. The sensitivity of the apparatus in terms of these parameters has not yet been tested. Experiments on the solid-state transformations are reactions in the system Mo-C, where the approximate enthalpy changes are known from other data, showed that an enthalpy change of approximately 20 calories produced a signal: average experimental noise ratio of about 20:1 ($T \sim 2000°C$).

e. Measurements in the System Molybdenum-Carbon

For the investigations in the system molybdenum-carbon, graphite was solely used as the container material.

In order to study the carburization rate of metal-rich alloys, a molybdenum-carbon alloy with 17At% C (composition of the metal-rich eutectic) was inserted into the sample container and cycled between room temperature and 2000°C. The conditions in this system are specially favorable, since three solid state reactions occur in the range from 34 to 40 At% carbon, i.e. excessive formation of the higher carbon phases will produce signals corresponding to these isothermal reactions.

The experiments were conducted to a constant heating and cooling rate of 4°C per second. A first faint peak was noticed after the 12th run, which could be identified as being due to the formation of the η-MoC_{1-x} phase from Mo_2C and graphite. The intensity of the peak increased somewhat with the number of reruns, but remained comparatively small. The experiment was stopped after the 17th run and the sample analyzed. The outer surface reaction zone which was approximately 1mm thick, consisted of a mixture of Mo_2C, η-MoC_{1-x} and free graphite. A second zone, approximated 0.3 mm thick and separated by sharp boundaries from the outer zone and the bulk of the sample, was identified as pure Mo_2C. The carbon concentration of the center-portion of the sample remained unchanged.

In agreement with the findings of R. T. Dolloff and R. V. Sara[46] on tungsten-carbon alloys, the carburization rates decrease considerably once free metal is absent and the alloys consist of carbide phases only. It was also experienced, that the melting equilibria in the metal-rich portions of the system could be reproducibly investigated as long as the maximum temperatures of the experiments did not exceed the temperature of the carbon-rich eutectic (2584°C) in the system. At temperatures above, carburization was almost instantaneous and the equilibria

observed on subsequent cooling referred to the carbon-rich portion of the system.

Summarizing the results of these tests, it was found, that graphite containers are suitable for the DTA-investigations on the molybdenum-carbon system, provided that only the first runs on a given sample are used for interpretation and that the temperature of the carbon-rich eutectic is not exceeded in the experiments.

7. Determination of Melting Points

In view of the difficulties encountered in finding adequate container materials, which limits the applicability and usefulness of a number of methods[8], as well as of the shortcomings of induction heating, the resistive heating method was chosen for the determination of the melting points.

In this method, a small sample bar with a black body hole in the center is heated resistively to the temperature of the phase change. The temperature is measured pyrometrically.

The method has the advantage of being fast and yields, with proper care taken in the measurements, very reliable results.

a. Furnace Design

The essential parts of the furnace consist of two water-cooled copper electrodes enclosed in a double-jacketed vacuum-tight housing. The specimen, which is held between two tungsten platelets, is clamped directly onto the water-cooled electrodes (Figure 11). A constant force, applied through a lever arm by weights (visible in Figure 11 in front of the electrodes) ensures good electrical contact between specimen and electrode. The thermal expansion of the specimen is accounted for by having one movable electrode.

A gravity balancing system, firmly connected to the movable electrode on the outside of the chamber allows the specimen to be put either under axial tension or compression. The maximum axial force, which can be exerted in this way on the sample is $\pm$ 2000 g. and can be controlled to within $\pm$ 30 g. The furnace can be operated either under vacuum or under inert gas of up to 2 1/2 atmospheres.

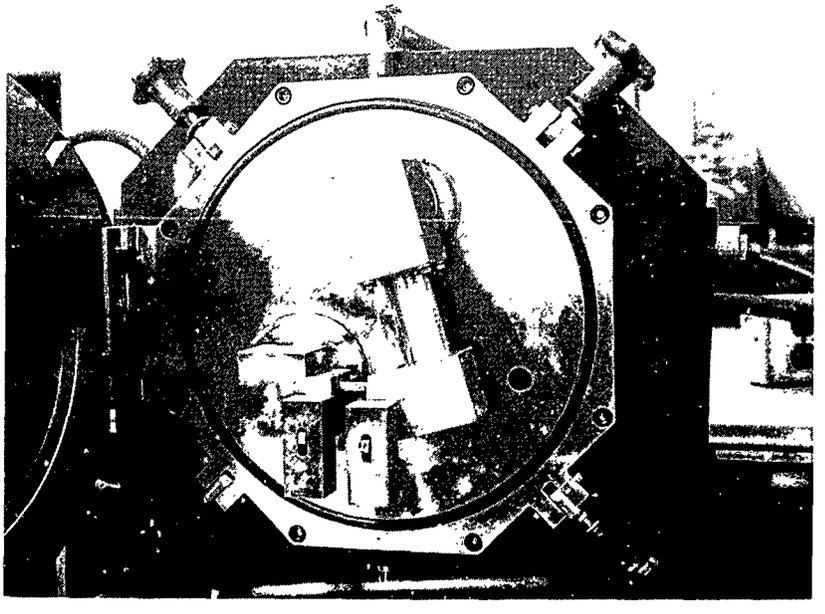

Figure 11. Interior View of the Melting Point Furnace

The power supply consists of a 50 KVA saturable core-reactor —— step down transformer system. The power control is effected via the DC-supply of the saturable reactor by means of a potentiometer with continuously variable DC-speed drive. Power application rates can be varied between 20 and 15,000 watts per second, and are controlled by foot switches at the operator's site.

b. Specimen Preparation

Two types of samples, differing in the way they are clamped to the electrodes, are in use. They are (a) rectangular bars of the dimensions 5 x 5 x 50 mm (Figure 12), and (b) cylindrical specimens of approximately 10 mm in diameter and 30 mm in length with a

Figure 12. Pirani Melting Point Specimen, Cold-Pressed to Size and Sintered (actual size)

rectangular or cylindrical groove in the center (Figure 13). Ductile metal specimens or samples containing excess ductile metal phases are pressed to final shape (with 0.6 mm diameter, and 3 mm deep hole) in a split die system with retractable center-pin (Figure 14) and are used in the as-pressed state.

Samples of more brittle materials are sintered after cold-pressing to provide sufficient strength for further handling. Specimens of such alloys, whose interaction with graphite is negligible or can be controlled (carbide solutions, diborides of the refractory transition metals) are hot pressed in a die system similar to that used for the cold-compaction of the bar-type specimens, and is shown in Figure 15. Where it can be applied, this method has the advantage of yielding dense and strong compacts in comparatively short times.

c. Temperature Measurements

The temperature of the sample is measured optically with a disappearing-filament type micropyrometer through a quartz window in the furnace wall. A small hole, generally in the order of 0.6 to 1.0 mm diameter, drilled or pressed into the sample, serves as the reference point for the temperature measurements. The micropyrometers are

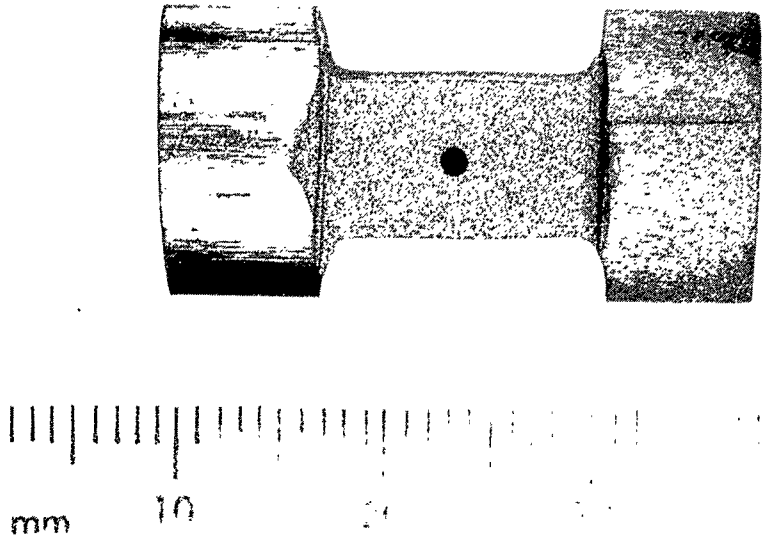

Figure 13. Pirani Melting Point Specimen, Hot Pressed and Ground

periodically calibrated against standard lamps, which were calibrated and certified by the National Bureau of Standards. As a further means of assurance of the calibration, the pyrometers are periodically checked directly against a standard pyrometer, calibrated and certified by the National Bureau of Standards.

d. Temperature Correction Terms

From Planck's law, and under the assumption that the temperature correction terms are small compared to the temperature itself, the following equation can be derived from the correction (ΔT_{corr}) to be applied to the observed temperature (T_m):

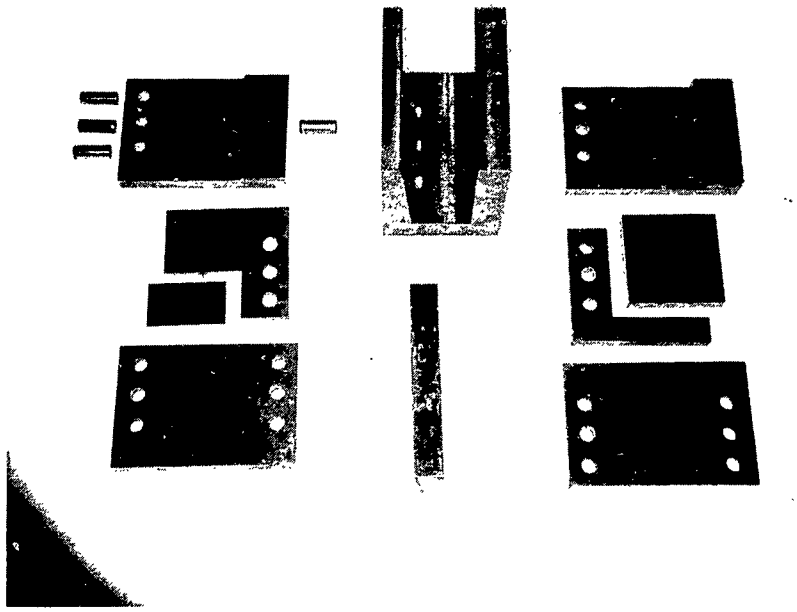

Figure 14. Die Components for Cold-Pressing Pirani Melting Point Specimens

$$\Delta T_{corr} \simeq -T_m^2 \cdot \frac{C_2}{\lambda} \cdot \ln D \cdot A \cdot \epsilon \qquad (1)$$

ϵ = Emissivity Coefficient of the black body hole

λ = Wave length of the radiation used in the measurement (0.65μ)

$C_2 = \frac{h \cdot c}{k}$ = const = 1.4384 [cm.deg.]

T_m = Measured Temperature

D = Relative reflection loss at the quartz window

A = Relative absorption loss in the quartz window

$D \cdot A = T_{tr}$ = Transmission of the quartz system

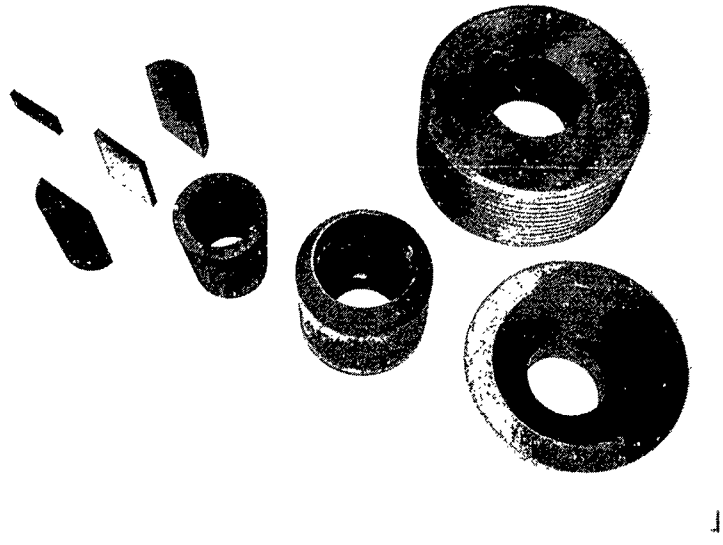

Figure 15. Die Components for the Preparation of Pirani Melting Point Specimens by Hot-Pressing

The terms D and A can be calculated from the known absorption data and the refractive index of quartz for the particular wave length. For the brand used (GE-grade 101, d = 5 mm) n = 1.4585. With Fresnel's formula for the reflected intensities at vertical incidence,

$$D = \frac{J_R}{J_o} = \left[\frac{n-1}{n+1}\right]^2 \qquad (2)$$

A reflection loss of 3.48% per surface is calculated. Together with a transparency coefficient of 0.98 per cm for the wave length (0.65 μ) used a total transmission of the quartz system of $D \cdot A = 0.92$ is obtained.

An experimental check of this value was performed in a way, which was originally proposed by A. Taylor, et.al.[47]. Provided that n is not too large, the total transmission of a system of n equal quartz windows is

$$T_{tot}(n) = (D \cdot A)^n, \qquad (3)$$

i.e. the temperature correction per quartz window is practically constant and equal to ln D·A. By measuring the apparent temperatures through a varying number of equal quartz windows, the transmission D·A can then be calculated from equation (1).

Experiments were performed using 1, 2, and 3 quartz windows. As reference point for the measurements served a 0.5 mm dia and 10 mm deep hole in graphite. At 2245°C, the chosen equilibrium temperature, the following readings were obtained (Table 6). The mean temperature difference derived from a large number of measurements was 25.5°C, yielding a product of $D \cdot A = 0.915$ (formula 1) which is in excellent agreement with the theoretical value.

Another factor which influences the accuracy of the final data and therefore has to be established are the emissivity coefficients of the reference holes in the samples. These coefficients were

determined independently by measuring the apparent temperature of sample holes of varying dimensions. A 0.5 mm dia x 10 mm deep hole in porous graphite served as the source for "black" radiation and the measurements were carried out at the same temperature as the previous experiments, i.e. 2245°C.

Table 6. Effect of the Number of Quartz Windows on the Apparent Temperatures of a Black Body Hole

Number of Quartz Windows	Measured Temperature (°C)	Difference (Mean Value)
1	2245 ± 4	-
2	2220 ± 4	25
3	2193 ± 4	26

The observed emissivities, as calculated from equation 1, were only slightly dependent on the alloys used, but are affected significantly by the dimensions of the black body hole, as shown from the data in Table 7. In order to minimize the corrections to be applied for non-black body conditions, the initially selected hole diameter of 1.0 mm was changed to 0.6 mm. Figure (16) shows the temperature correction chart as computed from equation 1 for the interesting range of emissivity factors and for the quartz window.

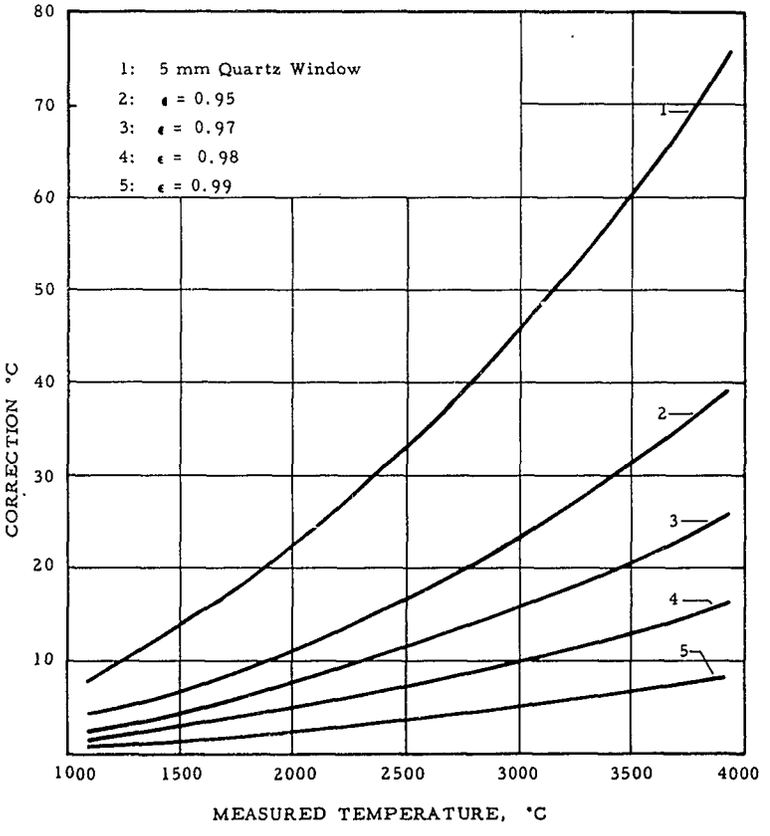

Figure 16. Temperature Correction Chart

Table 7. Mean Emissivity Coefficients of Black Body Hole in Metallic Specimens

Hole Dimensions (dia x length), mm	Mean Emissivity Coefficient
1.3 x 3	0.97
1.0 x 3	0.98
0.6 x 3	0.995

e. Reproducibility of Results

The reproducibility of the measurements in terms of the mean deviations in the individual measurements is about $\pm$ 4°C at 2000°C, $\leq \pm$ 10°C at 2700°C, and approximately $\pm$ 15°C at 3300°C. These figures are based on sample materials where no side reactions or compositional changes falsify the test results.

The temperature figures attached to the phase diagrams refer to the mean value and the standard deviation in the measurements. To obtain the overall uncertainties, the errors of the pyrometer calibration have to be taken into account. Since these are comparable in magnitude with the data given above, the overall uncertainties in the temperatures are obtained by multiplying the reported standard deviations by $\sqrt{2}$.

f. Interpretation of the Results

One draw-back of the method lies in the fact, that the exact course of the liquidus lines in a two-phase region cannot be determined. The reason for this is that the sample loses its strength and tends to collapse, once liquid phase is present; moreover, the observation

hole tends to fill up with liquid and the temperature measurements become inaccurate.

Sagging of the sample, sometimes observed at temperatures close to melting, tends to distort the observation hole and can be prevented by minimizing the axial force on the sample with the force-balancing system described in paragraph (a).

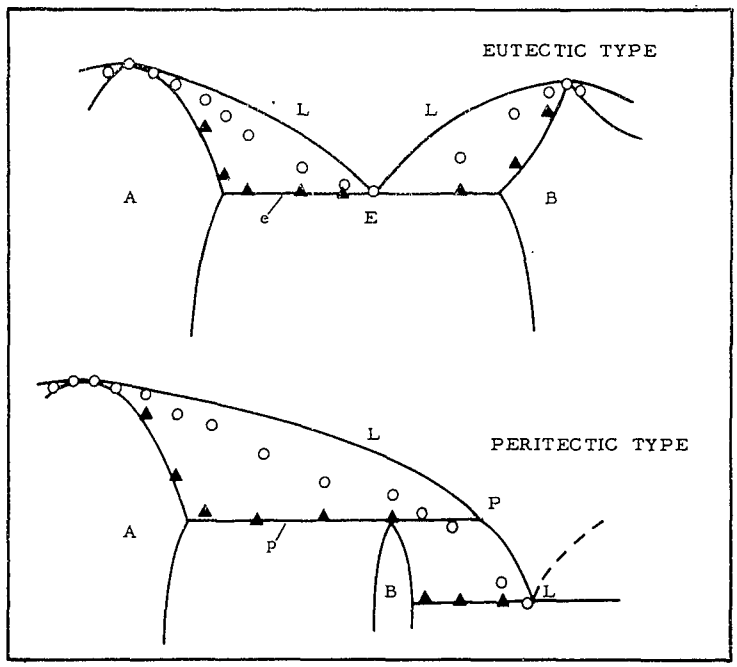

A, B	Intermediate Phases
L	Liquidus Lines
e, P	Eutectic and Peritectic Line
E, P	Composition of the Eutectic and the Peritectic
▲	Incipient Melting Observed
O	Sample Collapses Due to Loss in Strength

Figure 17. Typical Melting Behavior Observed with the Pirani Method (Schematic)

Usually, the incipient melting temperatures can be observed very accurately by the sudden emissivity change of the inner hole surface, the formation of droplets in the hole, as well as by the discontinuity occurring in the temperature-time history of the sample upon linear power increase (Thermal arrest).

The differentiation between peritectic and eutectic reaction types, as well as the approximate location of the corresponding concentrations, can be achieved by an analysis of the observed melting pattern. Typical cases are presented in Figure 17. At concentrations approaching the location of the melting point maxima as well as those of eutectics, the difference between observed incipient melting temperature and the temperature at which the sample collapses narrows; they coincide when these respective concentration points are reached.

g. Measurements on Molybdenum-Carbon Alloys

(1) Molybdenum

For the determination of the melting point of molybdenum, approximately 10 grams of the powder material (cf. analysis in Section 1) were placed in a steel die (Figure 4) and compacted under a pressure of 5 tons/cm^2. The green density of the compacts was approximately 75% of theoretical. The cold-compacted material was then placed on tantalum sheets and sintered for 1 hour at 1600°C under a vacuum of 1×10^{-5} Torr.

After insertion of the sample into the clamping device of the melting point furnace, the chamber was evacuated three times to 10^{-3} Torr, and each time refilled with high purity helium to atmospheric pressure.

Measurements were carried out under vacuum (10^{-3} Torr) as well as under helium (1.3 atm). The results were identical.

(2) Molybdenum-Carbon Alloys

The melting point specimens were prepared by hot pressing mixtures of the elemental powders to a density of approximately 70% of theoretical. After hot-pressing, the specimens were ground to size and a 1 mm diameter x 3-4 mm deep hole was drilled into the center portion of the sample (Figure 13). The specimens were then clamped between the two copper electrodes (Figure 11) and held under slight compression (~ 200 g) while heated. The initial runs under vacuum resulted in carbon losses from 2 to 5 atomic % in the alloys, and later experiments were therefore carried out under a helium pressure of 1.3 atmospheres.

It was found that porous compacts (20-40%) were preferable to fully dense material, since considerably less sputtering of the melt was encountered during the experiment and the temperature readings could be performed more accurately. The steep temperature gradient in the sample causes the melt to form first in the interior. After the melting temperature has been reached, the observation hole in dense samples fills immediately with liquid, which, after partial refreezing on the colder outer portions, causes the sample to burst upon further power increase. However, in porous melting point specimens the colder outer shell of the sample soaks up the melt from the interior, creating in this way a cavity in the center. Slight power raises do not increase the temperature, but merely affect the amount of melt formed. Thus, the observer

has sufficient time to focus the pyrometer and to match the filament exactly against the radiation coming from the observation hole. Upon continued power increase the size of the cavity reaches finally the outer sample surface and the specimen collapses. These various phases are shown in Figures 18 to 20.

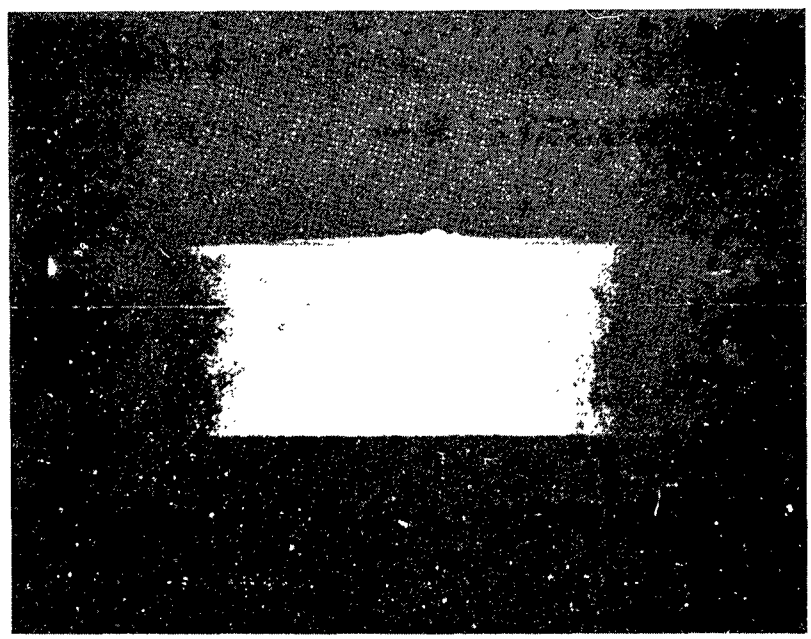

Figure 18. View through the Observation Window at a Melting Point Specimen at Temperature.

Figure 18 shows a melting point sample at temperature as viewed through the observation window. The magnification corresponds to approximately one-half of that of the micropyrometer.

Figure 19 shows a section of a sample shortly after incipient melting was noted. A cavity in the center section of the specimen has already formed by partial melting, but the observation hole is still intact.

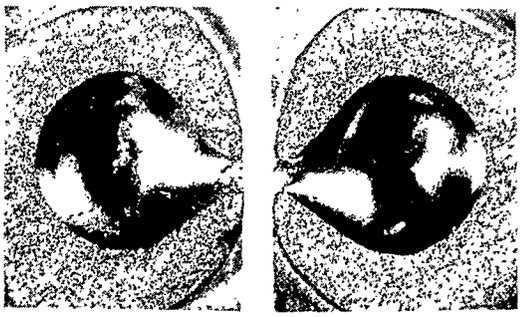

Figure 19. Section of a Melting Point Sample after Incipient Melting was Noted

Figure 20 shows a sample from an experiment which was stopped shortly before the sample collapsed. The observation hole has already filled with melt and the boundaries of the vacuole have nearly reached the outer sample surfaces. The sharply separated regions melt-solid give an indication of the steep temperature gradients existing between center and outer portions of the specimen.

8. X-ray Investigations

After the heat-treatments and quenching experiments, powder diffraction patterns (Cu-Kα and Cr-Kα) were prepared from each alloy. The X-ray readings were done with a Siemens-Kirem coincidence scale. The precision micrometer allows the measurements to be accurate to $\pm$ .01 mm.

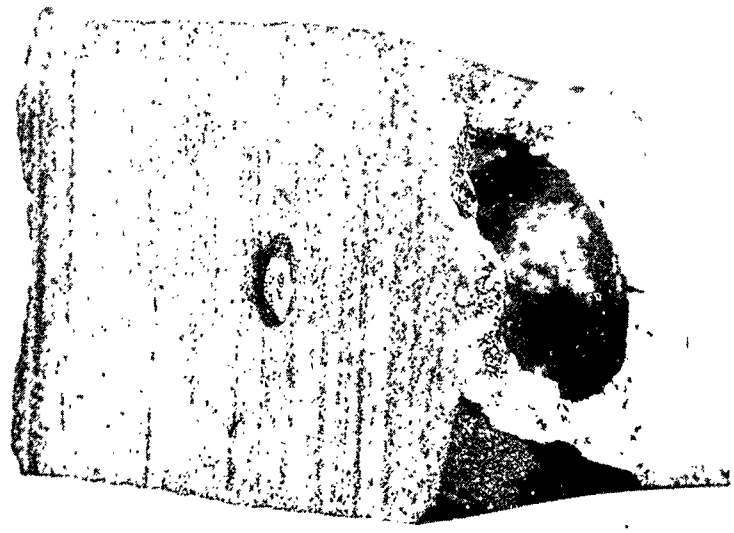

Figure 20. Section of a Melting Point Specimen Shortly Before Collapse. (Note the observation hole filled with melt)

The spontaneous transformation of α-MoC_{1-x} on severe grinding is known and therefore diffractometer runs were performed on α-MoC_{1-x} containing alloys.

9. Metallographic Investigations

The specimen preparation was done by grinding the mounted specimens on silicon carbide papers with grit sizes down to 600. Polishing was performed on microcloth, using Linde "B" alumina (0.05 μ) in Murakami's solution. From the various etchants, including electro-etch in 2% NaOH, a solution of 4g$KMnO_4$ and 4g NaOH in 100 ml water gave the best results. The samples were etched at room temperature; the times required to produce sufficient development of the microstructure varied from 3 to 10 seconds. The micrographs were examined and photographed on a Zeiss Ultraphot II Metallograph.

10. Chemical Analysis

Free and bound carbon was determined using the standard combustion technique*. For the determination of free carbon, the alloys were dissolved in a mixture of nitric and hydrofluoric acid, the undissolved graphic carbon filtered off and determined by combustion.

The carbon-dioxide content of the gas mixture resulting from the combustion was determined gasometrically by absorption in KOH. For low carbon contents (below 0.1 Wt%) the gas analysis was performed conductometrically.

In all cases standards were used for calibration of the equipment and the results of both methods were periodically counter-checked with gravimetric techniques. The results obtained are believed to be accurate to within $\pm$ .05 Wt%. The oxygen content of a number of alloys was determined by gas-fusion analysis.

*We acknowledge the help and advice received from Dr. Erik Lassner, Metallwerk Plansee, AG.

B. RESULTS

1. The α-Molybdenum-Phase

Nine melting temperature determinations were performed on pure molybdenum and yielded a melting point of 2619 ± 4°C, which is in perfect agreement with recent observations by B. Riley[48] of 2618 ± 3°C.

The solubility of carbon in molybdenum was not specifically investigated since the data are already well established and indicate only extremely low solubilities. Alloys with nominal carbon contents of 0.5, 1.0 and 1.5 atomic percent and which were quenched from 2000°C were all two-phased and contained Mo_2C carbide in precipitates at the metal grain boundaries. The solubility must therefore be less, which is in agreement with the earlier observations.

2. The Concentration Range α-Mo-α-Mo_2C

Melting point determinations on alloys in the concentration range from 5 to 26 atomic percent carbon showed incipient melting temperatures close to 2200°C (Table 8). At compositions between 15 and 20 atomic percent carbon melting occurred fairly sharply indicating that the approximate location of the eutectic α-Mo-α-Mo_2C had been reached.

Based on the results of the melting point determinations, the eutectic line was found to occur at 2200 ± 5°C; this was confirmed by DTA-measurements (Figure 21) which also showed the eutectic reaction to be the only isothermal phase change in the temperature range from 1100 - 2300°C occurring in this concentration region. The eutectic concentration was determined metallographically on alloys, which were quenched in the range from 2210 - 2250°C.

Table 8. Melting Temperatures of Molybdenum-Carbon Alloys

No	At% C Nom.	At% C Anal.	Number of Runs	Melting Temperatures °C (Corrected) Incipient	Melting Temperatures °C (Corrected) Sample Collapsed	Conditions	Melting
1	0	0	9	2619 ± 4	2619 ± 4	1,2	Sharp
2	5.0	5.2	1	2211	2451	2	Very Heterog
3	10.0	10.3	2	2208 ± 4	2260 ± 10	2	Heterog.
4	15.0	14.0	2	2205 ∓ 5	2205 ∓ 5	2	Sharp
5	20.0	18.5	2	2201 ∓ 4	2201 ∓ 4	2	Sharp
6	22.0	20.0	2	2198 ∓ 4	2198 ∓ 4	1	Sharp
7	24.0	21.6	2	2200 ∓ 4	2206 ∓ 5	1	Fairly Sharp
8	25.0	22.8	2	2206 ∓ 5	2221 ∓ 0	1	Heterog
9	26.0	24.1	2	2208 ∓ 4	2226 ∓ 4	1	Heterog
10	27.0	25.0	2	--	2229 ∓ 10	1	Very Heterog
11	28.0	26.3	2	2235 ± 10	2309 ∓ 8	1	Very Heterog
12	29.0	27.5	2	2267 ∓ 8	2313 ∓ 5	1	Very Heterog
13	30.0	28.9	1	2390	2410	1	Slightly Heterog
14	31.0	30.1	2	--	2427 ± 5	1	Slightly Heterog
15	32.0	30.2	2	2430 ± 5	2451 ∓ 4	1	Slightly Heterog
16	33.0	31.0	2	2475 ∓ 4	2475 ∓ 4	1	Sharp
17	33.5	32.2	2	2480 ∓ 3	2480 ∓ 3	1	Sharp
18	34.0	32.0	3	2486 ∓ 4	2486 ∓ 4	1	Sharp
19	34.5	32.6	3	2469 ∓ 4	2469 ∓ 4	1	Sharp
20	35.0	33.0	3	2486 ∓ 5	2486 ∓ 5	1	Sharp
21	35.2	33.5	3	2510 ∓ 6	2510 ∓ 6	1	Slightly Heterog
22	35.2	34.2	2	2522 ∓ 4	2522 ∓ 4	1	Sharp
23	36.0	35.0	2	2512 ∓ 10	2512 ∓ 0	1	Sharp
24	37.0	35.8	2	2513 ∓ 3	2513 ∓ 3	1	Sharp
25	38.0	36.6	2	2512 ∓ 4	2512 ∓ 4	1	Sharp
26	39.0	37.4	2	2533 ∓ 6	2533 ∓ 6	1	Sharp
27	40.0	38.1	2	2540 ∓ 6	2540 ∓ 6	1	Sharp
28	41.0	38.8	2	2550 ∓ 2	2550 ∓ 2	1	Sharp
29	39.0	38.9	2	2547 ∓ 3	2547 ∓ 3	2	Sharp
30	39.5	39.5	2	2547 ∓ 3	2547 ∓ 3	2	Sharp
31	40.0	39.8	2	2547 ∓ 4	2547 ∓ 4	2	Sharp
32	40.5	40.5	2	2576 ∓ 8	2576 ∓ 8	2	Sharp
33	40.9	41.0	2	2589 ∓ 2	2589 ∓ 2	2	Sharp
34	42.0	42.0	2	2599 ∓ 4	2599 ∓ 4	2	Sharp
35	42.5	42.6	2	2594 ∓ 3	2594 ∓ 3	2	Sharp
36	43.0	43.4	2	2578 ∓ 4	2578 ∓ 4	2	Sharp
37	45.0	45.4	2	2580 ∓ 4	2580 ∓ 4	2	Sharp
38	47.0	47.3	2	2584 ∓ 6	2584 ∓ 6	2	Slightly Heterog
39	50.0	--	2	2584 ∓ 6	2590 ∓ 8	2	Slightly Heterog
40	55.0	--	2	2585 ∓ 6	2594 ∓ 8	2	Heterog
41	60.0	--	2	2594 ∓ 6	2655 ∓ 10	2	Very Heterog
42	100	--	2	3800 ∓ 50	(Pc_x = 1 atm.)	3	Sublimation

Legend to Table 8:
(1) Vac., 10^{-2} Torr. The Measurements were carried out under slight helium flow to prevent fogging of observation window.
(2) He, 1.3 atm pressure
(3) He, 1.1 to 1.3 atm pressure

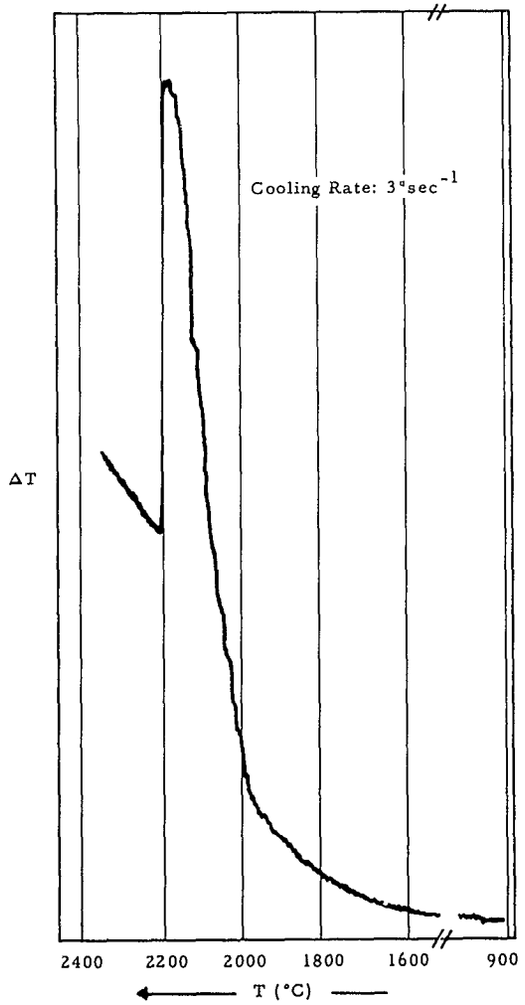

Figure 21: Differential Cooling Curve of a Molybdenum-Carbon Alloy with 20 Atomic % C

The microstructure shown in Figure (22) reveals the existence of primary molybdenum in a matrix of α-Mo —— α-Mo_2C - eutectic, while an alloy with 17 At% C (Figure 23) which was quenched from 2210°C is purely eutectic.

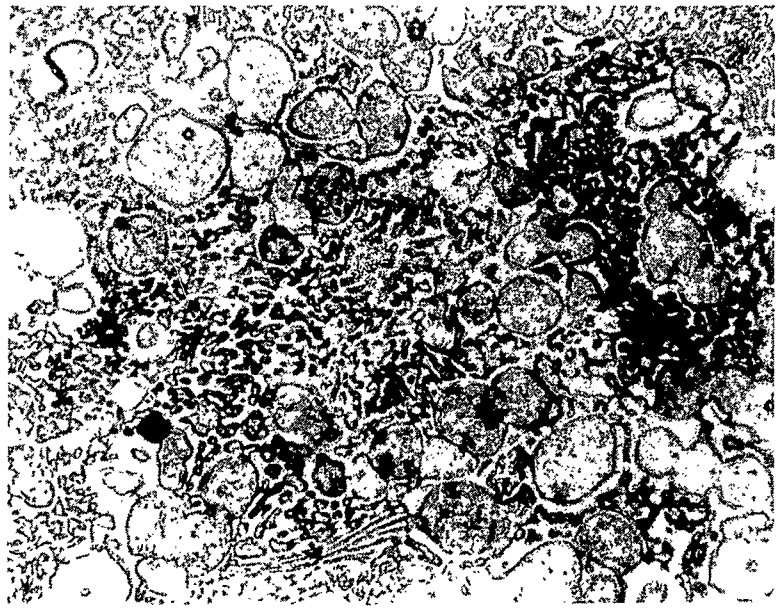

Figure 22. Mo-C (14 At% C), Quenched from 2230°C X500
Primary Crystallized Molybdenum in Matrix
of α-Mo —— α-Mo_2C - Eutectic.

The alloy with 18 At% carbon (Figure 24) quenched from the same temperature, shows already small amounts of primary Mo_2C, recognizable on the banded structure (preferential precipitation of molybdenum on preferred crystal planes).

An alloy with 25.5 At% carbon shows small amounts of traces at the grain boundaries (Figure 25), whereas apart from precipitation effects occurring during cooling, the alloy with 26 At% carbon is single phase (Figure 26).

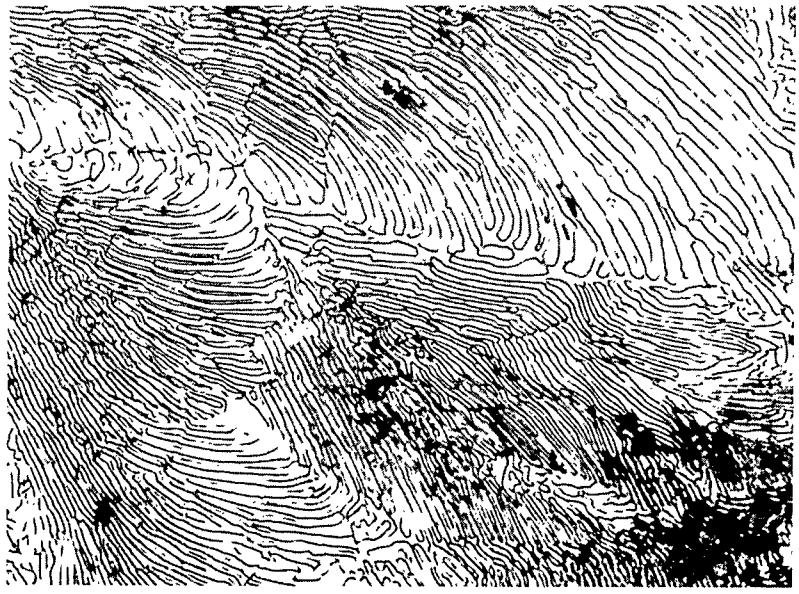

Figure 23. Mo-C (17 At% C), Quenched from 2210°C X1000
α-Mo —— α-Mo_2C Eutectic

3. α- and β-Mo_2C

Within the homogeneous range of the Mo_2C the melting temperatures increase steadily with the carbon concentration, reaching a maximum 2486 ± 5°C at a composition of 32 At% C. Increasing the carbon concentration further, the melting temperature drops again, reaching a minimum at 32.6 At% C, (2469 ± 6°), after which it reaches a second maximum (2522 ± 5°C) at a composition of 34 At% C.

The metallographic examination of alloys, which were quenched from a number of temperatures, revealed some interesting features:

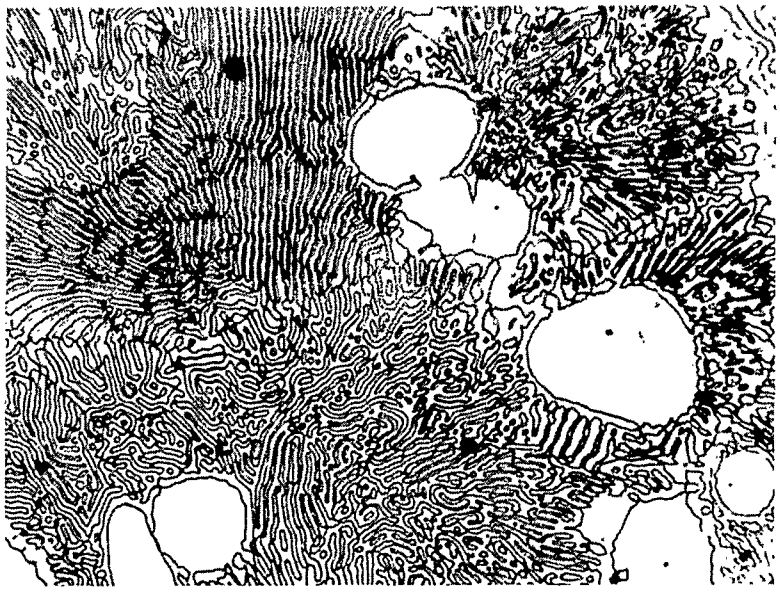

Figure 24. Mo-C (19 At% C), Quenched from 2210°C X1000
Primary α-Mo_2C and Eutectic.

Up to a total carbon concentration of 32 At% the alloys were single phase, as was found also by X-ray examination. It was also noticed that the localized molybdenum precipitations from the Mo_2C-phase, visible in the more metal-rich samples, disappeared after the total carbon concentration exceeded approximately 30 At%.

An alloy with 32.8 At% carbon, quenched from 1600, 2000, 2300 and 2400°C showed a two-phase structure, although the appearance varied with the quenching conditions. The microstructure resembled in many respects a typical Widmannstätten-type decomposition structure.

Figure 25. Mo-C (25.5 At% C), Quenched from 2210°C. X750
α-Mo_2C with Precipitations within the Grain
and Traces of Molybdenum at the Grain Boundaries

Since an alloy with 34 atomic percent carbon again showed only one phase, it became apparent that, presuming a second phase did exist in the neighborhood of Mo_2C, the corresponding two-phase field had to be very narrow and was therefore likely to escape the experimental observation. An attempt was therefore made to determine the existence of the

possible two-phase field by heating a sample with fixed composition under a temperature gradient. A concentration-temperature dependent two-phase field should in this experiment show up in the existence of a temperature zone, where the two phases are in equilibrium.

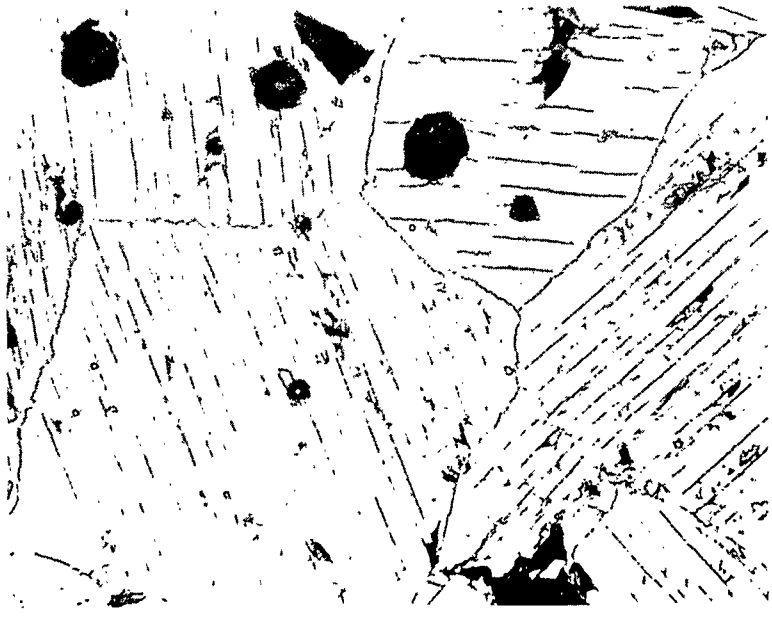

Figure 26. Mo-C (26 At% C), Quenched from 2220°C X500
α-Mo_2C with Precipitations and Pores (black)

For this purpose a sample similar to that used for the melting point determinations was prepared, having a carbon concentration of 32.8 At% C. The diameter of the sample was 10 mm. The specimen was heated by direct resistance until the temperature, observed with an micropyrometer in a black body hole, which was drilled into the center of

the specimen, reached 2460°C. The measured temperature at the outside of the specimen was 2170°C, yielding a temperature gradient 580°C per cm from the interior to the surface. After equilibration for about 5 minutes, the sample was quenched by dropping it into a tin bath. The result is shown in the micrograph in Figure 28, revealing the coexistence of two phases at high temperatures.

Figure 27. Mo-C (32.2 At% C), Quenched from 2480°C. X1000
Single Phase α-Mo_2C (Cracks are due to Rapid Cooling)

Since no second phase could be detected by X-ray methods in furnace cooled specimens, a series of alloys was prepared under varying quenching conditions and subjected to X-ray and metallographic

analyses. In alloys, which contained less than approximately 32 At% C, only the hexagonal close-packed pattern of the Mo_2C-phase could be observed in the powder pattern. A splitting of certain diffraction lines was observed in quenched alloys in the concentration range 32.5 - 33.5 At% C. This effect disappeared again, once the carbon concentration exceeded 34 At% C.

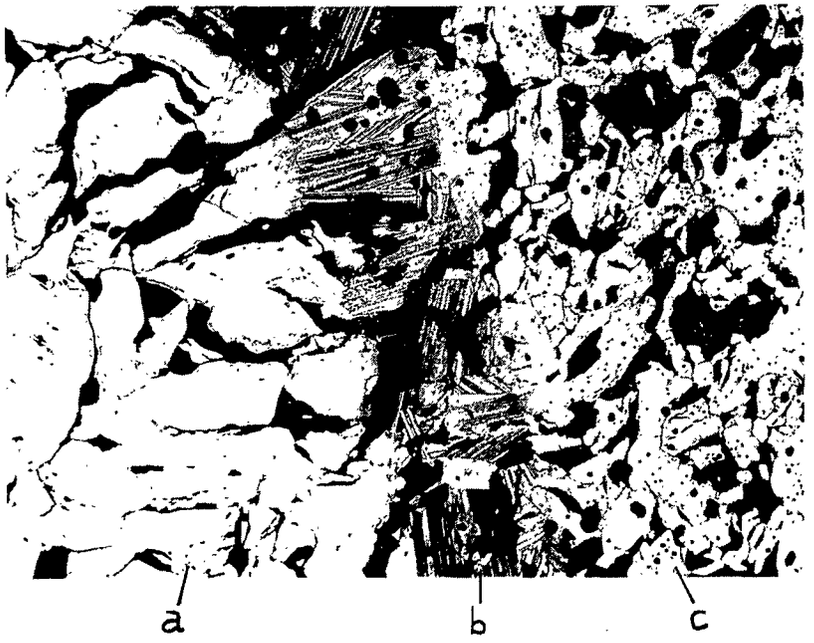

Figure 28. Mo-C (32.8 At% C), Heated Under a Temperature Gradient and Quenched X25

Zone a: β-Mo_2C (T = 2460°C)

Zone b: α- + β-Mo_2C (T ~ 2300°C)

Zone c: α-Mo_2C (T <2300°C)

At carbon concentrations in excess of 35 - 36 At%, small amounts of η-MoC_{1-x} were present, indicating that the two-phase range Mo_2C-η-MoC_{1-x}

Figure 29. Mo-C (34.0 At% C), Quenched from 2450°C X750
Single Phase β-Mo_2C (Cracks are due to Rapid Cooling)

had been reached. The X-ray findings are in accordance with the metallographic examination (Figures 29 and 30) of these specimens.

A closer inspection of the diffraction lines revealed that the line splitting was not accidental and also that it was restricted to certain diffraction lines only while the majority remained single and sharp.

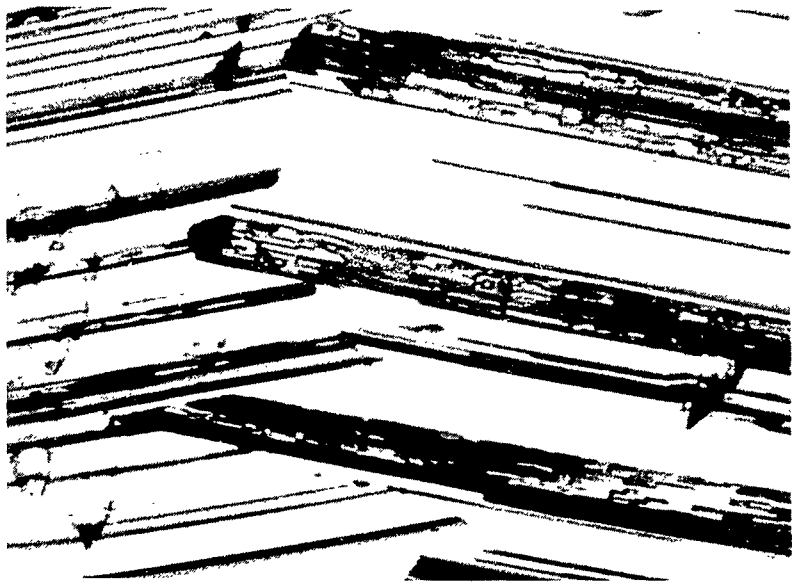

Figure 30. Mo-C (35.8 At% C), Quenched from 2400°C X2500
Localized Precipitations of η-MoC_{1-x} in
β-Mo_2C

Since such phenomena are commonly related to lattice distortions, an attempt was made to index the powder pattern on the basis of an orthorhombic setting of the hexagonal axes. These attempts were not successful and no usable structure proposal along these lines could be derived. Comparing

the indices of the planes which produced the double or diffuse lines, and by taking exposures with chromium radiation for further line resolution, it was noticed that all diffraction lines having indices $(hk\bar{i}o)$ remained sharp, while the diffraction lines from planes (000ℓ) showed the greatest separations; the diffraction lines $(hk\bar{i}\ell)$ showed an intermediate behavior, with the line separation increasing with increasing (ℓ). Based on intensity measurements on the diffraction lines, the existence of a phase mixture seemed to be the most plausible solution and the films were indexed on the basis of two isostructural (hexagonal close-packed) phases, having the same a-spacing but differing in the size of the c-spacing.

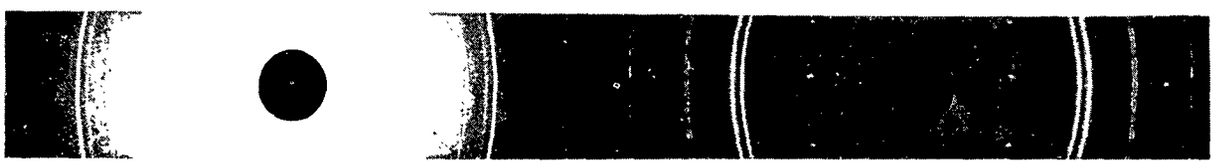

Figure 31. Diffraction Pattern (Cr-Kα) of a Molybdenum Carbon Alloy with 33 At% Carbon, Quenched From 2000°C

The evaluation of the diffraction of a molybdenum carbon alloy with 33.0 At% C, containing both phases in about equal amounts, is listed in Table 9 and accounts for all observed diffraction lines. A chromium-K_α exposure is shown in Figure 31.

Summarizing the high temperature experimental findings in the concentration range from 30 - 35 At% C, it has been found that Mo_2C separates into two isostructural phases at high temperatures.

The concentration gap between the two phases is extremely narrow and at any temperature does not exceed 1.0 At% C.* No upper critical solution temperature has been found and instead, both phases melt congruently. In view of the small concentrational differences involved, which preclude the exact experimental verification, the existence of a eutectic reaction between both phases is deduced from the melting point determinations.

The next question which arises concerns the lower temperature stability of the carbon-rich modification (β-Mo_2C).

Metallograph examination of the pure β-Mo_2C-phase which was obtained by quenching under varying cooling rates revealed growth of a second phase once the cooling rates were below a critical value. The fact that no β-phase could be detected in very slowly cooled material and also not in alloys which were heat-treated below 1400°C, indicated that β-Mo_2C is not stable at low temperatures, decomposing either to α-Mo_2C + η-MoC_{1-x} or to α-Mo_2C + graphite. The differential cooling and heating diagrams of an alloy with 33 Atomic % carbon are shown in Figure 32 and reveal a thermal arrest at 1470°C. The reaction proceeds very sluggishly, as can be seen by the same diagram on an expanded temperature scale (Figure 33). The significant feature representative of the true temperature of the isothermal phase change is the onset of the reaction (recognizable on the change of slope of the ΔT-T curve) in the cooling cycle.

The decomposition of the β-Mo_2C-phase proceeds by nucleation of the α-Mo_2C-phase (+ carbon), and subsequent growth of the α-Mo_2C-phase at the expense of the β-phase, as shown in Figures 34 and 34a.

---

* As a matter of convenience for the subsequent discussions, we shall refer to these phases as α- and β-Mo_2C.

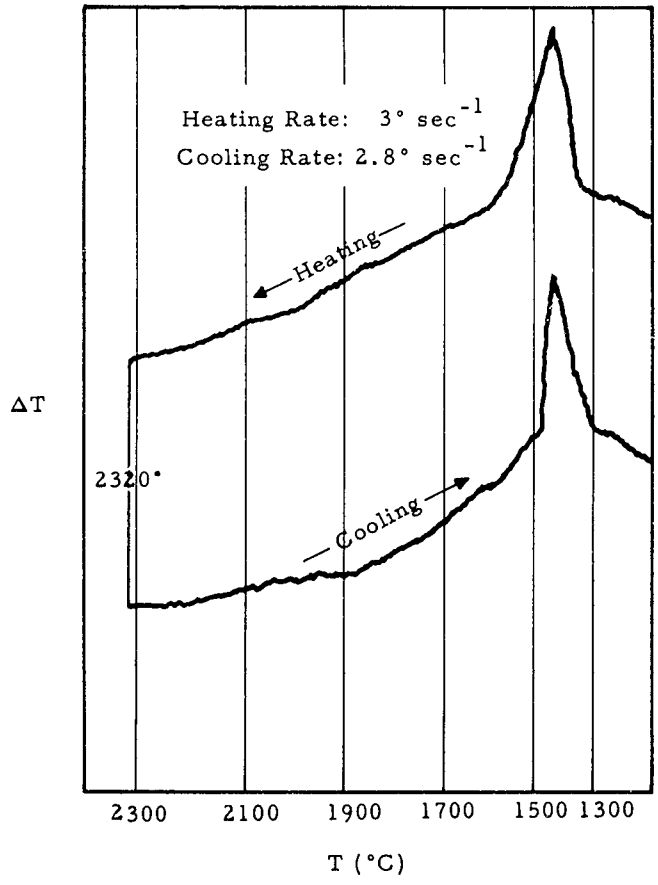

Figure 32. Differential Heating and Cooling Curve of a Molybdenum-Carbon Alloy with 33 Atomic % Carbon

The growth of the α-phase is oriented and it may be assumed[49] that the initial nucleation and growth (platelets) proceeds along the matching $(10\bar{1}0)$ plane of both structures

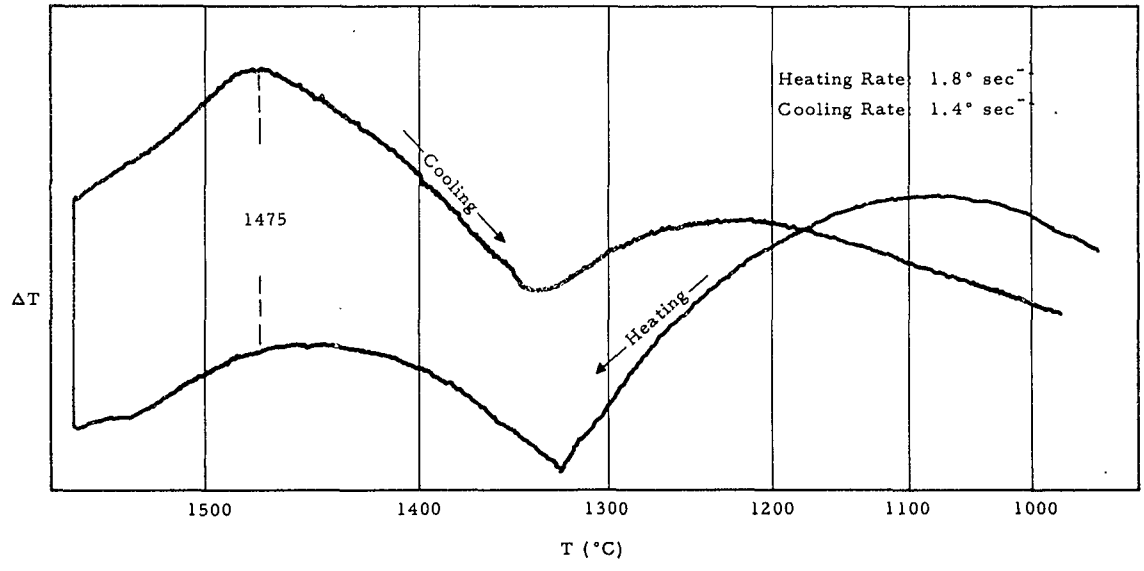

Figure 33. Differential Heating and Cooling Curve of a Molybdenum-Carbon Alloy with 33 Atom % Carbon. Medium Temperature Scale

The homogeneous range of the Mo_2C-phase was determined on rapidly quenched alloys which were prehomogenized by arc melting.

The metal-rich boundary of the α-Mo_2C at the eutectic temperature as deduced from metallographic examinations (Figures 25 and 26) from the results of the melting point investigations (Table 9) is located

Table 9. Powder Pattern of a Molybdenum-Carbon Alloy with 33.0 At% Carbon, Rapid Quenched from 2000°C

No	$10^3 \sin^2\theta$ calc.(1)	$10^3 \sin^2\theta$ Observ.	I (2) observ.	hkil β	hkil α
1	87.49	86.86	5	$10\bar{1}0$	$10\bar{1}0$
2	103.95 105.76	104.28*	6	0002	0002
3	113.47 113.93	113.60	10	$10\bar{1}1$	$10\bar{1}1$
4	191.44 193.25	191.76*	5	$10\bar{1}2$	$10\bar{1}2$
5	262.45	262.50	5-6	$11\bar{2}0$	$11\bar{2}0$
6	321.38	322.12	5 s.d.	$10\bar{1}3$	
7	325.45	325.80			$10\bar{1}3$
8	349.94	349.80	1	$20\bar{2}0$	$20\bar{2}0$
9	366.41 368.22	367.60	5 s.d.	$11\bar{2}2$	$11\bar{2}2$
10	375.93 376.38	375.49	4	$20\bar{2}1$	$20\bar{2}1$
11	415.81	415.80	1	0004	
12	423.04	422.80	1	-	0004
13	453.89 455.70	454.16	3 s.d.	$20\bar{2}2$	$20\bar{2}2$
14	503.29	503.63	1-	$10\bar{1}4$	
15	510.53	510.47	1-	-	$10\bar{1}4$
16	583.83	584.00	3 d	$20\bar{2}3$	
17	587.90	588.00			$20\bar{2}3$
18	612.40	612.48	2	$21\bar{3}0$	$21\bar{3}0$
19	638.38 638.83	638.74	5	$21\bar{3}1$	$21\bar{3}1$
20	678.27	678.53	3	$11\bar{2}4$	
21	685.50	685.47	3		$11\bar{2}4$
22	716.35 718.16	717.00	3 s.d.	$21\bar{3}2$	$21\bar{3}2$
23	737.19	737.22	2	$10\bar{1}5$	
24	748.49	748.72	2-3		$10\bar{1}5$
25	765.75	766.00	1- v.d.	$20\bar{2}4$	
26	772.98	773.10			$20\bar{2}4$
27	787.37	787.40	3	$30\bar{3}0$	$30\bar{3}0$
28	846.29 850.36	848.0	6 v.d.	$21\bar{3}3$	$21\bar{3}3$
29	889.31 893.13	891.70	5 d	$30\bar{3}2$	$30\bar{3}2$
30	935.57	936.06	1	0006	
31	951.84	951.74	1		0006

Legend to Table 9:

(1) The calculated lattice parameters are based on a=3.007 Å, c=4.737 Å for α-Mo_2C, and a=3.007 Å, c=4.778 Å for the β-Mo_2C phase.

(2) Visual estimate, intensity scale 0 - 10

*Lines resolved with Cr-Kα - radiation

s.d. - Slightly diffuse

d. - Diffuse

v.d. - Very diffuse

at 26 At% C. The lattice dimensions at this composition could not be determined, since even by using rapid quenching techniques, the precipitation of molybdenum from the carbide matrix could not be prevented. No disproportionation of the alloys was encountered in the alloy series which was quenched from 2000°C. Homogeneity was found to exist between 30 and 32.7 At% C (α-Mo_2C) and 33.5 and 34 At% C (β-Mo_2C). The X-ray results on the chemically analyzed alloys are summarized in Table 10 and the cell dimensions are presented in graphical form in Figure 35.

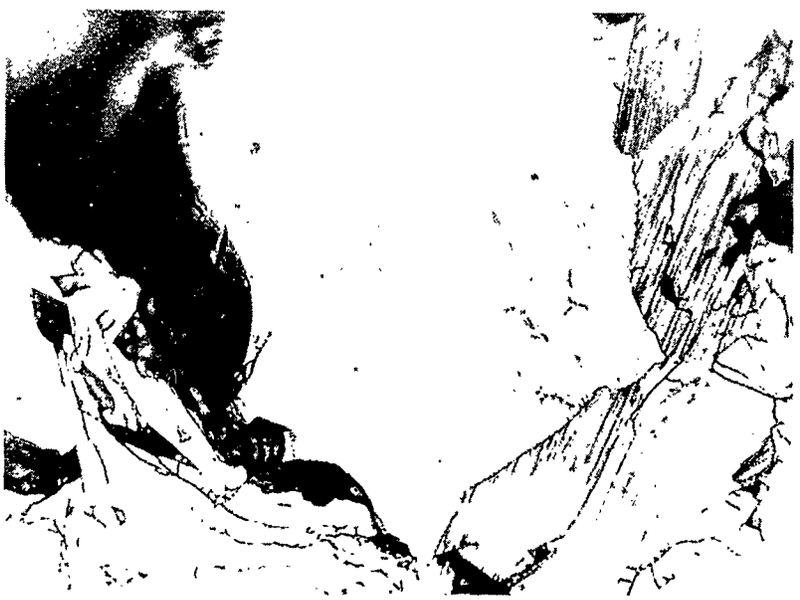

Figure 34. Mo-C (34 At% C), Cooled with Approximately 20°C per Second From 2400°C X750

Decomposition of β-Mo_2C: Oriented Growth of the New Phase (α-Mo_2C) in Originally Homogeneous Grains of β-Mo_2C.

Table 10. Homogeneous Range of the α-Mo_2C-Phase at 2000°C
X-Ray and Analytical Results on Quenched Alloys

No	Anal.Determ. Composition At% C.	Lattice Parameters, Å Mo_2C a	Mo_2C c	Mo a	Phases Present (X-Ray)
1	26.4	2.9905±2	4.729±1	3.147_0	α-Mo_2C + α-Mo
2	27.0	2.9908±4	4.729±1	3.147_3	α-Mo_2C + α-Mo
3	27.4	2.9910±4	4.728±1	-	α-Mo_2C + α-Mo
4	28.9	2.9910±5	4.728±1	-	α-Mo_2C + α-Mo
5	29.3	2.9905±5	4.729±1	-	α-Mo_2C + Traces α-Mo
6	30.1	2.9895±5	4.728±1	-	α-Mo_2C
7	30.5	2.9930±5	4.730±1	α-Mo_2C	α-Mo_2C
8	30.9	2.9960±5	4.732±1	-	α-Mo_2C
9	31.8	3.0000±5	4.732±1	-	α-Mo_2C
10	32.0	3.0015±5	4.734±1	-	α-Mo_2C
11	32.3	3.0040±5	4.734±1	-	α-Mo_2C
12	32.7	3.005±1	4.733±1	-	α-Mo_2C
13	33.0	3.006±1	4.734±1	-	α-Mo_2C + β-Mo_2C
14	33.5	3.007±1	4.778±1	-	α-Mo_2C + β-Mo_2C
15	34.0	3.010±1	4.780±1	β-Mo_2C	β-Mo_2C
16	35.0	3.0105±5	4.780±1	-	β-Mo_2C + Traces η-Mo_{1-x}
17	36.0	3.0105±5	4.782±1	-	β-Mo_2C + η-MoC_{1-x}

The a-axis of the unit cell increases practically linearly with the carbon concentration and shows no marked discontinuity. The c-axis, which is nearly constant over the entire homogeneous range of the α-phase, shows an abrupt change to higher values at the α-β-phase boundary.

Towards lower temperatures the metal-rich phase boundary moves to higher carbon concentrations. Alloys with 29, 30 and 31 At% C, heat treated at 1400°C, were all two phase and contained excess molybdenum, while an examination of an alloy with 32.3 At% C, heat treated at 1300°C revealed only the existence of the carbide phase. These findings are in accordance with earlier observations[9,15,16]

Figure 34a. Mo-C (34 At% C), Cooled with Approximately 20°C per Second from 2400°C X2500

Formation and Growth of α-Mo_2C-Nuclei in a Homogeneous Matrix of β-Mo_2C.

The homogeneous ranges of the α- and β-Mo_2C-phase obtained from X-ray lattice parameter data (Table 10 and Figure 35) are consistent with the metallographic observations. However, a slight dependence of the relative

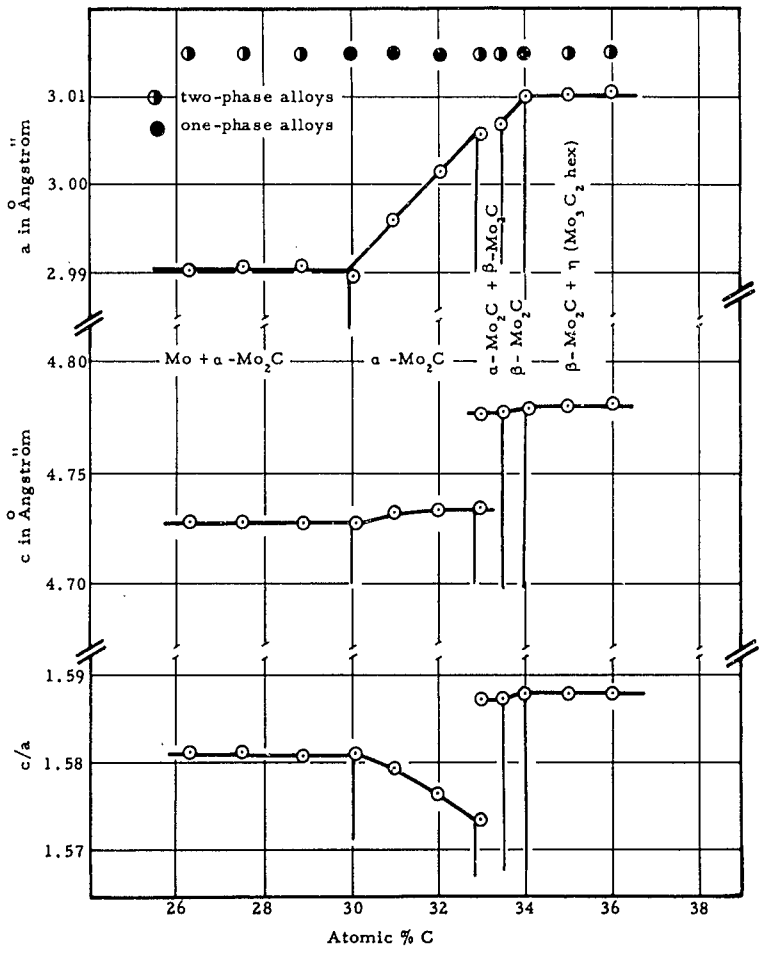

Figure 35. Lattice Parameters of α- and β-Mo_2C (Alloys quenched from 2000°C)

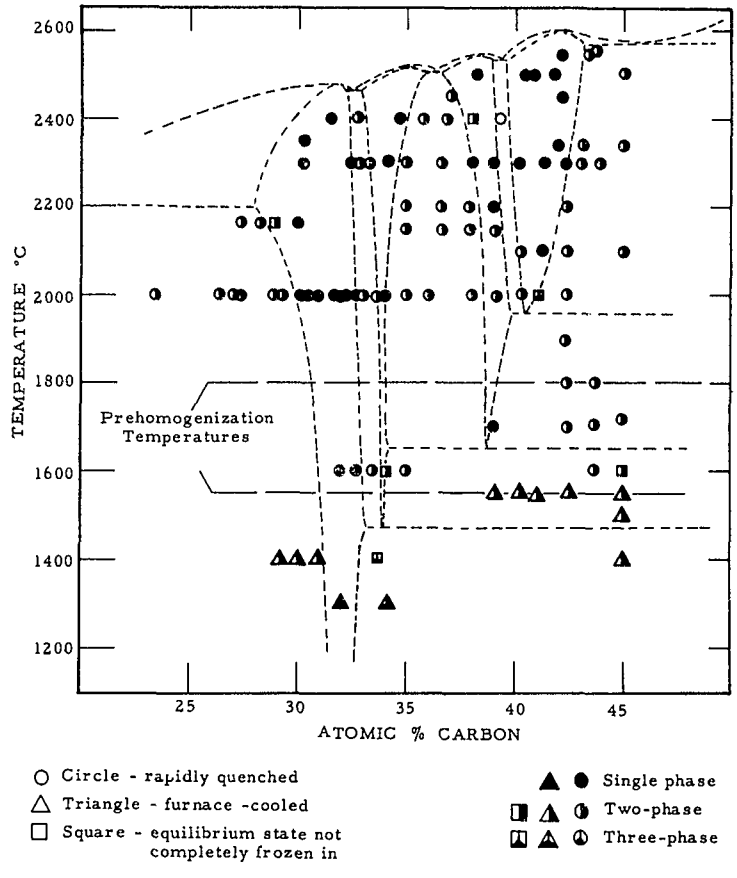

Figure 36. Positions of Alloys in the System Molybdenum- Carbon

lattice dimsneions (c/a) on the quenching temperature has been observed and there is some uncertainty with regard to the relative extent to which the high temperature equilibrium states had been retained in the α- and β-phase, respectively.

Without going into detail, it may be indicated at this point that the anomalous lattice changes may be related to homogeneous disordering reactions of the carbon sublattice. We shall return to a discussion of this question in a later section.

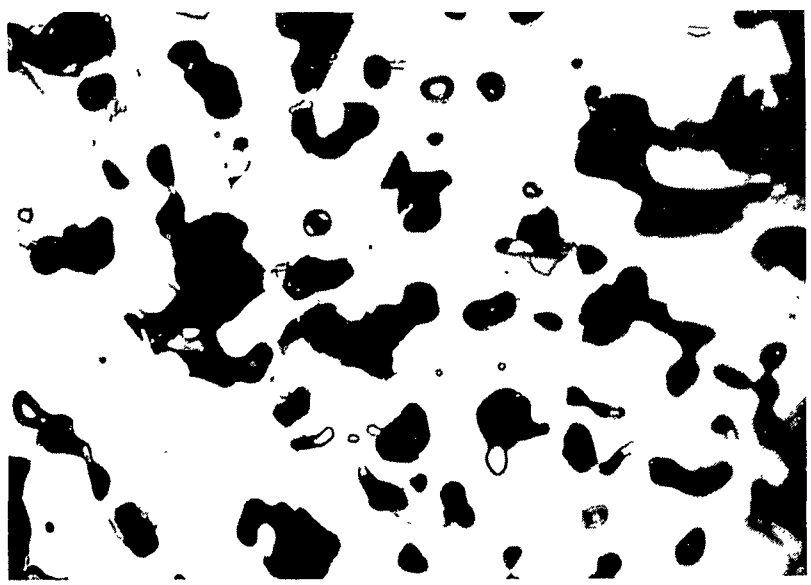

Figure 37. Mo-C (38At% C), Quenched from 2500°C. X1000
Single Phase η-MoC_{1-x} with Pores (Black)

4. The Concentration Range Between 33 and 39 At% Carbon. The Thermal Stability of the η-Phase.

An examination of the melting temperatures (Table 8) of molybdenum-carbon alloys in this concentration region indicates, that

melting occurs virtually isothermally in the range from 34 to 37 At% C. Starting at about the latter composition, the melting temperatures increase slightly, reaching a maximum of 2550°C at a composition of 38.8 atomic percent carbon. Quenched alloys in the concentration range from 35 to 37 atomic percent carbon were two-phase (Figure 36), and the X-ray patterns showed β-Mo_2C and η-MoC_{1-x} to be present in varying amounts.

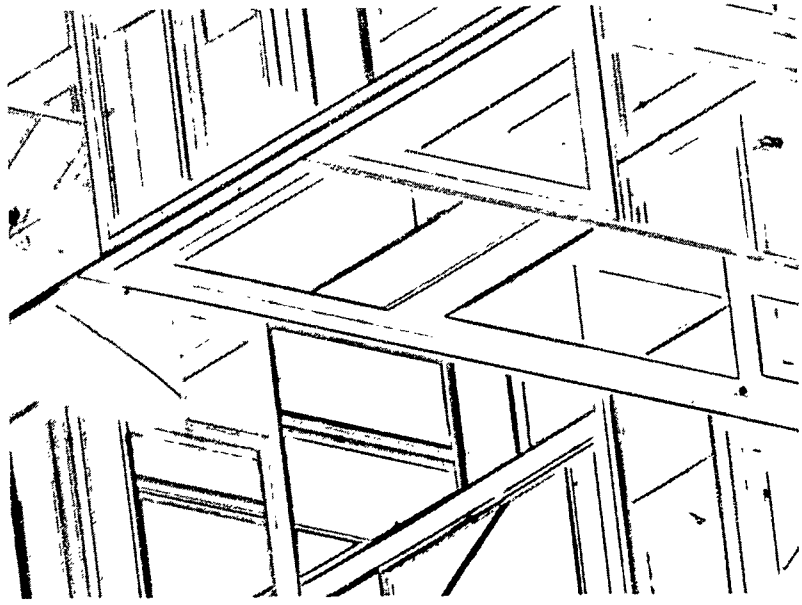

Figure 38. Mo-C (38 At% C), Cooled from 2500°C and Approximately 20°C per Second. X1000

Early Stages of Decomposition of the η-phase into β-Mo_2C and Graphite.

Alloys with carbon concentrations higher than 38 At% and which were quenched from temperatures above 1800°C were generally single phase (Figure 37), although in some instances partial decomposition

of the η-MoC_{1-x}-phase into β-Mo_2C and graphite could not be fully prevented. This applies especially to those instances, where slower cooling rates were used, (Figure 38). Similar to the findings at the metal-rich phase-boundaries of the Mo_2C-phase at high temperatures, samples at the carbon-rich phase boundary of the β-Mo_2C-phase, and at the metal-rich phase-boundary of the η-MoC_{1-x}-phase at high temperatures cannot be retained as a single phase even by using the rapid quenching techniques described in Section A-4.

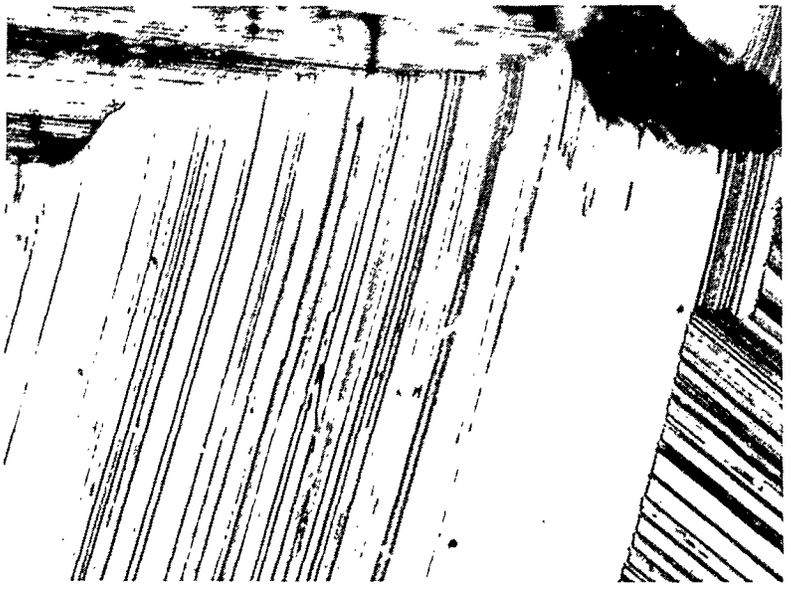

Figure 39. Mo-C (35.8 At% C), Rapidly Quenched from 2470°C. Localized Precipitations of η-MoC_{1-x} in Originally Homogeneous Matrix of β-Mo_2C. X2000

The alloys disproportionate extremely fast and homogeneity at high temperatures can often be deduced only from the appearance of the microstructures. Figure 39 shows the microstructure of a molybdenum carbon alloy with 35.8 At% C, which was rapidly quenched from 2470°C. The X-ray

examination of the alloy revealed the main constituent to be β-Mo_2C, accompanied by smaller amounts of η-MoC_{1-x}. There were also a few weak diffraction lines present which could not be attributed to either the β-or the η-phase. These lines were only observed in alloys which were quenched from temperatures above 2400°C, and were not present when the quenching experiments were performed with lower cooling speeds. Since these lines were only occasionally observed, and also only, where heavy precipitation could be expected to occur, it was concluded that the diffraction lines did not correspond to an equilibrium phase.

An explanation of the appearance of non-equilibrium (transition) phases may be sought in the structural similarities of both phases. Precipitation from β-Mo_2C as well as from η-MoC_{1-x} (Figures 38 and 39) initiates on preferred crystal planes [probably on (0001), because of the nearly identical dimensions and occupational densities] and epitaxial phenomena may lead to the formation of structures with faulty stacking during the initial stages of precipitation, i.e. while the layer thickness of the precipitate phase is still very small.

Differential-thermoanalytical measurements were carried out on alloys with carbon contents of 35 and 38 At%. While for the alloy with 35 At% C the thermal arrest associated with the decomposition of the β-Mo_2C-phase was still fairly well developed, it could not be differentiated with certainty from the experimental background for the alloy with 38 At% C.

A second sharp thermal arrest was observed at temperatures between 1640 and 1690°C, and was identified as being due to the formation (heating) or decomposition (cooling) of the η-MoC_{1-x}-phase. The temperature difference observed in the onset of the reaction in the heating

or cooling cycle (Figure 40) is a kinetic effect and approaches zero, as the heating or cooling rates approach zero. Using measurements with heating and cooling rates from 1.5 to 10°C per second, the true temperature of the non-variant (eutectoid) equilibrium was extrapolated to be 1655 $\pm$ 20°C. No further thermal arrests in this concentration region were observed in the DTA-runs, which were extended up to 2400°C.

The low temperature decomposition of η-MoC_{1-x} was studied in some detail by metallographic, X-ray, and analytical methods.

Table (11) shows the result of the X-ray and analytical investigations on quenched alloy material. The findings are in agreement with the conclusions reached from the differential-thermoanalytical investigations. Samples with total carbon contents varying from 39 to 45 atomic percent after an initial equilibration treatment of 30 hours at 1550°C showed α-Mo_2C, β-Mo_2C, and graphite as main constituents, and traces of η-MoC_{1-x}. The average content of bound carbon in these alloys corresponded close to the stoichiometric composition of the Mo_2C-phase. Rapid quenching of this prehomogenized material at 1600°C revealed only β-Mo_2C and graphite, sometimes with traces of η-MoC_{1-x} present.

In this connection it may be mentioned, that while the initiation of the decomposition of η-MoC_{1-x} shows itself to be a comparatively fast process, fairly long annealing times at temperatures below the eutectoid line are necessary to complete the reaction, i.e. to decompose the η-MoC_{1-x}-phase completely. The presence of small amounts of η-phase in the low temperature quenching experiments have therefore to be understood as arising from kinetic effects.

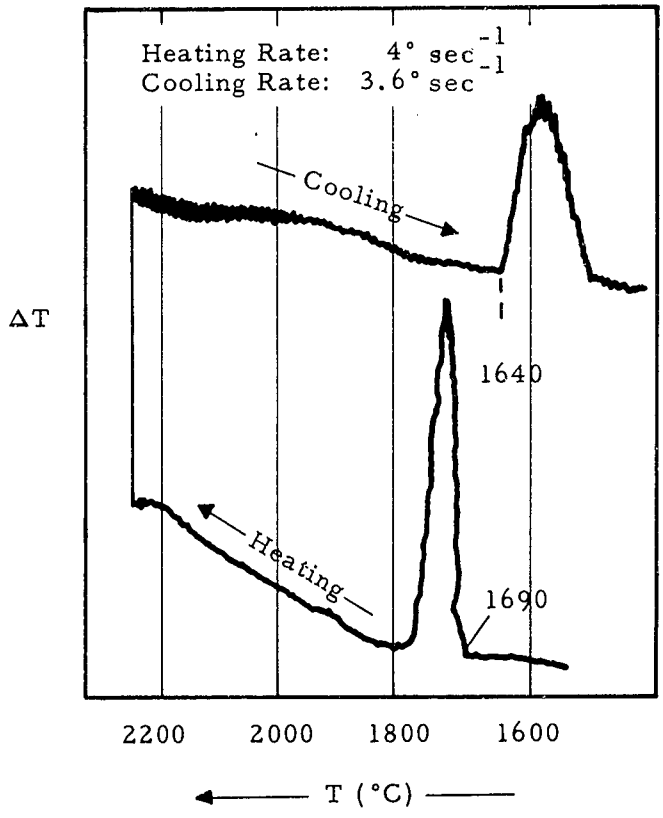

Figure 40. Differential Heating and Cooling Curve of a Molybdenum-Carbon Alloy with 38 Atomic % Carbon

Table 11. Formation of η-MoC_{1-x} from β-Mo_2C and Graphite: Analytical and X-Ray Results on Quenched Specimens*

No	Quenching or Annealing Conditions	Analyt.Determ.Composition Atomic % Total	Combined	Phases Present (X-ray)	Lattice Parameters	Remarks
1	30 hrs/1500°C	42.5	33.6	α-Mo_2C + β-Mo_2C +graphite + traces η-MoC_{1-x}	n.d.	η-MoC_{1-x} not completely decomposed
2	25 min/1600° ↓	45.0	~34.0	β-Mo_2C + traces η-MoC_{1-x}	n.d.	η-MoC_{1-x} not completely decomposed
3	8 min/1700° ↓	39.0	39.0	η-MoC_{1-x}	a=3.010Å, c=14.64Å } η-MoC_{1-x}	
4	10 min/1700° ↓	42.5	38.9	η-MoC_{1-x} + C	n.d.	
5	10 min/1720° ↓	45.0	38.3	η-MoC_{1-x} + C	n.d.	
6	10 min/1800° ↓	42.4	39.5	η-MoC_{1-x} + C	a=3.011Å, c=14.64Å } η-MoC_{1-x}	
7 **	10 min/1700° + 25 min/ 1500° ↓	42.6	~34.1	β-Mo_2C + C + trace η-MoC_{1-x}	n.d.	η-MoC_{1-x} not completely decomposed

* Alloys homogenized for 30 hrs at 1550°C prior to quenching

** Sample of run number 4

↓ Rapid Quench

If the quenching temperature is raised to 1700-1800°C, the amount of bound carbon increases to approximately 39 atomic percent, and the X-ray examination reveals only the presence of the η-MoC_{1-x}-phase (Table 11). The process is reversed if alloys which were initially quenched from temperatures above the eutectoid line and which therefore contained only the η-phase (with or without excess graphite) were reheated at lower temperatures and quenched (sample 7 in Table 11).

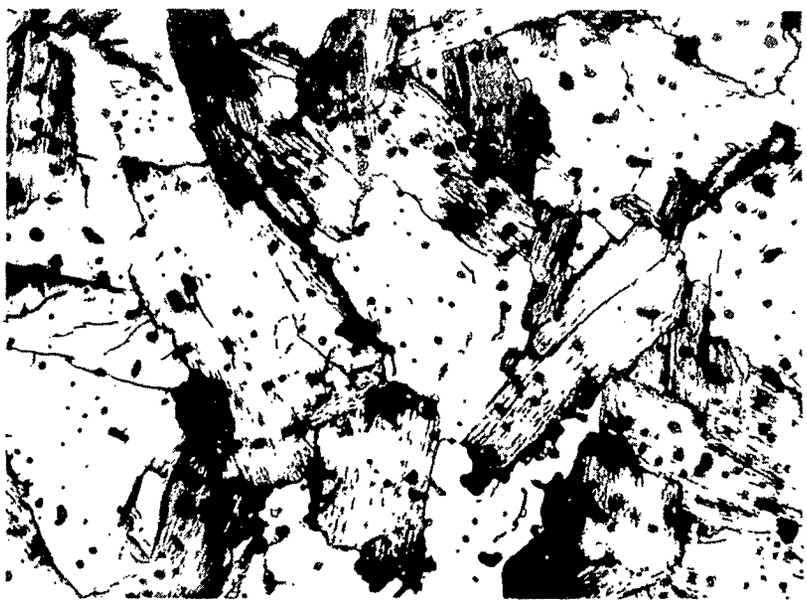

Figure 41. Mo-C (45 At% C), Annealed for 30 Hours X500 at 1550°C under 10^{-5} Torr, and Slowly Cooled. α-Mo_2C + Graphite.

The microstructure of a molybdenum carbon alloy with 45 At% C, annealed for 30 hours at 1550°C is shown in Figure 41. The structure shows two phases and consists of Mo_2C and graphite. The

microstructure of the same alloy, but quenched from 1720°C is shown in Figure 42. Most of the graphite initially present has reacted with Mo_2C to form η-MoC_{1-x}, the excess graphite being distributed along the subgrain-boundaries of the structure. The striated structure of the metallic phase indicates that nucleation of the β-Mo_2C in the η-MoC_{1-x} phase has already taken place.

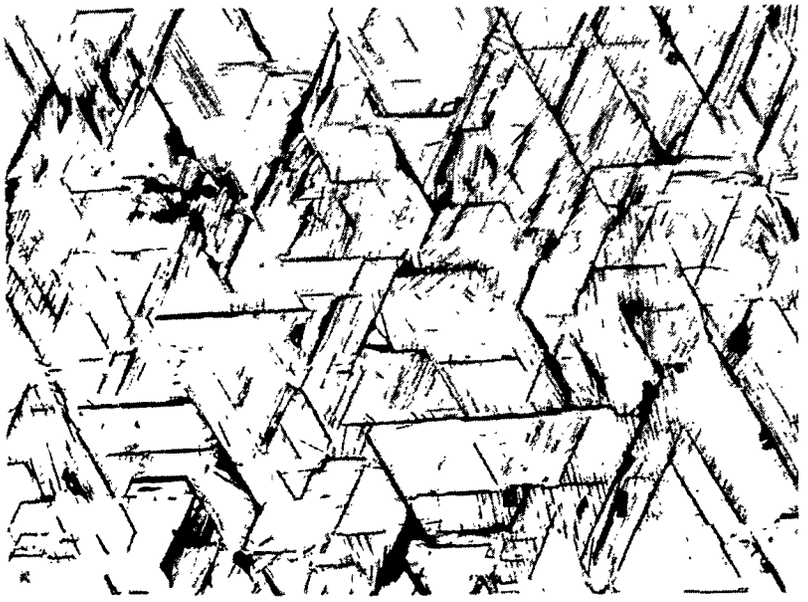

Figure 42. Mo-C (45 At% C), Equilibrated for 10 min. X500
at 1720°C and Quenched.
η-MoC_{1-x} (in the Initial Stages of Decomposition)
and Excess Graphite on Subgrain Boundaries.

The same alloy (Figure 42) was equilibrated for 25 hours at 1550°C and quenched from this temperature. The X-ray examination revealed as main constituents β-Mo_2C and graphite, with only small

amounts of undecomposed η-MoC_{1-x} left. The resulting microstructure (Figure 43) shows a typical, partly reannealed decomposition structure.

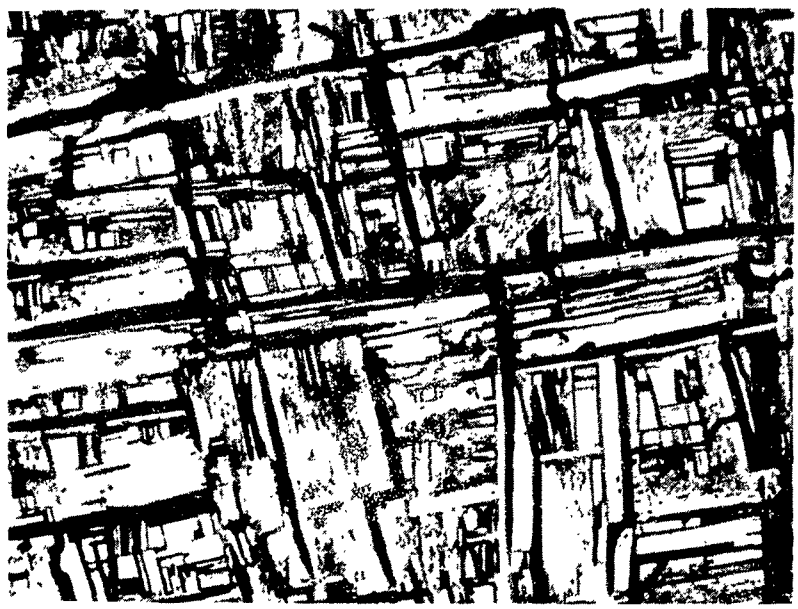

Figure 43. Mo-C (45 At% C), Sample from Figure 42, Equilibrated for 25 Hours at 1550°C and Quenched. X1000
β-Mo_2C with Graphite on Subgrain Boundaries

The graphite has collected mainly at subgrain boundaries as displayed in Figure 44, which shows the same structure at a lower magnification.

In summarizing the experimental findings in this concentration region, it could be shown that η-MoC_{1-x} decomposes in a eutectoid reaction at 1655°C into β-Mo_2C and graphite. At higher temperatures the homogeneity range of η-MoC_{1-x} extends to lower carbon concentration, reaching 36.7 At% C at the eutectic temperature β-Mo_2C —— η-MoC_{1-x} (2510 ± 3°C).

In the β-Mo_2C-phase additional interstitial positions are being filled at higher temperatures, bringing the overall composition of this phase to 36.3 At% C at 2510°C.

Figure 44. Mo-C (45 At% C), Sample from Figure 42. X500
Equilibrated for 25 Hours at 1550°C and Quenched.
Decomposed η-MoC_{1-x} with Graphite Precipitated at Subgrain Boundaries

The existence of a critical solution temperature (complete transition) between the β-Mo_2C and the η-MoC_{1-x} phase could not be established, although the concentration gap between both phases becomes very narrow at high temperature. Due to the narrow separation of both phases

at high temperatures, the eutectic between η-MoC_{1-x} and β-Mo_2C was not observed metallographically, but was deduced from the variation of the melting points with the carbon concentration.

5. The Concentration Range Above 39 Atomic Percent Carbon. The α-MoC_{1-x}-Phase.

An examination of the melting temperatures of molybdenum carbon alloys (Table 8) in this concentration range indicates that after reaching a maximum of 2550°C at a composition of ~39 At% C, melting within the next larger atomic percent range is virtually isothermal. A sharp increase of the melting temperatures is noted at approximately 40 At% C, reaching again a maximum (2600°C) at a composition of 42 At% C. In alloys with carbon in excess of 43 At% C the presence of free graphite could be visually observed. Alloys in the range from 43 to 55 melted sharply at approximately 2584°C, while the alloy with 60 atomic percent carbon showed first signs of heterogeneous melting. This indicates that the concentration of the carbon-rich eutectic had been passed. Since the existence of the cubic (B 1) phase as a high temperature phase in the concentration region around 40 At% C was known from our previous investigations, attempts were made to determine its temperature and concentration range of stability.

DTA-runs were performed on samples containing 40, 41, 43, 47, 50 and 63 atomic percent carbon and the investigations were in some cases extended up to 3200°C.

Recalling that in the DTA-run of the alloy with 38 Atomic percent carbon (Figure 40) only one thermal arrest was observed in the solidus region above 1500°C, (indicating that only one solid state

reaction occurred at this concentration up to melting) the behavior of the alloy with 40 atomic percent carbon is quite different (Figure 45). The thermal arrest slightly above 1600°C, appearing on the heating as well as on the cooling curve, can, by comparison with the preceding diagram (Figure 40), easily be identified as being due to the formation of the η-phase from β-Mo_2C and graphite. A second, sharply defined thermal arrest is observed at 1960°C. The temperature lag of this reaction is much smaller than that observed with the η-phase, i.e. the underlaying solid state reaction proceeds comparatively faster than that associated with the formation or decomposition of the η-phase. The only other phase known to occur in the system molybdenum-carbon is the cubic phase, and we therefore attribute the second thermal arrest as being due to the appearance of the cubic phase.

The melting temperatures observed by the DTA-runs, although not comparable in accuracy with the results obtained by the resistive heating method, are in good agreement with the measured values in Table 8.

With the exception of a slight change in the melting temperature, the DTA-diagrams of the more carbon-rich alloys were identical as displayed by Figure 46, which shows a heating and a cooling curve of an alloy with 50 atomic percent carbon.

An effect worth mentioning concerns the very strong supercooling effects observed in the solidification of carbon-rich alloys. This effect, never noticed in alloys with a carbide as the primary crystallization product, was consistently observed, once the alloys had carbon contents in excess of the eutectic concentration, i.e. at concentrations, where graphite was the primary crystallization product. Figure 47 shows the solidification curves of an alloy which originally contained 40 atomic percent carbon.

After several remelts, which increased the total carbon content above the eutectic composition, the solidification curve shown in the lower portion of Figure 47 was obtained repeatedly. Supercooling of the melt by more than 100°C was observed until solidification, followed by a sudden rise in temperature, started. It may be assumed that the carbon atoms in the melt also mainly occupy interstitial positions, and the effect may be due to hindered nucleation of carbon from the melt.

The formation of the cubic α-MoC_{1-x} phase from η-MoC_{1-x} and graphite was studied by X-ray and analytical, as well as by metallographic techniques, using rapidly quenched alloy specimens. Since it was observed that the decomposition of the cubic high temperature phase was a much faster process than the disproportionation of η-MoC_{1-x}, very thin sample platelets (1 - 2 mm) were used to achieve effective quenching conditions.

In agreement with the DTA-findings, the X-ray patterns of alloys quenched from 1900°C showed the pure η-MoC_{1-x}-phase. The average content of bound carbon in these alloys was approximately 39 atomic percent (Table 12). With sufficient graphite present, the alloys quenched from 2000°C showed only α-MoC_{1-x}. In some cases quenching was not complete, and small amounts of η-MoC_{1-x}, formed by partial decomposition of the cubic high temperature phase, were noted. The bound carbon content in the α-MoC_{1-x} phase slightly above the peritectic temperature is ~40.9 At%, and therefore somewhat higher than the carbon content of the η-phase, proving them to be two distinct phases.

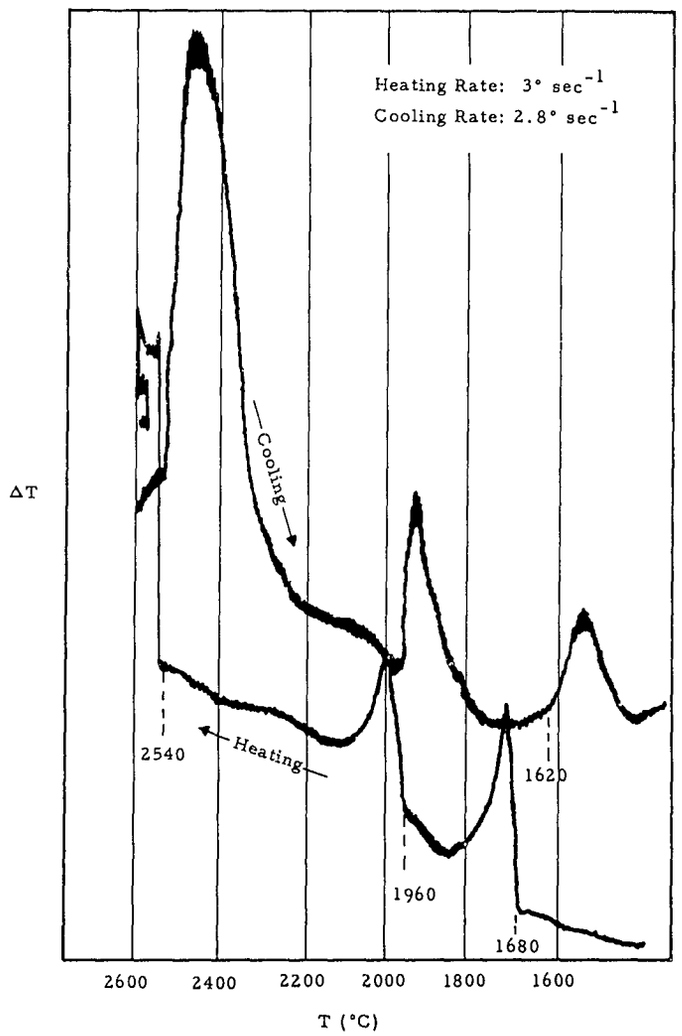

Figure 45. Differential Heating and Cooling Curve of a Molybdenum-Carbon Alloy with 40 Atomic % Carbon

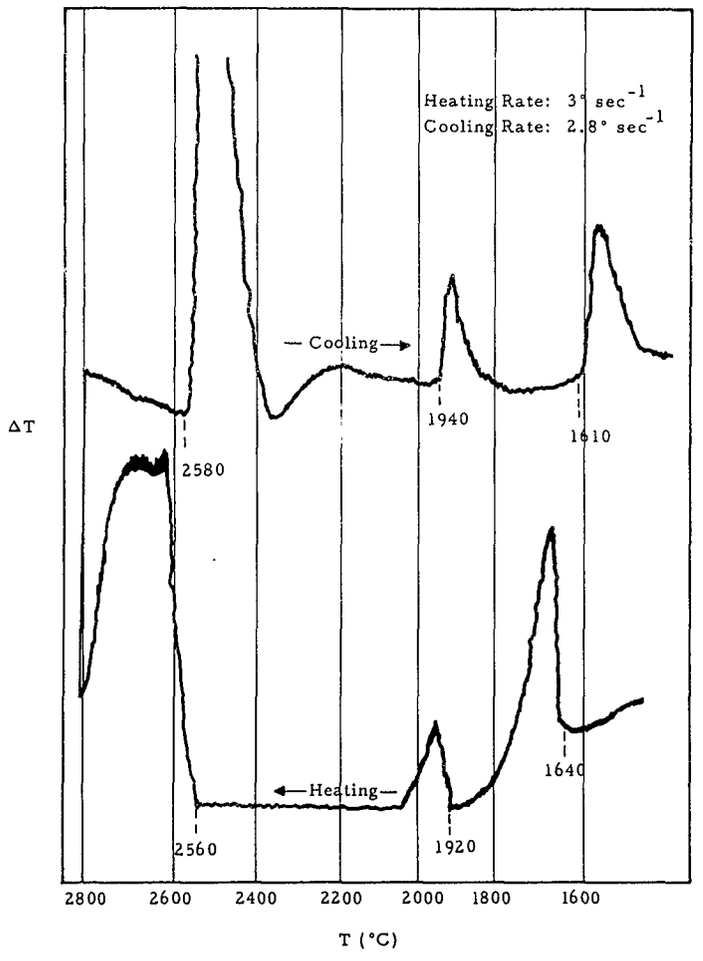

Figure 46. Differential Heating and Cooling Curve of a Molybdenum-Carbon Alloy with 50 Atomic % Carbon

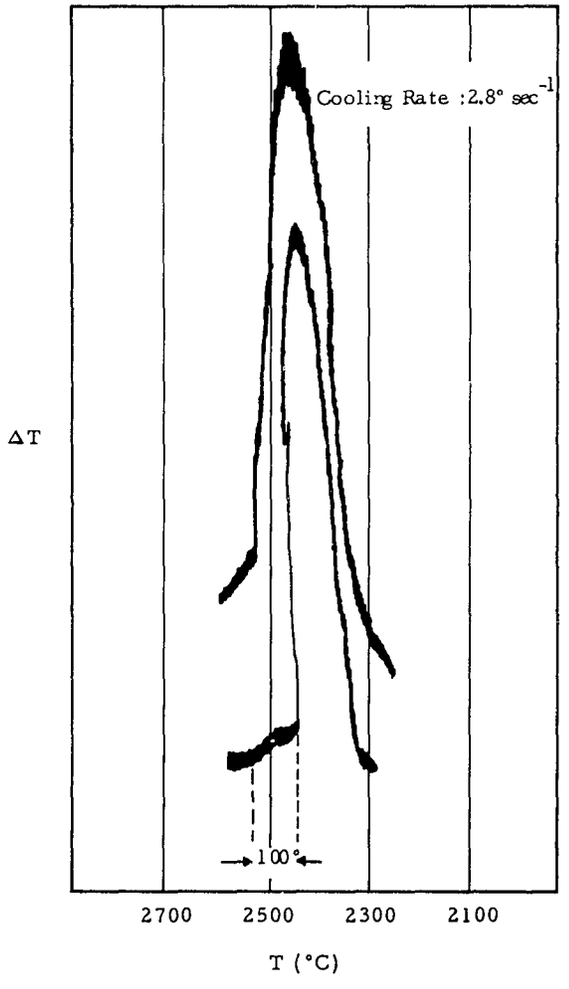

Figure 47. Supercooling in Carbon-Rich (< 45 At% C) Molybdenum-Carbon Alloys

Table 12. Formation of α-MoC_{1-x} from η-MoC_{1-x} and Graphite: Analytical and X-Ray Results on Quenched Alloys.

No	Quenching or Anneal. Temp. °C*	Analyt. Determ. Composition At% C			Phases Present (X-ray)	Lattice Parameters	Remarks
		Total	Free	Bound			
1	20 min/2000°C ↓	42.3	2.7	39.6	η-MoC_{1-x} + traces C	n.d.	- -
2	20 min/2000°C ↓	39.1	-	39.1	η-MoC_{1-x}	a=3.010 Å c= 14.64 Å } η-MoC_{1-x}	- -
3	20 min/2000°C ↓	40.3	0.1	40.2	α-MoC_{1-x} + traces η-MoC_{1-x}	a=4.266 Å α-MoC_{1-x}	- -
4	20 min/2000°C ↓	41.2	0.5	40.7	α-MoC_{1-x} + traces η-MoC_{1-x}	n.d.	quenching not complete
5	20 min/2000°C ↓	42.3	1.4	40.9	α-MoC_{1-x}	a=4.268 Å α-MoC_{1-x}	
6**	20 min/2000°C ↓	42.3	4.4	37.9	η-MoC_{1-x} + α-Mo_2C β-Mo_2C	n.d.	not in equilibrium

* Alloys homogenized prior to quenching for 30 hrs at 1550°C

** Sample of run number 5

↓ Rapid Quench

The decomposition of α-MoC_{1-x} was studied by prehomogenizing alloys above the eutectoid line and quenching them from temperatures slightly below the decomposition temperature.

The presence of significant amounts of α- and β-Mo_2C in addition to η-MoC_{1-x} in the alloys, which were held only for short times below the decomposition temperature indicates that at this temperature α-MoC_{1-x} decomposes first into metastable phase mixtures of Mo_2C and graphite, which then form the equilibrium phases in a second reaction step. The decomposition process of α-MoC_{1-x} can therefore be presented as proceeding in the following steps:

$$MoC_{0.693}\ (\alpha) \xrightarrow[k_1]{1960°C} MoC_{\sim 0.50} + 0.19\ C \qquad (a)$$

$$MoC_{\sim 0.50} + 0.14\ C \xrightarrow[k_2]{1655° < T < 1960°C} MoC_{\sim 0.64}\ (\eta) \qquad (b)$$

with the rate constant k_1 being greater than k_2. Below 1655°C reaction (b) proceeds from the right to the left. Effects of this kind have been frequently observed with other substances (Ostwald'sche Stufenregel).

The close structural relationships between α-MoC_{1-x} and the hexagonal η-MoC_{1-x}-phase did not rule out the possibility for the existence of a critical solution temperature of both phases. However, an analysis of carefully quenched alloys in the concentration region from 39 to 40.2 alloys revealed a two-phase structure in most of the alloys. While at lower temperatures, the alloys up to 39 atomic percent carbon were single phase η-MoC_{1-x}, an alloy with 39.2 atomic percent carbon contained significant amounts of the B1-phase. Alloys with 40.3 atomic percent carbon,

which were quenched from 2000° and 2100°C contained as the major constituent α-MoC_{1-x}, with only small amounts of η-MoC_{1-x} present. The same alloy quenched from 2300°C was single phase α-MoC_{1-x}.

The extremely fast decomposition rate of the cubic high temperature phase is well known and the argument that the quenching experiments might not be fully representative of the high temperature equilibrium state, cannot be entirely rejected. However, the results of the melting point measurements, as well as the fact that both phases could be practically completely retained in their respective concentration domains point more towards the existence of a small, but finite concentration gap between both phases over the entire temperature range. Also in favor of this interpretation are the DTA measurements as well as the results of the chemical analyses which identify them, at least in the low temperature range, as two distinct phases.

The eutectoid decomposition of α-MoC_{1-x} was studied metallographically, and the results are shown in Figures 48-51. The X-ray examination of the alloy in Figure 48 showed only the cubic high temperature phase to be present, although the striae visible in the structure indicates that the nucleation reaction had already initiated in certain areas. The structure shown in Figure 49 seems to be representative of slightly subcritical cooling speeds, i.e. cooling-rates which are slightly lower than those required to prevent decomposition of the α-MoC_{1-x} phase.

Cooling rates of approximately 40°C/sec. produce structures as shown in Figure 50, containing about equal amounts of unconverted α-MoC_{1-x} and η-MoC_{1-x} and Mo_2C as reaction products. Figure 51 shows a microstructure of an alloy which was cooled with

approximately 80°C per second from 2300° to 1850°C, held for approximately half a minute at this temperature, and then rapidly quenched. The X-ray examination showed only the η-phase to be present, i.e. Mo_2C, formed in the initial steps of the decomposition, has already completely reacted to the equilibrium products at this temperature.

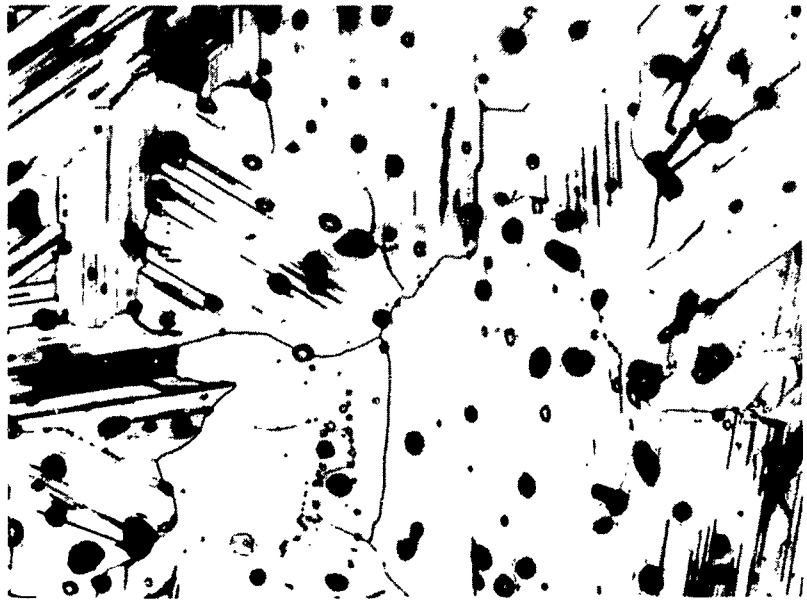

Figure 48. Mo-C (43.8 At% C), Rapidly Quenched X1000 from 2550°C.
α-MoC_{1-x} with Traces of Free Carbon.
The Striae Visible in Some Grains are Signs of the Beginning Decomposition.

The carbon-rich boundary of the α-MoC_{1-x} as a function of temperature was determined by analysis of rapidly quenched alloy material with excess carbon. The samples used for the quenching

studies were thin-sliced cylinders of approximately 1 mm height, and the crystal phases presented after quenching were examined by X-rays. In nearly all cases quenching was practically (Figure 52) complete.

Figure 49. Mo-C (41 At% C), Cooled with Approximately 80°C/sec. 1000X

Growth of Nuclei in Originally Homogeneous Matric of α-MoC_{1-x}. (X-ray: α-MoC_{1-x}, Mo_2C, and η-MoC_{1-x})

The results of these studies are summarized in Table 13. Carbon content and lattice parameters of the α-MoC_{1-x}-phase (Figure 53) increase steadily with temperature, reaching 43 atomic percent carbon and 4.281 Å, respectively, at 2580°C, the carbon-rich eutectic line.

Table 13. Carbon-Rich Boundary of α-MoC_{1-x} : X-Ray and Analytical Results on Quenched Alloys

No.	Quench. Temp. °C	Analyt. Determ. Composition Atomic % C		Phases Present (X-ray)	Lattice Parameters
		Total	Bound		
1	2100	41.2		α-MoC_{1-x}	4.267
2	2100	42.4	41.6	α-MoC_{1-x}	4.270
3	2200	42.3	41.9	α-MoC_{1-x}	4.275
4	2300	41.3	41.25	α-MoC_{1-x}	4.267
5	2300	42.3	42.25	α-MoC_{1-x}	4.275
6	2300	43.0	42.2	α-MoC_{1-x}	4.273
7	2300	43.8	42.0	α-MoC_{1-x}	4.274
8	2340	42.0	42.0	α-MoC_{1-x}	4.273
9	2340	43.1	42.3	α-MoC_{1-x}	4.274
10	2340	44.9	42.1	α-MoC_{1-x}	4.274
11	2540	42.1	42.1	α-MoC_{1-x}	4.274
12	2540	43.4	42.9	α-MoC_{1-x}	4.278
13	2550	43.8	43.0	α-MoC_{1-x}	4.281

The homogeneous melting behavior of the alloys with carbon contents from 43 to 55 atomic percent (Table 8) already gave an indication for a rather flat liquidus curve in the carbon-rich portion of the system. For the experimental determination of the composition of the graphite-saturated melt alloys with initial carbon concentrations varying between zero and forty atomic percent were equilibrated with graphite at temperatures above the carbon-rich eutectic line of the system.

The alloys were held for approximately 20 minutes at the chosen equilibrium temperature and then quenched in order to avoid segregation of graphite from the higher density melt.

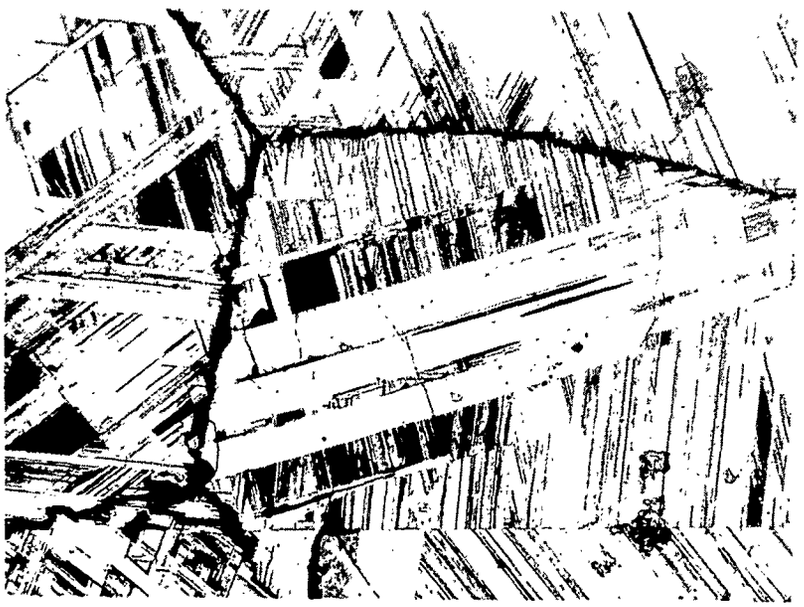

Figure 50. Mo-C (41 At% C), Cooled with Approximately 40°C/sec. from 2300°C. X250
Subgrain Decomposition of α-MoC_{1-x}
(X-ray: α-MoC_{1-x}, η-MoC_{1-x}, and Mo_2C in About Equal Amounts.)

The results of the chemical analysis, obtained on duplicate runs (Table 14) are presented in graphical form in Figure 54.

An alloy with 43.4 atomic percent carbon, which was quenched from 2590°C showed α-MoC_{1-x} to be the primary product of crystallization, while the alloy with 45 At% C (Figure 55) was practically

pure eutectic. The eutectic structure is not characteristic. An alloy with 48 atomic percent carbon, quenched from 2630°C, already contains significant amounts of primary crystallized graphite (Figure 56).

Figure 51. Mo-C (41 At% C) Cooled from 2300°C to 1850°C (~ 80°C/sec), Held for 30 sec at 1850°C and then Quenched (X-ray: η-MoC_{1-x}) X1000

6. Investigations in the Low Temperature Range

The results of additional investigations performed in the temperature range from 1300°to 1600°C are summarized in Table 15. The studies were performed on quenched as well as on annealed and furnace-cooled alloy material. The results are in accord with the findings at higher temperatures, although in many cases equilibrium could not be attained.

This is probably to be ascribed to the low reaction rates at these temperatures.

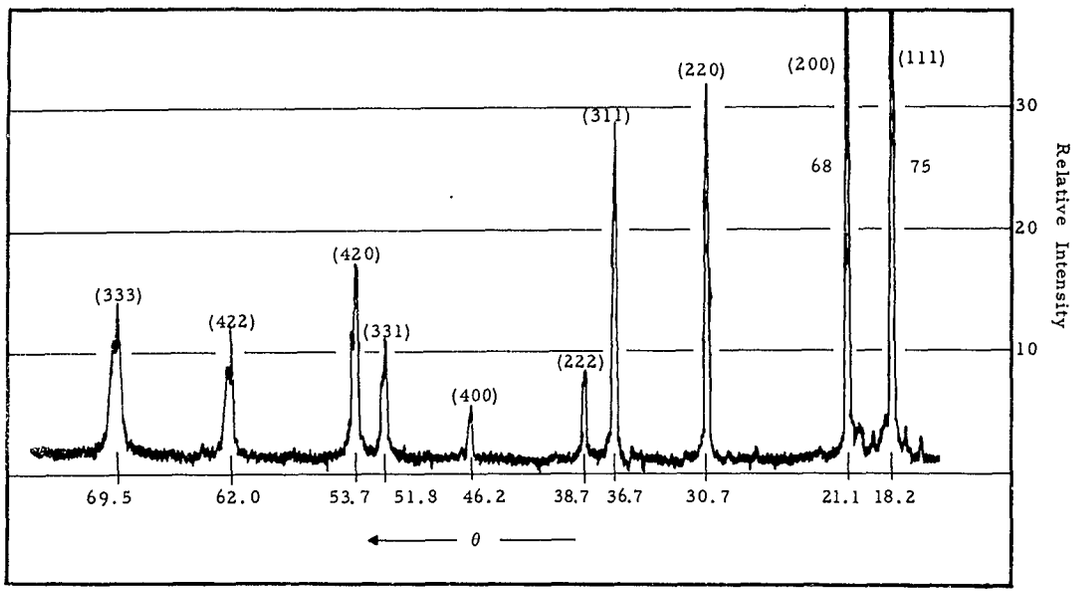

Figure 52. Diffraction Pattern of the Cubic (B1) High Temperature Phase in the System Molybdenum-Carbon

7. Assembly of the Phase Diagram

The melting temperatures of molybdenum-carbon alloys are summarized in graphical form in Figure 57. The size of the experimental points corresponds to the average temperature-concentration uncertainties encountered in the experiments. The melting temperatures obtained by DTA-techniques agree within the experimental error with the results from direct resistance method.

The differential-thermoanalytical investigations over the entire concentration range are summarized in Table 16, and are presented in graphical form in Figure 58.

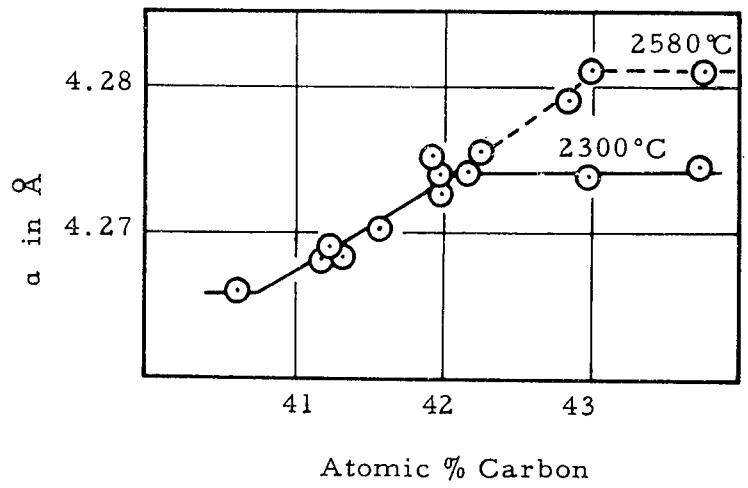

Figure 53. Lattice Parameters of the Cubic (B1) Phase in the System Molybdenum-Carbon

The experimental results are combined in the complete phase diagram shown in Figure 59.

C. THE α-β-PHASE SEPARATION OF THE Me_2C-PHASES

Before we proceed with an attempt to discuss the phase-separation of the Me_2C-phases on a thermodynamic basis, we shall briefly review the experimental evidence. It then will be useful, to correlate the experimental findings with the structural properties of the Me_2C-phases, in order to arrive at a model for the calculations, and to examine present theories for their applicability to our problem.

In the course of a thermodynamic analysis of the phase-equilibria occurring in the system W-Cr-C agreement between experiment and calculation could be achieved only by assuming an essentially disordered

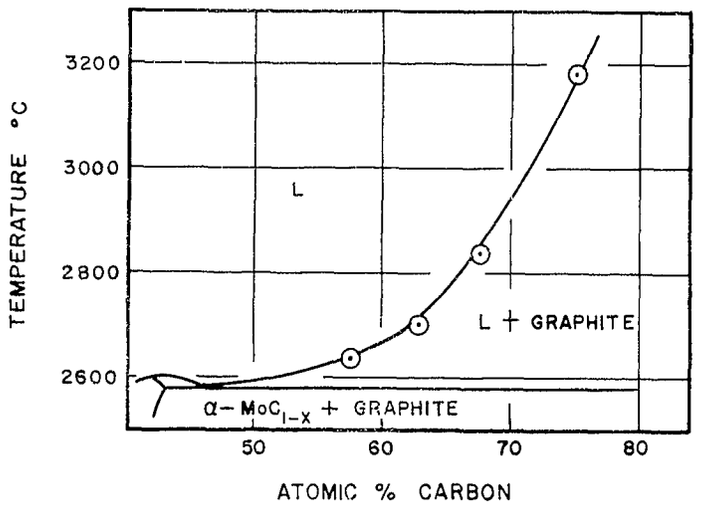

Figure 54. Liquidus Curve in the Carbon-Rich Section of the System Molybdenum-Carbon

carbon sublattice of the $(W,Cr)_2C$ solid solution at higher temperatures[52]. Based on this indirect evidence, the investigations were extended to the respective binary carbides, with the specific intent to search for phenomena, which may be related to homogeneous disordering reactions occurring in the carbon sublattice of these compounds. For these investigations, the system molybdenum-carbon appeared to be the most attractive, since Mo_2C is the only stable phase in the lower temperature range, and therefore no interference from higher carbides would be expected. Moreover, the free

Table 14. Equilibrium Mo-C $_{melt}$ —— Graphite$_{(s)}$: Equilibrium Concentration of the Melt at Various Temperatures.

Temperature °C	Starting Composition At% C	Composition after Equilibration with Graphite At% C	Number of Runs
2650	20	57.7 ± 2	2
2700	35	62.7 ± 2	2
2800	35	65.8 ± 3	3
2850	0	66.8 ± 3	3
3190	0	74.4 ± 3	3

Figure 55. Mo-C (45 At% C), quenched from 2620°C X500
Carbon-rich eutectic

energies of formation of molybdenum carbides are fairly small quantities, and therefore entropy effects due to disordering reactions should play an important role in the overall behavior of these phases.

Figure 56. Mo-C (48 At% C), Quenched from 2630°C X250
Primary Crystallized Graphite (Black)
and Eutectic.

Differential-thermoanalytical studies carried out in the critical concentration region from 32-34 atomic percent carbon showed a thermal arrest at 1475°C. No signal was observed with alloys, which contained less than 32 At% C. Metallographic as well as chemical analytical studies

Table 15. Temperature Range 1300 - 1600°C: Analytical and X-ray Results on Quenched and Annealed Alloys

No	Quenching or Anneal. Temp. °C	Anal. Determ. Composition At% C		Phases Present (X-ray)	Lattice Parameters
		Total	Bound		
1	1300*	32.0	31.9	α-Mo_2C	a= 2.998 Å c= 4.728 Å
2	1300*	34.3	33.0	α-Mo_2C+traces β-Mo_2C and η-MoC_{1-x}	a= 3.001 Å, c= 4.728 Å } α-Mo_2C
3	1400 ↓	29.3	29.3	α-Mo_2C+α-Mo	a= 2.998 Å, c= 4.728 Å } α-Mo_2C a= 3.147 Å α-Mo
4	1400 ↓	30.0	30.0	α-Mo_2C+α-Mo	a= 2.998 Å, c= 4.728 Å } α-Mo_2C a= 3.147 Å α-Mo
5	1400 ↓	33.5	33.1	α-Mo_2C+traces β-Mo_2C and η-MoC_{1-x}	a= 3.006 Å, c= 4.730 Å } α-Mo_2C
6	1400 ↓	45.1	32.8	α-Mo_2C+traces β-Mo_2C, η-MoC_{1-x} and graphite	a= 3.004 Å, c= 4.731 Å } α-Mo_2C
7	1500 ↓	44.9	33.4	β-Mo_2C+graphite	a= 3.006 Å, c=4.773 Å } β-Mo_2C
8	1600 ↓	32.0	32.0	α-Mo_2C	a= 3.003 Å, c= 4.731 Å } α-Mo_2C
9	1600 ↓	32.8	32.0	α-Mo_2C	a= 3.004 Å, c= 4.732 Å } α-Mo_2C
10	1600 ↓	33.5	33.5	α-Mo_2C + β-Mo_2C	a= 3.006 Å, c= 4.731 Å } α-Mo_2C a= 3.006 Å, c=4.773 Å } β-Mo_2C
11	1600 ↓	34.1	33.6	β-Mo_2C+ sml. amts. α-Mo_2C	a= 3.008 Å, c= 4.776 Å } β-Mo_2C
12	1600 ↓	35.0	34.0	β-Mo_2C	a= 3.008 Å, c= 4.776 Å } β-Mo_2C

Legend to Table 15. *40 hrs/1300°C/10^{-5} Torr annealed

↓ Rapid Quench in Tin.

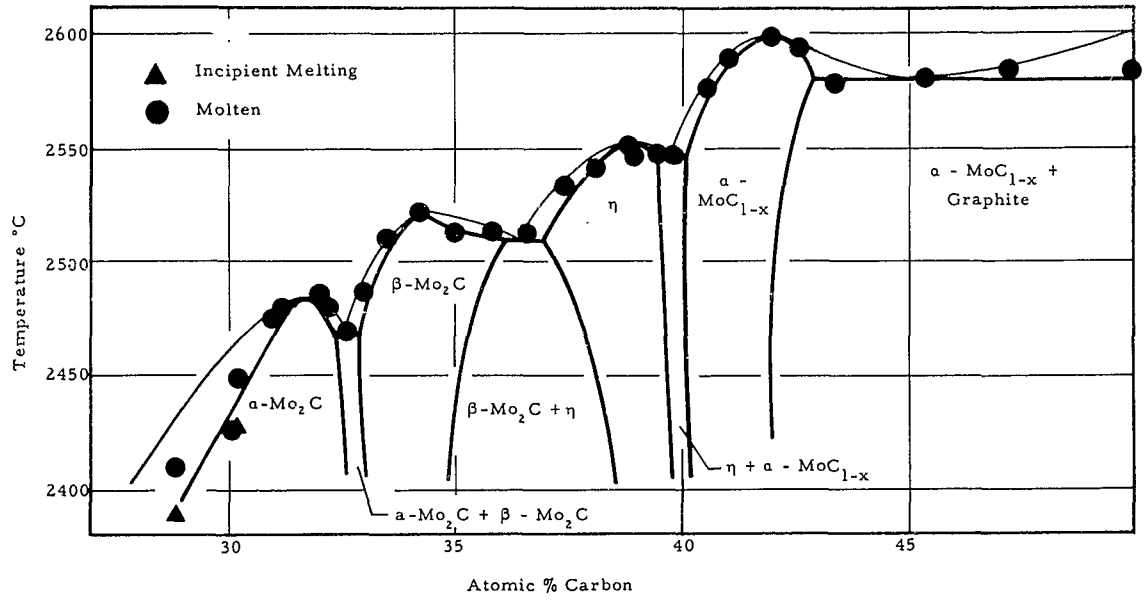

Figure 57. Molybdenum-Carbon: Melting Points and Partial Phase Diagram.

Table 16. Summary of Differential-Thermoanalytical Investigations in the System Molybdenum-Carbon

Concentr. Range At% C	Thermal Arrests (°C) Heating / Cooling / T max	Reaction Associated with Thermal Arrests
0-25	2200±20 {2280} 2200±20	α-Mo + α-Mo_2C → L (eutect. react) L → α-Mo + α-Mo_2C (eutect. react)
32.5-33	1100-1500 2460±20 {2500} 2470±20 1500-1200	α-Mo_2C + C → β-Mo_2C α-Mo_2C + β-Mo_2C → L (eutect. react)
34-39	(1450)* 1650±15 {2360} 1610±20	α-Mo_2C + C → β-Mo_2C β-Mo_2C + C → η-MoC_{1-x} η-MoC_{1-x} → β-Mo_2C + C
39-40.5	(1450)* 1660±15 1960±15 2540±20 {2580} 2550±20 1970±15 1640±20	α-Mo_2C + C → β-Mo_2C β-Mo_2C + C → η-MoC_{1-x} η-MoC_{1-x} + C → α-MoC_{1-x} η-MoC_{1-x} + α-MoC_{1-x} → L (eutect. react) L → η-MoC_{1-x} + α-MoC_{1-x} (eutect. react) α-MoC_{1-x} → η-MoC_{1-x} + C η-MoC_{1-x} → β-Mo_2C + C
43-90	1650±15 1930±20 2570±15 {3000} 2590±20 1960±20 1630±20	β-Mo_2C + C → η-MoC_{1-x} η-MoC_{1-x} + C → α-MoC_{1-x} α-MoC_{1-x} + C → L (eutect. react.) L → α-MoC_{1-x} + C (eutect. react.) α-MoC_{1-x} → η-MoC_{1-x} + C η-MoC_{1-x} → β-MoC_{1-x} + C

Legend to Table 16. * Very faint signals

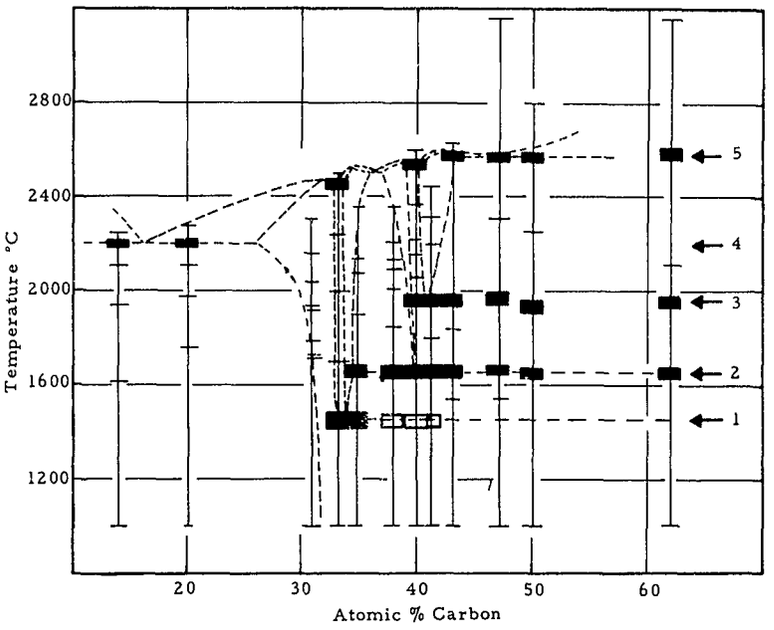

Isothermal Reactions:

(1) $\alpha\text{-}Mo_2C + C \rightleftharpoons \beta\text{-}Mo_2C$
(2) $\beta\text{-}Mo_2C + C \rightleftharpoons \eta\text{-}MoC_{1-x}$
(3) $\eta\text{-}MoC_{1-x} + C \rightleftharpoons \alpha\text{-}MoC_{1-x}$
(4) $\alpha\text{-}Mo + \alpha\text{-}Mo_2C \rightleftharpoons L$ (eutectic reaction)
(5) $\alpha\text{-}MoC_{1-x} + C_{(gr.)} \rightleftharpoons L$ (eutectic reaction)

Figure 58. Summary of Differential-Thermoanalytical Investigations in the System Molybdenum-Carbon.

— Maximum Temperatures of Intermediate Runs

▬ Temperature Arrests

▭ Signal very weak

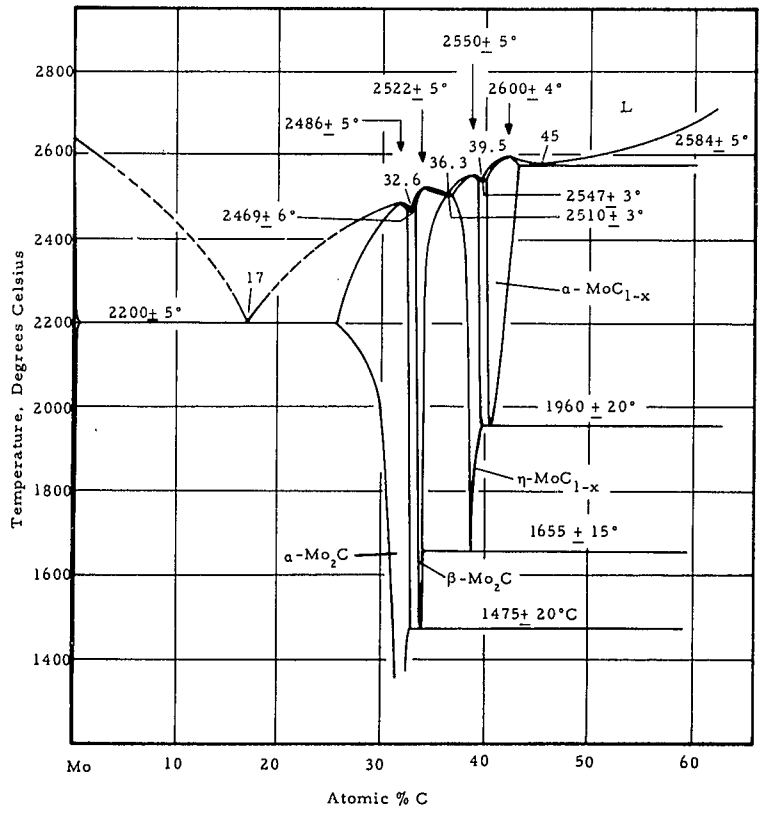

Figure 59. The Phase Diagram of the System Molybdenum-Carbon

indicated, that there are two phases separated by a small but finite two-phase region, the maximum separation of the two phases being < 1.0 atomic percent carbon over the entire temperature range.

Especially important for our discussion are the X-ray findings:

Beginning with the metal-rich limit of the homogeneous range of the Mo_2C-phase, the cell volume increases steadily with the

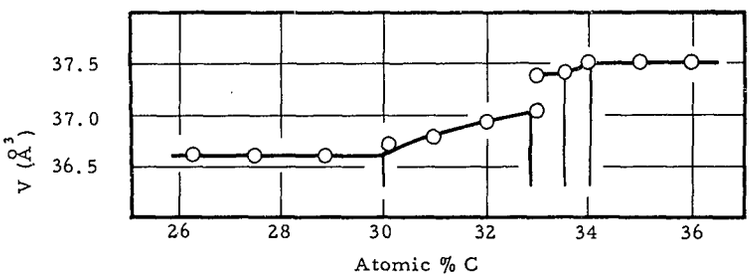

Figure 60. Unit Cell Volume of Mo_2C as a Function of the Carbon Concentration.

degree of filling of the available interstitial sites (Figure 60); this is a common feature of defect structures and is shown by all carbides. At the α-β-Mo_2C phase boundary, the cell volume undergoes an abrupt change, the volume of the β-phase being larger by about one percent.

Examining the change of the individual cell parameters (Figure 35), we find that the a-axis increases steadily with the carbon

concentration, and shows no marked discontinuity at the α-β-phase boundaries. The c-spacing of the unit cell is affected only to an insignificant degree by the filling of the vacancies within the stability range of the α-phase, but increases abruptly from 4.73 to 4.78 Å, once the concentration domain of the β-phase is reached.

In discussing the X-ray findings, it is worthwhile to remember that these results were obtained on quenched material and may, therefore, not be fully representative of the actual unit cell volume conditions at temperature. Nevertheless, the data will show the average trend, and may therefore be used for comparison purposes in the discussion.

In summarizing the experimental findings on the Mo_2C-phase, it has been established that:

1. Separation of the Mo_2C-phase into two phases with crystallographically identical arrangements of metal atoms, but with different unit cell volumes, occurs above 1475°C.

2. The maximum width of the two-phase field separating both phases at all temperatures does not exceed 1.0 At% C, and is probably much less at temperatures close to melting. The gap at the eutectoid temperature is symmetrical with regard to the stoichiometric composition.

3. The Mo_2C-phase can accommodate carbon in excess of the stoichiometric composition (boundary at 2500°C: 36 At% C).

4. The rearrangement of the carbon sublattice at high temperatures tends to increase the c-spacing of the hexagonal close-packed metal lattice, while the a-axis remains practically unaffected.

5. The phase-separation is accompanied by a marked volume increase.

While it is well established, that the molybdenum atoms occupy hexagonal close-packed positions, two different ways by which the carbon atoms might fill the octahedral interstices in the lattice, have been proposed originally, resulting in the following proposals for the structure of Mo_2C.

1. The anti-cadmium iodide (C6-type) structure, where the carbon atoms occupy only one of the two octahedral sites available in the unit cell. The occupied point positions in the cadmium-iodide type structure are:

2 Mo in 2 (d): 1/3. 2/3., z; 2/3; 1/3, $\bar{z}$;

with z = 1/4

1 C in 1 (a) : 0, 0, 0

2. The L' 3-type structure, where the $n_c = N_L$ carbon atoms are statistically distributed among the $2n_c = n_{Me} = 2N_L$ crystallographically equivalent octahedral lattice sites. The occupied point positions for the L' 3-type are:

2 Mo in 2 (c): 1/3, 2/3, 1/4; 2/3, 1/3, 3/4,

with the carbon occupying the two-fold position:

1 C in 2 (a): 0, 0, 0; 0, 0, 1/2.

While in the C6-structure the carbon atoms arrange themselves in one layer (0) only, they are in the L' 3-structure statistically distributed over the (0) and (1/2) positions.

Using room temperature neutron diffraction techniques, E. Parthé and V. Sadagopan[10] were able to show, that the carbon atoms arrange themselves in a systematic (ordered) way between both layers (0)

and (1/2) such, that every molybdenum atom has three equidistant carbon neighbors. Neglecting coordination differences, the latter structure proposal corresponds in a way to the C6-structure, in allowing only one of the two interstitial lattice sites per unit cell to be occupied by a carbon atom.

In order to account for the hyper-stoichiometric compositions found at high temperatures, the following types of defects or combinations of these defect types have to be considered:

1. Formation of metal vacancies.

2. Occupation of additional interstitial lattice sites by carbon atoms.

The relative significance of both defect reactions in terms of their contribution to the free energies will depend to a large degree on the energies associated with the formation of the respective defect type.

Both defect types are known to occur in related compound classes[53]. In TiO (P. Ehrlich 1939), there are 15% vacant oxygen and titanium sites at the stoichiometric composition, and the isostructural NbO[54, 55, 56] contains 25% ordered vacancies in both sublattices.

There are indications, however, that in carbides[57] defect formation at the concentration of order is much smaller. The weaker interaction Me-C as compared to the interaction Me-O is to a large degree responsible for the observation, that creation of a carbon vacancy requires less energy than the formation of a metal vacancy. Although no detailed treatment of group VI metal carbides is available at the present time, the relatively low free energies of formation of the group VI metal carbides suggest comparatively weak or metal-carbon bonds. We may therefore assume that the free energy of formation of a metal vacancy will be much more positive

than that for creating a carbon vacancy, and we may regard changes resulting from defects in the semi-metal lattice as so preponderant that contributions from other kinds of defects can be neglected. As a further support for these simplifying assumptions we use the argument that, from structural considerations, the net energy change resulting from an interchange of carbon atoms among two (structurally equivalent) lattice sites is expected to be much lower than the energy required to create a carbon vacancy. Having chosen process (2) as the relevant defect type, we may think of building up the carbide in the following way.

First, we convert the stable body centered cubic modification of molybdenum into a hexagonal close-packed structure in order to achieve structural equality. Having the proper lattice, the octahedral interstices are now being filled with carbon atoms, and we collectively attribute all changes occurring in the electronic structure of the parent metal lattice as being due to metal-carbon interaction (bond formation). Secondly, the metal lattice expands upon incorporation of the semi-metal atoms and this will reflect in a positive (endothermic) term in the free energy —— concentration relationships.

We may also think, that in order to minimize the strain energy of the lattice at a given total semi-metal concentration, sites in the immediate neighborhood of already occupied interstitial lattice positions become less favored, i.e. require an extra amount of energy for their occupation. Specifically for the Me_2C-lattice, once one of the two available octahedral sites (either in the layer 0 or 1/2) is filled, occupation of the other octahedral hole, having the same (x, y)-coordinates, but being half the c-spacing apart

from the already occupied hole, would become accessible only by expenditure of an amount of energy ΔE in excess of that required for the occupation of a lattice site of the first kind.

In this model, substantial occupation of the B-sites will tend to affect mainly the c-spacing of the lattice, since a new (buckled) layer of carbon atoms has to be accommodated, while the conditions perpendicular to the c-axis remain essentially unchanged. We take this agreement with the experimental observations as a further support for the chosen model.

Depending on the size of this energy gap ΔE between the two sites, at any given total carbon concentration and fixed temperature (p = const.) there will exist a distribution of the carbon atoms among the two kinds* of lattice sites.

For a mathematical description, the first step to be taken is the establishment of the conditions of internal equilibrium, that is, to calculate the equilibrium distribution of the carbon atoms, as a function of the energy ΔE, the temperature, and the concentration.

From the knowledge of the available number of sites and the distribution among the accessible sites, the contribution of the disordering effects to the thermal free energy can then be computed. The configurational terms, superimposed on the thermal free energy should then be capable of describing the thermal stability of the system, and also to account for the observed phase-separation phenomena.

---

* We shall refer to the two kinds of lattice sites as "A" and "B" sites.

The basic principles of the theory of essentially ordered phases, i.e. phases, where the number of defects at the concentration of order is small compared to the number of lattice sites, were laid down in the work by W. Schottky and C. Wagner[58]. As pointed out by C. Wagner[59], relatively simple expressions can be derived for the limiting cases, i.e. essentially ordered or disordered systems, but the equations become rather involved when intermediate cases are being considered. Generally, simplifying assumptions have to be introduced in order to reduce the mathematical difficulties.

Most calculations on systems exhibiting gross departure from stoichiometry have been performed on gas-solid systems where from the known activities of the gaseous component in the solid phase the necessary parameters in the theoretical expressions can be derived. Using the concept of pair interactions[60], J. R. Lacher[61] obtained satisfactory expressions for the conditions existing in the palladium-hydrogen system. Extending Lacher's concept, and under certain simplifying assumptions, J.S. Anderson[62] formulated the conditions for the stability of the nonstoichiometric crystal, and considers the mutual attraction of atoms in interstitial positions or of cation holes as the driving force behind phase segregations. In this way, he was able to reproduce semiquantitatively the phase behavior in gas-metal systems, and also to account for critical solution phenomena occurring in these system types.

A.L.G. Rees[63] considered the succession of phase equilibria in systems resulting from incorporating interstitial atoms into two or more types of interstitial sites in a metal parent lattice for cases

where the phases show certain structural similarities. With the concept of pair interaction, he was able to fit the theoretical equations to the observed phase equilibria in the zirconium-hydrogen system[64]. The limitations of these models were discussed by A.L.G. Rees[65], J. S. Anderson[53,62], and C. Wagner[59]. Although the concept of pair interaction for the description of critical phenomena is certainly useful, its physical meaning is not quite obvious, and one would think that the relatively wide separation of the interstitial atoms would not allow direct interaction (attraction) to any significant extent. Another point, which has to be considered are the energetical differences between the different lattice types, which may be of the same order of magnitude as the interaction energies.

The point that volume changes accompanying order-disorder transformations may be of significant importance for the thermodynamic description of the system was presented by C. Wagner[9]. He also considered the problem of whether the transition between a substantially ordered structure and a substantially disordered structure involves a discontinuous (heterogeneous) transformation, or whether the degree of order decreases continuously with increasing temperature. The same subject has also been stressed by R. Smoluchovsky[66] who showed on examples, that the ordering reaction for substitutional type alloys proceeds as a heterogeneous reaction, with the volume of the ordered phase gradually increasing at the expense of the disordered phases.

Returning from this review of pertinent previous work to our problem, it becomes obvious that these previous concepts are not applicable to our problem. We have no upper critical solution temperature,

which a system with pair interactions would yield, but instead we observe phase separation to occur above a certain temperature. A second problem arises from the relatively large volume changes, which probably will influence significantly the vibrational modes of the parent lattice. Since these changes in the parent lattice are intimately coupled with the energies of the interstitial lattice sites, the energies associated with the different degrees of freedom can very probably not be treated as additive, i.e. the grand partition function of the system cannot be presented as the product of the partition functions of the individual degrees of freedom.

Since the extra contributions to the thermal energy resulting from changes in the parent metal lattice due to disordering reactions in the semi-metal sublattice are unknown and can, therefore, not be accounted for, and also the free energies of formation of the Mo_2C-phase as a function of temperature are known to an inadequate degree only, we shall restrict our discussions to those contributions, which emerge directly from the disordering reactions in the semi-metal sublattice. We choose a completely ordered sublattice, (with the C-atoms on A-sites only) as the reference state for the calculations, and shall examine the resulting equations with respect to such terms which may under the given conditions give rise to the observed phase separation phenomena.

Two models will be considered:

1. The a priori existence of an equal number of A and B-sites is assumed, with the latter separated by an energy gap $\Delta E = G_{C(B)} - G_{C(A)}$ from the A-sites.

2. The energetically unfavored (B)-sites are created by occupation of the A-sites; specifically, we assume, that for each occupied site of the first kind, one site of the second kind is created.

Model (1) is certainly too restrictive inasmuch as it would allow long range interaction; especially in the low carbon concentration range it would deviate from model 2, but it would be expected to produce similar results as the refined model at the higher concentration end. Model (2) corresponds to the assumptions made by J. R. Lacher[61] for the palladium-hydrogen system.

As the first step we calculate the distribution of the interstitial atoms among the two lattice sites as a function of the concentration and the energy gap ΔE at a given temperature. Basing our considerations on one mole Me_2C, we have for model 1:

Total number of available sites	2N
Number of A-sites	N
Number of B-sites	N
Number of C-atoms on Sites A	n_{CA}
Number of C-atoms on Sites B	n_{CB}
Number of vacancies on Sites A	$N-n_{CA}$
Number of vacancies on Sites B	$n-n_{CB}$

Treating the energy difference as a gross phenomenon rather than as a sum of the individual contributions, we have to minimize the free energy function at fixed total concentration y, temperature, and pressure.

Denoting an interstitial hole, by the symbol Δ, we let one mole of an alloy $Me_2C_y\Delta_z$ disproportionate into ν_1 moles $MeC_{x_{CA}}\Delta_{x_{\Delta A}}$ and ν_2 moles $MeC_{x_{CB}}\Delta_{x_{\Delta B}}$, and, since we consider changes in the sublattices

only, we can omit the metal atoms in the formal characterization of the reactions and write

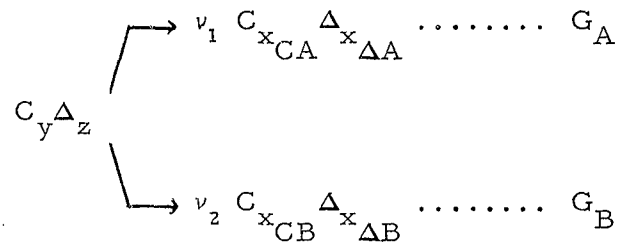

with

$$x_{CA} = \frac{n_{CA}}{N} \qquad x_{CB} = \frac{n_{CB}}{N}$$

$$x_{\Delta A} = \frac{n_{\Delta A}}{N} \qquad x_{\Delta B} = \frac{n_{\Delta B}}{N}$$

and G_A and G_B denoting the free energies of state A and B, respectively. Since G_A and G_B can be varied (y, T, p = const) by changing the relative occupation of the states, G_A becomes a function of x_{CA} and $x_{\Delta A}$, and G_B of x_{CB} and $x_{\Delta B}$. The total free energy of the sublattice system is given by

$$G = \nu_1 G_A + \nu_2 G_B. \tag{4}$$

Since $\nu_1 = \nu_2 = 1$, we can omit these terms, and G becomes then

$$G = G(x_{CA}, x_{\Delta A}, x_{CB}, x_{\Delta B}) \; (y, T, p = \text{const}) \tag{5}$$

The equilibrium state is characterized by the minimum of G, while observing the boundary conditions resulting from relationships between the concentration terms and the conservation of the atomic masses, i.e.

(a) $x_{CA} + x_{\Delta A} = 1$

(b) $x_{CB} + x_{\Delta B} = 1$

(c) $x_{CA} + x_{CB} = y$

(d) $x_{\Delta A} + x_{\Delta B} = z$

(e) $(y + z = 2)$

Using Lagrange's method for the evaluation of the extrema,

$$\frac{\partial G}{\partial v_i} - \sum_k \frac{\partial N_k}{\partial v_i} a_k = 0 \tag{6}$$

N_k Boundary condition (1 ..... k)

a_k Undetermined Lagrange multiplier assigned to boundary condition N_k

v_i Independent variables

we obtain the conditions

$$\frac{\partial G_A}{\partial x_{CA}} - a_1 - a_3 = 0 \tag{7}$$

$$\frac{\partial G_A}{\partial x_{\Delta A}} - a_1 - a_4 = 0 \tag{8}$$

$$\frac{\partial G_B}{\partial x_{CB}} - a_2 - a_3 = 0 \tag{9}$$

$$\frac{\partial G_B}{\partial x_{\Delta B}} - a_2 - a_4 = 0 \tag{10}$$

Combining the first and the second couple of equations we obtain

$$\frac{\partial G_A}{\partial x_{CA}} - \frac{\partial G_A}{\partial x_{\Delta A}} = a_4 - a_3 = \frac{\partial G_B}{\partial x_{CB}} - \frac{\partial G_B}{\partial x_{\Delta B}} \tag{11}$$

or, since

$$\partial x_{\Delta A} = \partial x_{CA}$$

and

$$\partial x_{\Delta B} = \partial x_{CB}$$

$$\left[\frac{\partial G_A}{\partial x_{CA}}\right]_{T,p,y} = \left[\frac{\partial G_B}{\partial x_{CB}}\right]_{T,p,y} \tag{12}$$

$$\left[\frac{\partial G_A}{\partial x_{\Delta A}}\right]_{T,p,y} = \left[\frac{\partial G_B}{\partial x_{\Delta B}}\right]_{T,p,y} \tag{13}$$

Equations 12 or 13 characterize the internal equilibrium of carbon atoms and vacancies in the crystal structure.

Formally, these conditions are equivalent to the distribution equations for a two-phase equilibrium in a ternary system with fixed boundaries of the one-phase ranges[67], and we can adopt the same graphical method for the determination of the equilibrium concentrations in the sublattices A and B.

The meaning of equilibrium condition 12 becomes especially clear, if we neglect lattice interactions and write

$$G_A = G_{Me} + x_{CA} \cdot G_{C(A)} + G^{mix}_{(A)} \tag{14}$$

and

$$G_B = G_{Me} + x_{CB} \cdot G_{C(B)} + G^{mix}_{(B)} \tag{15}$$

Here G_{Me} is the free energy of the parent metal with the identical structure as the compound, $G_{C(A)}$ and $G_{C(B)}$ are the free energies of carbon on the sublattices A and B respectively, and $G^{mix}_{(A)}$ and $G^{mix}_{(B)}$ are the free energy changes due to the mixing of carbon atoms and vacancies on the sublattices A and B.

Taking the derivative, we have

$$\frac{\partial G_A}{\partial x_{CA}} = G_{C(A)} + \frac{\partial G^{mix}_{(A)}}{\partial x_{CA}} \tag{16}$$

$$\frac{\partial G_B}{\partial x_{CB}} = G_{C(B)} + \frac{\partial G^{mix}_{(B)}}{\partial x_{CB}} \tag{17}$$

or

$$\frac{\partial G^{mix}_{(A)}}{\partial x_{CA}} = G_{C(B)} - G_{C(A)} + \frac{\partial G^{mix}_{(B)}}{\partial x_{CB}} \tag{18}$$

Denoting the difference $G_{C(B)} - G_{C(A)}$ with ΔE, we finally obtain

$$\frac{\partial G^{mix}_{(A)}}{\partial x_{CA}} = \Delta E + \frac{\partial G^{mix}_{(B)}}{\partial x_{CB}} \tag{19}$$

For the graphical determination of the equilibrium concentrations, the derivatives of the free energies are plotted against the concentration variable x. Coexisting equilibrium concentrations of carbon atoms on the two sublattices correspond to the points of intersection of horizontal line

with the plotted curves of the values of the free energy derivatives. For an assumed value of one of the concentration variables, say x_{CA}, the concentration x_{CB} in the other sublattice can be found by extending a horizontal line from the point corresponding to x_{CA} on the curve for $\frac{\partial G^{mix}_{A}}{\partial x_{CA}}$ until it intersects the curve for $\frac{\partial G^{mix}_{B}}{\partial x_{CB}}$.

The equations take an especially simple form, if we neglect interactions between defects and assume ideal mixing behavior between the carbon atoms and the vacancies on both sublattices. The mixing terms become then:

$$G^{mix}_{(A)} = RT \cdot (x_{CA} \ln x_{CA} + x_{\Delta A} \ln x_{\Delta A}) \tag{20}$$

$$G^{mix}_{(B)} = RT \cdot (x_{CB} \ln x_{CB} + x_{\Delta B} \ln x_{\Delta B}) \tag{21}$$

$$\frac{\partial G^{mix}_{(A)}}{\partial x_{CA}} = RT \ln \frac{x_{CA}}{x_{\Delta A}} \tag{22}$$

$$\frac{\partial G^{mix}_{(B)}}{\partial x_{CB}} = RT \ln \frac{x_{CB}}{x_{\Delta B}} \tag{23}$$

Denoting the dimensionless quantity $\Delta E/RT$ with w, we obtain as the final condition governing the distribution of the interstitial atoms among the two lattice sites the equation:

$$\ln \frac{x_{CA}}{x_{\Delta A}} = w + \ln \frac{x_{CB}}{x_{\Delta B}} \tag{24}$$

For the graphical determination of the equilibrium concentrations as a function of the energy parameter w, a series of functions $w_i + \ln \frac{x}{1-x}$, starting with w = 0, is plotted against x (Figure 61). The horizontal intercepts between the curves corresponding to w = 0 and the given value w yield immediately the corresponding equilibrium concentrations x_{CB}.

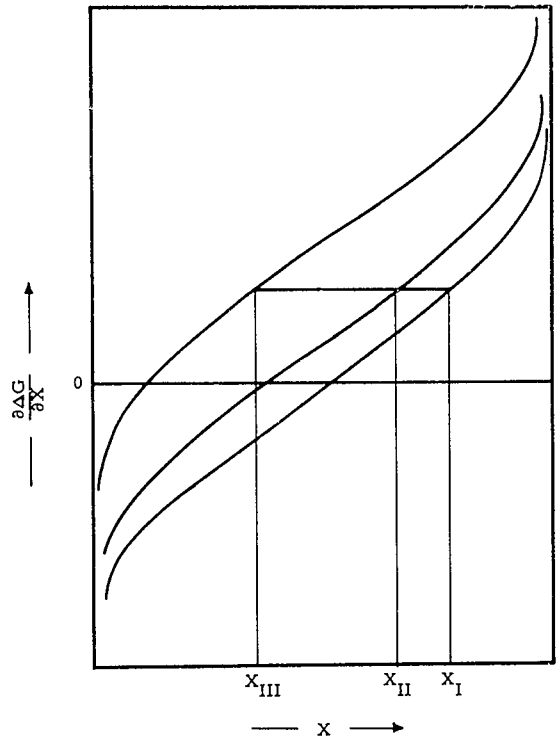

Figure 61. Graphical Determination of the Equilibrium Population in a Two-Level system.

At the concentration of order, y = 1, the equations take the simple form

$$\ln \frac{x_{CA}}{x_{\Delta A}} = + \frac{w}{2}, \quad \text{and} \tag{25}$$

$$\ln \frac{x_{CB}}{x_{\Delta B}} = - \frac{w}{2} \tag{26}$$

Returning to our original discussion, we rearrange the terms in the distribution equation and write:

$$RT \ln \frac{x_{CA}}{x_{\Delta A}} \cdot \frac{x_{\Delta B}}{x_{CB}} = \Delta E, \tag{27}$$

and identify the term

$$\frac{x_{CA}}{x_{\Delta A}} \cdot \frac{x_{\Delta B}}{x_{CB}} = K \tag{28}$$

as the equilibrium constant of the reaction*

$$C \mid \Delta_A + \Delta_B \longrightarrow C \mid \Delta_B + \Delta_A \ldots\ldots\ldots \Delta E,$$

with ΔE as the free energy change of the reaction, i.e. the free energy change associated with the transfer of one mole carbon atoms from lattice sites A to lattice sites B.

The derivation of the equilibrium condition for the second model is analogous:

The reaction to be considered is

$$C_y\Delta_z \begin{cases} \longrightarrow \nu_1 \, C_{x_{CA}} \Delta_{x_{\Delta A}} \ldots\ldots G_A \\ \longrightarrow \nu_2 \, C_{x_{CB}} \Delta_{x_{\Delta B}} \ldots\ldots G_B \end{cases}$$

---

*The symbolism used follows the nomenclature introduced by A.L.G. Rees[65]

and

$$G = \nu_1 G_A + \nu_2 G_B , \tag{29}$$

the boundary conditions to be considered are:

(a) $\nu_1 + \nu_2 = 1$

(b) $x_{CA} + x_{\Delta A} = 1$

(c) $x_{CB} + x_{\Delta B} = 1$

(d) $\nu_1 x_{CA} + \nu_2 x_{CB} = y$

(e) $\nu_1 x_{\Delta A} + \nu_2 x_{\Delta B} = z$

(f) $z + y = 2$

The equilibrium condition obtained is identical to that of model (1), i.e.

$$RT \ln K = \Delta E, \tag{30}$$

with

$$K = \frac{x_{CA}}{x_{\Delta A}} \cdot \frac{x_{\Delta B}}{x_{CB}} \tag{31}$$

This means that the relative occupation of the two lattice sites at a given temperature and energy value ΔE, is independent of relative masses (ν_1 and ν_2) of the coexisting 'phases'.This behavior resembles and in this respect is also a perfect analogue to the forementioned case of a two-phase-equilibrium in a ternary system.

Having established the conditions governing the equilibrium occupations of both lattice sites, we proceed now to the calculation of the excess contribution of the carbon sublattice to the thermal free energy of

the system. According to our choice of reference state, we shall understand under excess terms the sum of excess enthalpy, resulting from occupation of the B-state, and the configurational terms of the sublattices, i.e.

$$\Delta G^{exc} = \epsilon \cdot n_{CB} - T \left(S^{conf.}_{(A)} + S^{conf.}_{(B)}\right) \tag{32}$$

ϵ is the free energy required to transfer one carbon atom from a lattice site A to a lattice site B, and $S^{conf.}_{(A)}$ and $S^{conf.}_{(B)}$ are the entropies of mixing of carbon atoms and vacancies on sublattice A and B, respectively.

Beginning with model (1), the number of distinct microscopical arrangements (thermodynamic probability) in sublattice A is given by

$$W_A = \frac{N!}{n_{CA}! \cdot n_{\Delta A}!} \tag{33}$$

Analogously, we obtain for the B-sites

$$W_B = \frac{N!}{n_{CB}! \cdot n_{\Delta B}!} \tag{34}$$

The total number of arrangements in the combined system A-B is given by

$$W_{A-B} = W_A \cdot W_B \, . \tag{35}$$

The thermodynamic probability of the system is related to the entropy by the Boltzmann relation

$$S_{A+B} = k \ln W_{A-B} \tag{36}$$

Using Stirling's approximation for the calculation of the $n_i!$,

$$\ln n_i! \simeq n_i \ln n_i - n_i \tag{37}$$

and substituting mole fractions for the n_i, i.e.

$$x_{CA} = \frac{n_{CA}}{N} \quad \text{and} \quad x_{CB} = \frac{n_{CB}}{N},$$

we obtain for the configurational entropy of the carbon sublattice

$$S_{A+B} = -R\,(x_{CA} \ln x_{CA} + x_{\Delta A} \ln x_{\Delta A} + x_{CB} \ln x_{CB} + x_{\Delta B} \ln x_{\Delta B}). \quad (38)$$

Thus, the excess free energy due to the disorder in the A and B-sublattice becomes:

$$\Delta G^{exc.} = \Delta E \cdot x_{CB} + RT\,(x_{CA} \ln x_{CA} + x_{\Delta A} \ln x_{\Delta A} + x_{CB} \ln x_{CB} + x_{\Delta B} \ln x_{\Delta B}) \quad (39)$$

For the calculation of the positional terms in the model (2) we proceed analogously. According to the chosen model, the enumeration of states is as follows:

Total number of lattice sites	$2N$
Number of B-sites	n_{CA}
Number of A-sites	$2N-n_{CA}$
Number of C-atoms on Sites A	n_{CA}
Number of C-atoms on Sites B	n_{CB}
Number of holes on Sites A	$2N-2n_{CA}$
Number of holes on Sites B	$n_{CA}-n_{CB}$

The thermodynamic probability of the sublattice A is given by

$$W_A = \frac{(2N-n_{CA})!}{n_{CA}!\,(2N-2n_{CA})!} \quad (40)$$

and for the sublattice B by

$$W_B = \frac{n_{CA}!}{n_{CB}!(n_{CA}-n_{CB})!} \tag{41}$$

Using Boltzmann's relation as well as Stirling's approximation for the factorial terms, and using mole fractions in place of the number of atoms, we have

$$x_{CA} = \frac{n_{CA}}{2N-n_{CA}} \qquad x_{CB} = \frac{n_{CB}}{n_{CA}}$$

$$x_{\Delta A} = \frac{2N-2n_{CA}}{2N-n_{CA}} \qquad x_{\Delta B} = \frac{n_{CA}-n_{CB}}{n_{CA}}$$

and we obtain

$$S^{conf.}_{A+B} = -\frac{2R}{1+x_{CA}} \cdot \left[x_{CA} \ln x_{CA} + x_{\Delta A} \ln x_{\Delta A} + x_{CA}(x_{CB} \ln x_{CB} + x_{\Delta B} \ln x_{\Delta B}) \right] \tag{42}$$

and for ΔH^{exc}, the excess enthalpy resulting from the occupation of the B-states:

$$\Delta H^{exc} = \epsilon \cdot n_{CB} = 2\Delta E \cdot \frac{x_{CB} \cdot x_{CA}}{1 + x_{CA}} \tag{43}$$

The excess free energy due to disorder in the carbon sublattice is given by

$$\Delta G^{exc} = \Delta H^{exc} - T \cdot S^{conf.}_{A+B} \tag{44}$$

The carbon concentrations on the respective lattice sites are related to the total carbon content according to the sum formula Me_2C_y by

$$\frac{2x_{CA}}{1+x_{CA}} (1 + x_{CB}) = y$$

In evaluating the equations for the two models, first the corresponding carbon equilibrium concentration on both sublattices (A and B) have to be calculated. Knowing the distribution, the positional terms for each sublattice as well as the change in enthalpy due to occupation of the B-sites can then be computed. The total excess free energy change due to the disordering reaction in the carbon sublattice is then obtained by addition of the individual terms.

The corresponding equations for both models are summarized below:

Model (1): $N_B = N_i$. The expressions refer to one mole Me_2C_y.

(a) Condition for the distribution of the atoms among the sublattices A and B

$$RT \ln \frac{x_{CA}}{x_{\Delta A}} \cdot \frac{x_{\Delta B}}{x_{CB}} = \Delta E$$

with ΔE denoting the free energy required to transfer one gramatcm of carbon atoms from lattice sites A to lattice sites B

(b) Concentration relationships:

$$x_{CA} + x_{CB} = y$$
$$x_{CA} + x_{\Delta A} = 1$$
$$x_{CB} + x_{\Delta B} = 1$$

(c) Entropy and Energy terms

$$S_A^{conf.} = -R\,(x_{CA} \ln x_{CA} + x_{\Delta A} \ln x_{\Delta A}) \tag{46}$$

$$S_B^{conf.} = -R\,(x_{CB} \ln x_{CB} + x_{\Delta B} \ln x_{\Delta B}) \tag{47}$$

$$S_{A+B}^{conf.} = S_A^{conf.} + S_B^{conf.} \tag{48}$$

$$\Delta H^{exc} = \Delta E \cdot x_{CB} \tag{49}$$

$$\Delta G^{exc} = \Delta H^{exc} - T\,S_{A+B}^{conf.} \tag{50}$$

Model (2): $N_B = n_{CA}$. The expressions refer to one mole Me_2C_y.

(a) Condition for the distribution of the carbon atoms among the sublattices A and B:

$$RT \ln \frac{x_{CA}}{x_{\Delta A}} \cdot \frac{x_{\Delta B}}{x_{CB}} = \Delta E \tag{51}$$

with ΔE having the same meaning as in model (1).

(b) Concentration Relationships

$$\frac{2x_{CA}}{1+x_{CA}}\,(1 + x_{CB}) = y$$

$$x_{CA} + x_{\Delta A} = 1$$

$$x_{CB} + x_{\Delta B} = 1$$

(c) Entropy and Energy Terms

$$S_A^{conf.} = -\frac{2R}{1+x_{CA}} \cdot (x_{CA} \ln x_{CA} + x_{\Delta A} \ln x_{\Delta A}) \tag{52}$$

$$S_B^{conf.} = -\frac{2R \cdot x_{CA}}{1+x_{CA}} (x_{CB} \ln x_{CB} + x_{\Delta B} \ln x_{\Delta B}) \tag{53}$$

$$S_{A+B}^{conf.} = S_A^{conf.} + S_B^{conf.} \tag{54}$$

$$\Delta H^{exc} = 2\Delta E \cdot \frac{x_{CB} x_{CA}}{1 + x_{CA}} \tag{55}$$

$$\Delta G^{exc} = \Delta H^{exc} - T S_{A+B}^{conf.} \tag{56}$$

In examining the excess free energy function of model 1 (Figure 62) we find that only <u>one</u> minimum exists over the entire range of carbon concentrations y and energy parameter $w = \frac{\Delta E}{RT}$. We further note, that for higher w-values, the minimum shifts towards smaller carbon concentrations and reaches as limiting value $y = \frac{1}{2}$ when w approaches infinity (B-states unoccupied, random mixing over the N A-states).

On the other hand, if w approaches zero (A and B-sites energetically equivalent), the minimum occurs at y = 1, as would be expected. Examining somewhat closer the minimum in the excess free energy concentration curve, we write

$$\frac{\Delta G^{exc}}{RT} = \Delta G = w \cdot x_{CB} + x_{CA} \ln x_{CA} + x_{\Delta A} \ln x_{\Delta A} + x_{CB} \ln x_{CB} + x_{\Delta B} \ln x_{\Delta B} \tag{57}$$

The distribution equation becomes:

$$\ln \frac{x_{CA}}{x_{\Delta A}} \cdot \frac{x_{\Delta B}}{x_{CB}} = w \qquad (58)$$

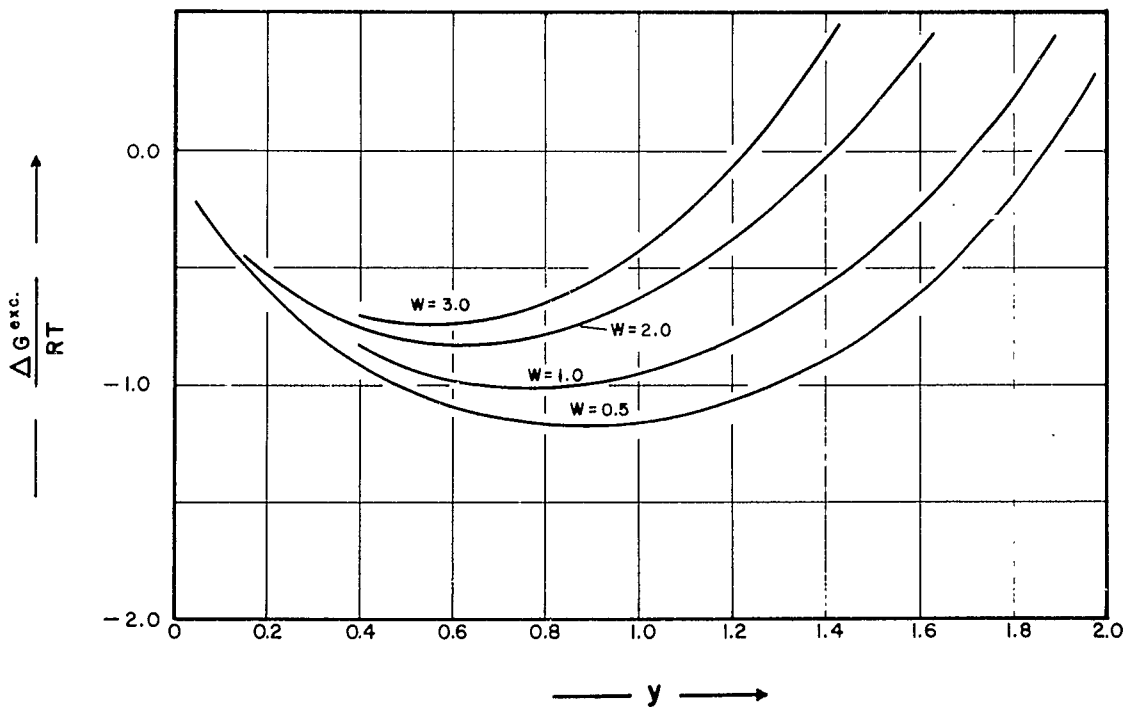

Figure 62. Model 1: Excess Free Energy Due to Disorder in the Carbon Sublattice

Parameter: $w = \frac{\Delta E}{RT}$ (Quantities per Mole Me_2C_y)

Substituting for

$$\ln \frac{x_{CA}}{x_{\Delta A}} = u, \text{ and for}$$

$$\ln \frac{x_{CB}}{x_{\Delta B}} = v,$$

we find for

$$\frac{\Delta G^{exc}}{RT} = \Delta G^{*} = f\left\{ x_{CA}(u),\ x_{CB}\ [u\ (v)]\right\} \tag{59}$$

$$\frac{\partial \Delta G^{*}}{\partial u} = \frac{\partial f}{\partial x_{CA}} \cdot \frac{\partial x_{CA}}{\partial u} + \frac{\partial f}{\partial x_{CB}} \cdot \frac{\partial x_{CB}}{\partial v} \cdot \frac{\partial v}{\partial u} \tag{60}$$

$$\frac{\partial f}{\partial x_{CA}} = u, \text{ and } \frac{\partial f}{\partial x_{CB}} = v + w = u,$$

yielding $\left[\frac{\partial v}{\partial u} = 1\right]$:

$$\frac{\partial \Delta G^{*}}{\partial u} = u \left(\frac{\partial x_{CA}}{\partial u} + \frac{\partial x_{CB}}{\partial v} \right) = 0 \tag{61}$$

Substituting for x_{CA} and x_{CB},

$$x_{CA} = \frac{e^{u}}{1+e^{u}}, \qquad x_{CB} = \frac{e^{v}}{1+e^{v}}$$

we obtain

$$\frac{\partial x_{CA}}{\partial u} = \frac{e^{u}}{(1+e^{u})^{2}} \ ; \qquad \frac{\partial x_{CB}}{\partial v} = \frac{e^{v}}{(1+e^{v})^{2}} \tag{62}$$

The condition for the extrema becomes then:

$$u \cdot \left[\frac{e^u}{(1+e^u)^2} + \frac{e^v}{(1+e^v)^2} \right] = 0 \tag{63}$$

Since the term in the bracket is always positive definite, the extrema must be defined by the condition, that $u = 0$.

Since

$$u = \ln \frac{x_{CA}}{x_{\Delta A}} = 0 \tag{64}$$

The extremum always occurs at $x_{CA} = \frac{1}{2}$, i.e. when half of the A-sites are filled.

For the case, that $w = \infty$, x_{CB} becomes zero, and the extremum is located at $x_{CA} = y = \frac{1}{2}$. For $w = 0$ x_{CB} is equal to $x_{CA} = \frac{1}{2}$, and in this case the extremum occurs at a total carbon concentration $y = x_{CA} + x_{CB} = 1$.

Taking the second derivative, we obtain

$$\frac{\partial^2 \Delta G^*}{\partial u^2} = \frac{e^u}{(1+e^u)^2} + \frac{e^v}{(1+e^v)^2} + u \left[\frac{e^u(e^{2u}-1)}{(1+e^u)^4} + \frac{e^v(e^{2v}-1)}{(1+e^v)^4} \right] \tag{65}$$

For $u = 0$, the location of the extremum, this expression becomes

$$\frac{\partial^2 \Delta G^*}{\partial u^2} \left(x_{CA} = \frac{1}{2} \right) = \frac{1}{4} + \frac{e^{-w}}{(1+e^{-w})^2} \tag{66}$$

The right hand side of the equation is always positive, i.e. the extremum is a minimum.

We also note from the second derivative that the free energy function has no λ-point, as would be indicated by the existence of an inflection point at the same concentration as the minimum of the free energy-concentration function

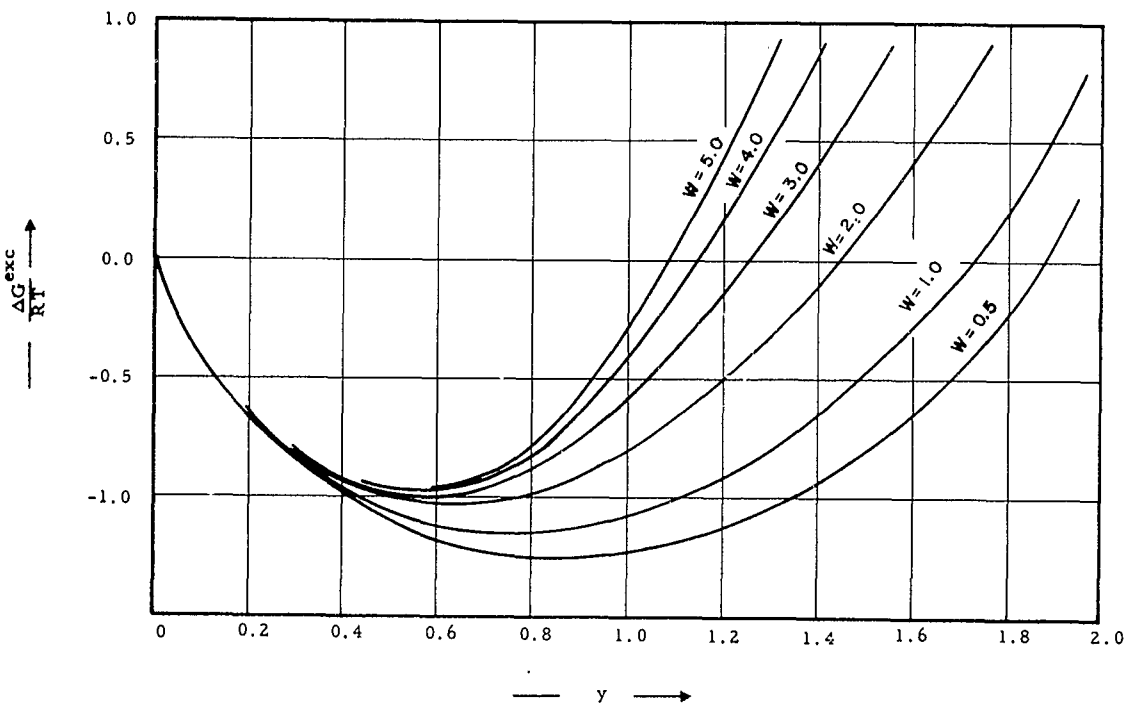

Figure 63. Model 2. Excess Free Energy due to Disorder in the Carbon Sublattice. Parameter: $w = \frac{\Delta E}{RT}$
(Quantities per Mole Me_2C_y)

A similar behavior of the excess free energy functions is derived from the expressions for the second model, although the functional

values at equivalent concentrations and energy parameters differ slightly from those obtained for the first model (Figure 63); c.f. the simple condition that the minimum occurs at $x_{CA} = \frac{1}{2}$ does not anymore hold.

It is not surprising that the combined excess functions of the carbon sublattice alone do not account for the observed phase separation. Since, as discussed earlier, the extra contributions from changes in the metal lattice are unknown, we have to relax our requirements and examine the individual terms for features, which might be responsible for the observed effects.

The excess enthalpies computed for both models show again a very similar behavior (Figure 64 and 65). At low carbon concentrations and high energy parameters (small fraction of the B-sites occupied), the excess enthalpy is correspondingly small; however, above $y = 1$ the excess quantities increase very rapidly to positive values, reaching at $y = 2$ the maximum value $\Delta H^{exc} (y = 2) = \Delta E$. Considering the two limiting cases, we find that for $w = 0$ (no energy gap), ΔH^{exc} is zero at all temperatures; for $w = \infty$, ΔH is a step function being zero for the range $0 \leq y \leq 1$, and rising to infinity at $y = 1$.

For a given value of ΔE, w decreases with temperature, and the data presented in Figure 64 and 65 can therefore be interpreted also as the excess enthalpy at different temperatures for a fixed value of ΔE.

Of special interest for our discussion are the free energy changes resulting from the configurational entropy of the carbon atoms on the different lattice sites, and also how the distribution of the carbon atoms will reflect itself in the overall behavior of the integrated functions.

Figure 66 shows the individual contributions of the interstitial sublattices A and B for a number of values of the energy parameter $w = \frac{\Delta E}{RT}$.

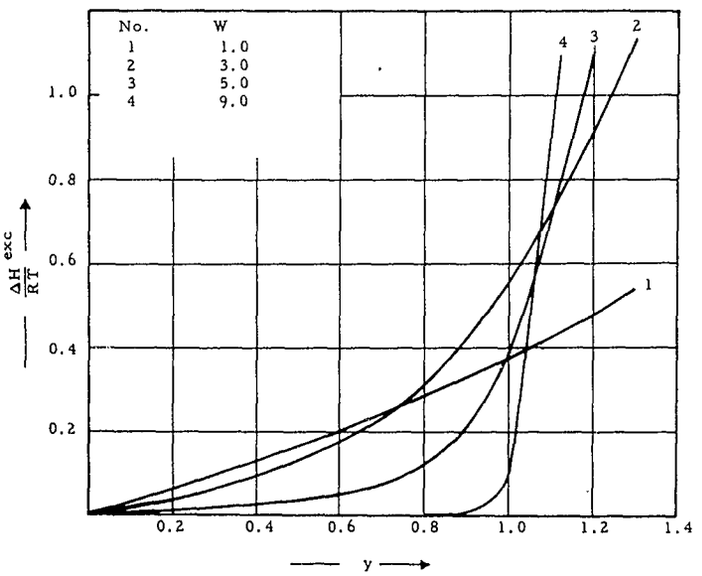

Figure 64. Model 1: Excess Enthalpy due to Occupation of Interstitial Sites of the Second Kind.
Parameter: $w = \frac{\Delta E}{RT}$. (Quantities per Mole Me_2C_y)

The curves are symmetrical with respect to y = 1, with the respective maxima at concentrations $y < 1$ (sublattice A) or $y > 1$ (sublattice B). The curves coincide for $w = 0$, with the minimum at $y = 1$. For $w = \infty$, the contribution of the sublattice A at $y = 1$ is zero (sites A completely filled, sites B unoccupied).

Mathematically, the location of the minima is given by

$$\frac{\partial \Delta G^{pos}}{\partial y} = 0 \qquad (67)$$

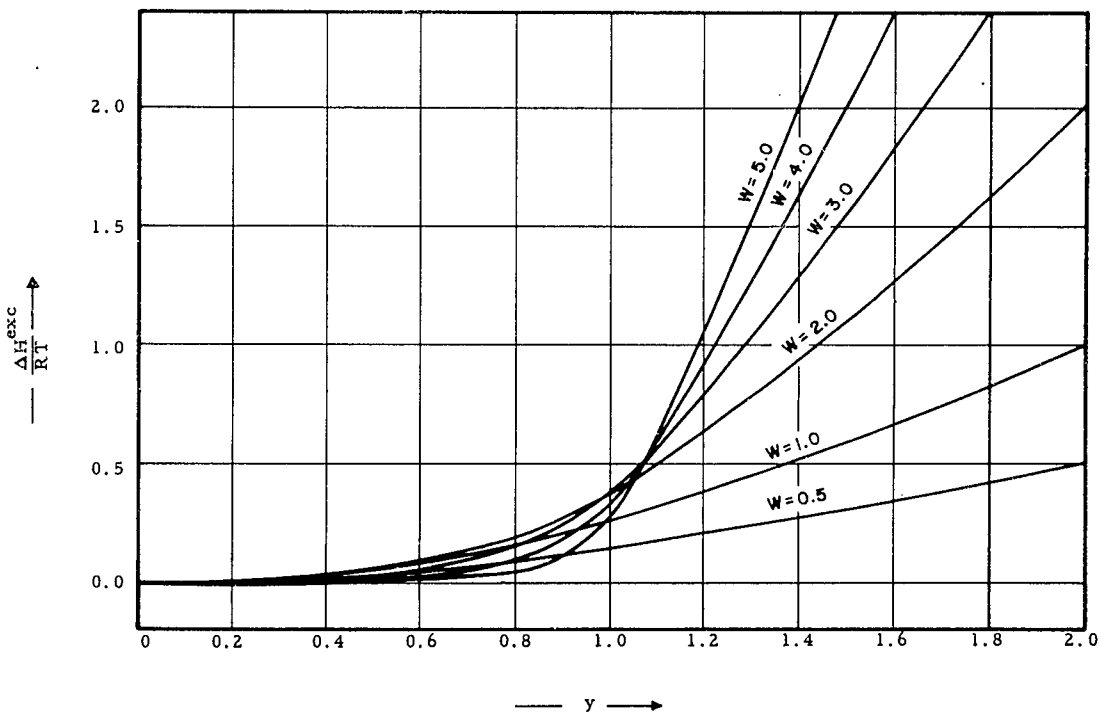

Figure 65: Model 2: Excess Enthalpy due to the Occupation of Interstitial Sites of the Second Kind.
Parameter: $w = \frac{\Delta E}{RT}$ (Quantities per Mole Me_2C_y)

Choosing y as the independent variable is impractical, since it leads to very complicated expressions. Instead, by making the analogous substitution as before, namely

$$u = \ln \frac{x_{CA}}{x_{\Delta A}}, \qquad v = \ln \frac{x_{CA}}{x_{\Delta A}}$$

differentiation after the substitution yields:

$$u \frac{\partial x_{CA}}{\partial u} + v \frac{\partial x_{CB}}{\partial v} = 0 \tag{68}$$

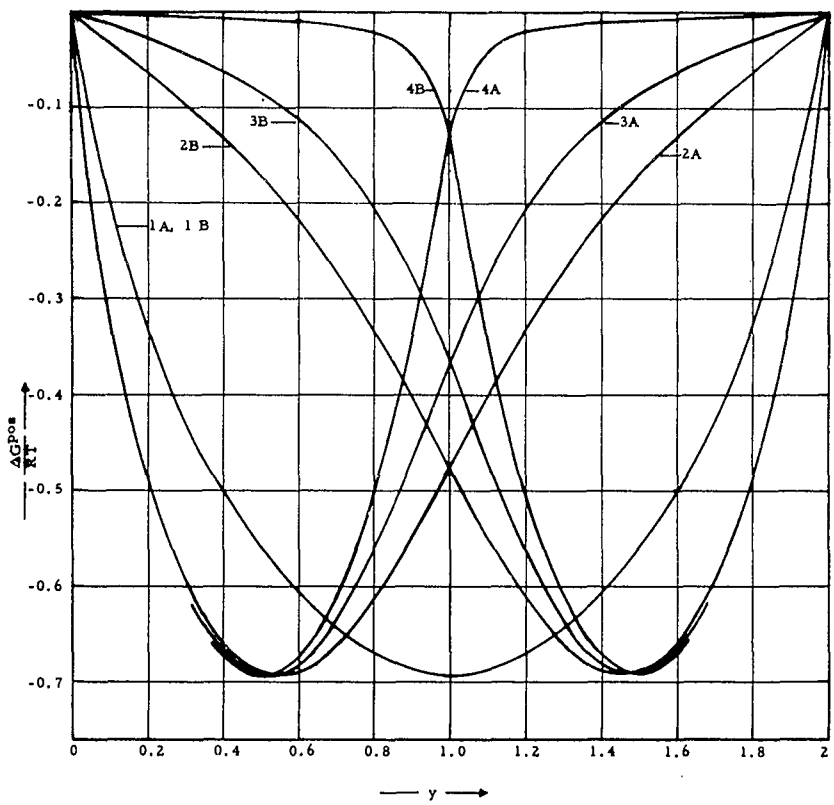

Figure 66: Model 1: Individual Contributions of the Interstitial Sublattices to the Positional Free Energy of a Two-Level System.

1 A,B; w = 0
2 A,B; w = 3
3 A,B; w = 4
4 A,B; w = 7

Recalling, that

$$\frac{\partial x_{CA}}{\partial u} = \frac{e^u}{(1+e^u)} = x_{CA} \cdot x_{\Delta A} \tag{69}$$

$$\frac{\partial x_{CB}}{\partial v} = \frac{e^v}{(1+e^v)} = x_{CB} \cdot x_{\Delta B} , \tag{70}$$

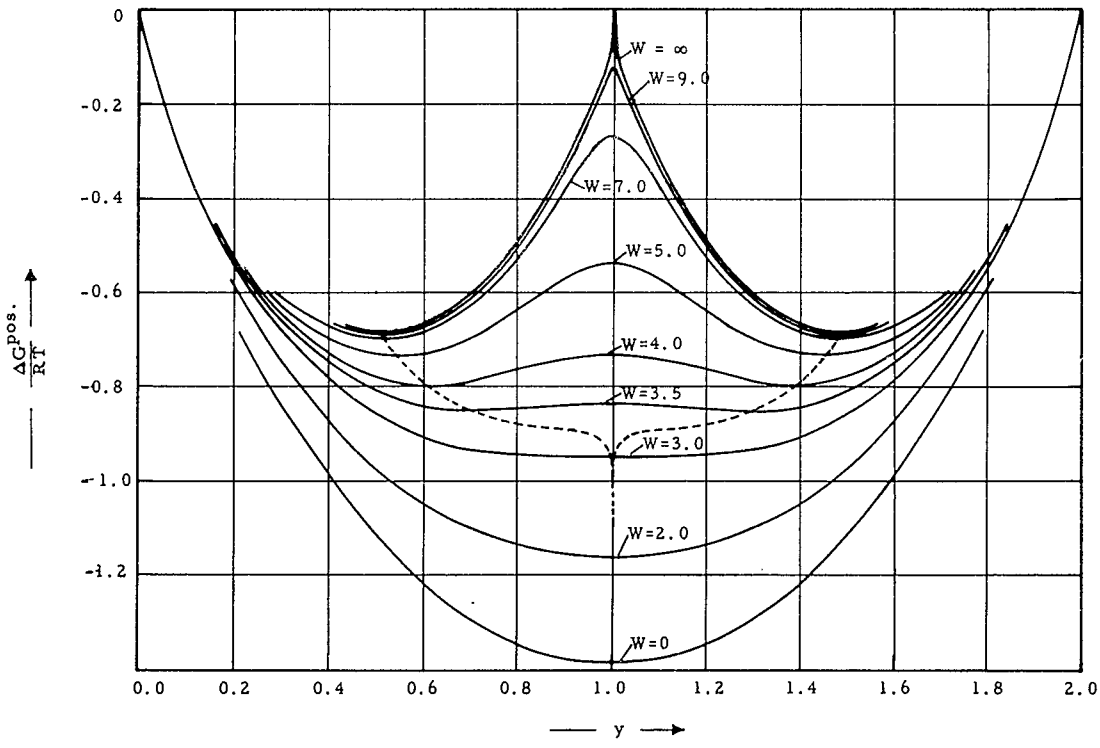

Figure 67: Model 1: Positional Free Energy Resulting from the Distribution of Interstitial Atoms Among Two Types of Interstitial Lattice Sites.

Parameter: $w = \frac{\Delta E}{RT}$ (Quantities per Mole Me_2C_y)

-------- Location of the Minima

we obtain the final equation for the minima:

$$x_{CA} \cdot x_{\Delta A} \ln \frac{x_{CA}}{x_{\Delta A}} = x_{CB} \cdot x_{\Delta B} \ln \frac{x_{\Delta B}}{x_{CB}} \tag{71}$$

With the aid of the distribution function, the above equation can be solved for x_{CA} or x_{CB}.

The numerical evaluation of the analogous equation for the second model yields the curves shown in Figures 68 and 69. Due to the larger number of A-states contributing to the positional terms, the functions for the refined model become asymmetrical, but show the same general behavior as the functions obtained with the simplified lattice model.

So far, we were mainly concerned with the discussion of the various contributions resulting from the changes occurring in the carbon sublattice. As pointed out, the thermal part, i.e. the change of the vibrational terms of the parent metal lattice is unknown. However, since the disordering reaction is homogeneous, it is safe to assume that there are no abrupt changes or discontinuities in the free energy functions to be expected, i.e. it will be possible to present the thermal part of the free energy of formation of an alloy Me_2C_y as a continuous function of concentration and temperature. Thus, the total free energy of formation can be presented as:

$$\Delta G_f(Me_2C_y) = \Delta G_f^{(thermal)}(y, T) + \Delta H^{exc} - T \cdot S^{pos}_{A+B} \tag{72}$$

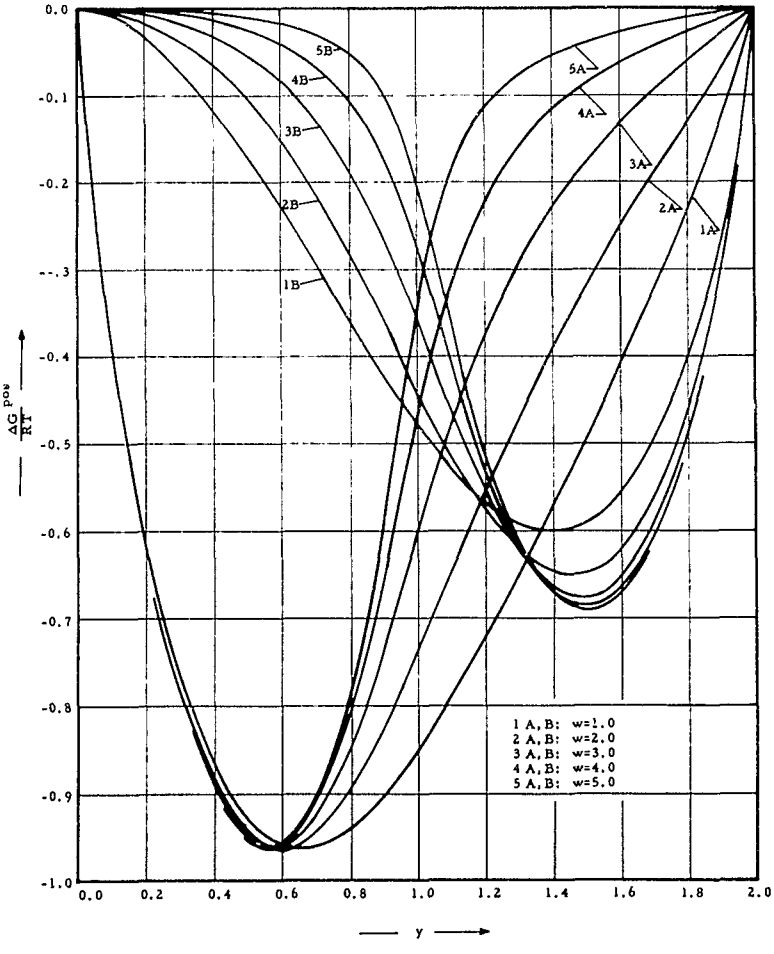

Figure 68. Model 2: Contributions of the Individual Interstitial Sublattices to the Positional Free Energy.
Parameter: $w = \frac{\Delta E}{RT}$. (Quantities per Mole Me_2C_y)

Considering only a small concentration range in the immediate vicinity of y = 1, it will be possible to present the thermal part as a linear function of the carbon concentration; we further may assume, that a given shape

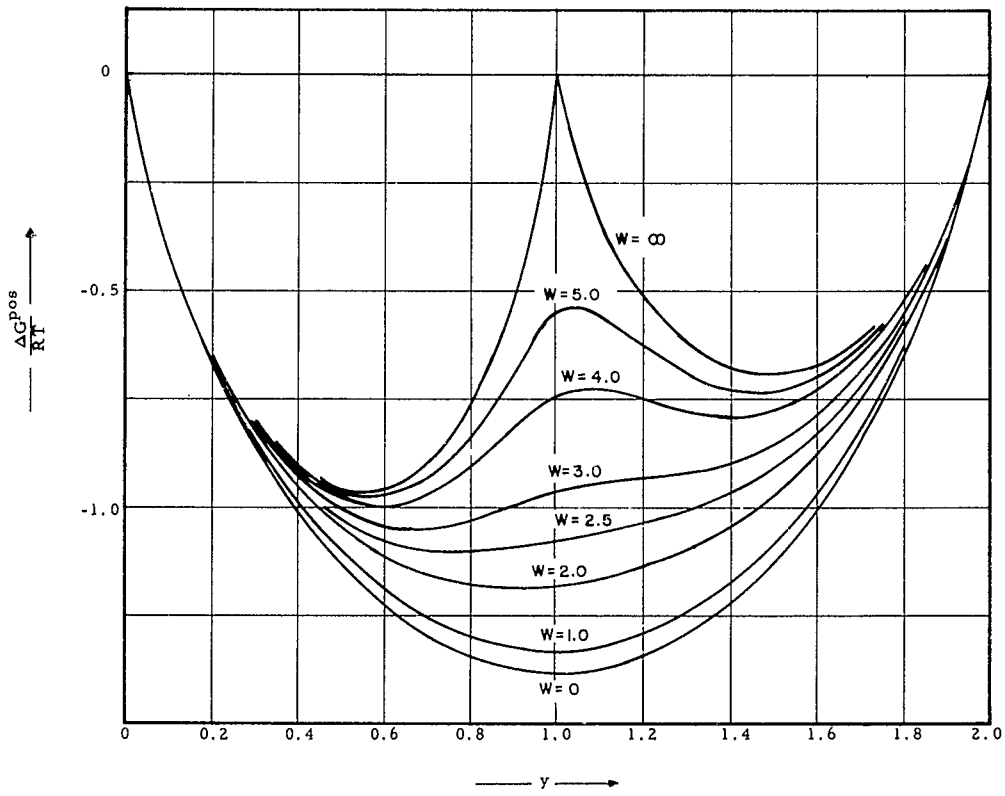

Figure 69. Model 2: Positional Free Energy Resulting From the Distribution of Interstitial Atoms Among Two Types of Interstitial Lattice Sites.
Parameter: $w = \frac{\Delta E}{RT}$ · (Quantities per Mole Me_2C_y)

of the thermal free energy-concentration curve, (in terms of the gradient) will be maintained over the temperature range of interest.

Examining the excess enthalpy function (Figures 64 and 65) we note, that at a given w-value, the gradient changes rapidly to more positive values at $y = 1$; towards higher temperatures (smaller w-values) the gradient for a given composition becomes smaller.

Any counterbalance of both effects at some temperature should therefore occur in the vicinity of $y = 1$, and in this case, the variation of the free energy curve will then be controlled by the positional terms.

From the observed variation of the gradients of ΔH^{exc} with temperature, we can derive the general statement, that for temperatures below the temperature of the isothermal reaction, (no further additional compounds at higher y-values).

$$\left[\frac{\partial \Delta G_f^{therm}}{\partial y} + \frac{\partial \Delta H^{exc}}{\partial y}\right]_{y = 1 \pm \delta} > 0 \text{ (no phase separation)} \quad (73)$$

At the temperature of the isothermal phase reaction

$$\left[\frac{\partial \Delta G_f^{therm}}{\partial y} + \frac{\partial \Delta H^{exc}}{\partial y}\right]_{y = 1 \pm \delta} = -\left[\frac{\partial G^{pos}}{\partial y}\right]_{y = 1 \pm \delta} \text{ (model 2)} \quad (74)$$

$$\left[\frac{\partial \Delta H_f^{therm}}{\partial y} + \frac{\partial \Delta H^{exc}}{\partial y}\right]_{y = 1 \pm \delta} = o \text{ (model 1)} \quad (75)$$

and at temperatures above the temperature of the isothermal phase reaction

$$\left[\frac{\partial \Delta G_f^{therm}}{\partial y} + \frac{\partial \Delta H^{exc}}{\partial y}\right]_{y = 1 \pm \delta} = \begin{cases} < o \text{ (model 1)} \\ < \left[\frac{\partial \Delta G^{pos}}{\partial y}\right]_{y = 1 \pm \delta} \text{ (model 2)} \end{cases} \quad (76)$$

These general considerations therefore would predict coexistence of both phases only above a critical temperature, which is accordance with the experimental observations. Furthermore, the phase-separation is to be expected to occur around the stoichiometric composition, with the carbon-rich boundary of the α(carbon-poorer)-phase moving to smaller carbon concentrations towards higher temperatures

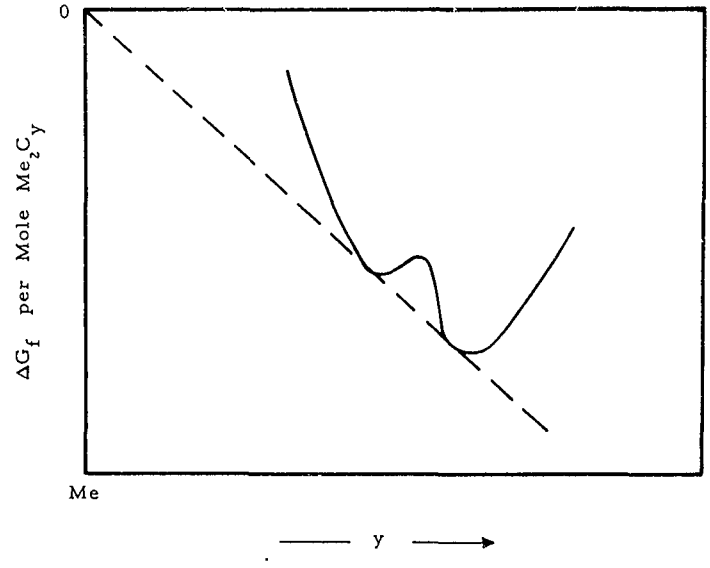

Figure 70. Stability Condition for the Coexistence of Two Separate Phases at the Metal Rich Side

If the sum of the gradients

$$\left[\frac{\partial \Delta G_f^{therm}}{\partial y} + \frac{\partial \Delta H^{exc}}{\partial y}\right]_{y = 1 \pm \delta} < k \qquad (77)$$

is more negative than a critical value k, the gradient of the tangent through the point ($\Delta G_f = 0$, $y = 0$) to the free energy curve of the compound (Figure 70), then only the β(carbon-richer)-phase is stable. In this case, the two-phase field crosses the homogeneous range of the phase and would, following the commonly used definition, be interpreted as a phase transformation.

Designating the eutectoid temperature at which the phase-separation occurs, i.e. the lowest temperature at which the β-phase is stable, as T_u, and the peritectoid temperature, at which the reaction

$$\alpha \longrightarrow \beta + Me$$

proceeds (highest temperature at which the α-phase is stable) as T_o, we deduce from the foregoing considerations that T_o should always be higher than T_u.

With fixed ΔE, T_u, the temperature of the phase-separation, will take its lowest value in those systems, where the phase under question is in direct equilibrium with the interstitial element, i.e. where no other intermediate phases with higher interstitial contents than the phase under consideration, are formed. This means that in all systems, where additional phases do occur, the temperature of the phase separation will be higher. Since the decomposition reaction of the α-phase at $T = T_o$ is independent of the free energy of formation of the higher interstitial phase, the difference $T_o - T_u$ should always be smaller in the latter system types presuming that the conditions for both transformations are being met within the solidus range. The difference $T_o - T_u$ is approaching the value zero, when the stability limit of the Me_2C_y-phase in the system is reached.

After these more general considerations, we shall return to our original problem and apply, at least in a semiquantitative manner, the theoretical findings to the observed phase relationships in the molybdenum-carbon system.

At the temperature of the phase-separation, $T \simeq 1748\,^{\circ}K$, the equilibrium concentrations of the coexisting phases are $y_I = 0.98$ and $y_{II} = 1.02$.

By comparison with the curves of the positional free energy of the refined model (Figure 69), we note that the curve corresponding to a w-value of 3 would predict too wide a concentration gap, while the curve with the energy parameter $w = 2$ would predict an extremely narrow gap only; the excess function computed for a w-value of $w = 2.5$ corresponds most closely to the experimental observations.

Taking $w = 2.5$ as the representative, value, we obtain from the relation

$$w = \frac{\Delta E}{RT}$$

and the temperature of the isothermal reaction ($T = 1748\,^{\circ}K$)

$$\Delta E\ (y \sim 1) = 8500 \text{ cal per two gramatoms metal}$$

Since we expect ΔE to vary somewhat with the composition, we understand this value to refer to a total carbon concentration corresponding to $y \sim 1$.

It is interesting to note, that the value of w, deduced from the simplified model (Figure 67), would fall into the same range.

Taking the obtained value for ΔE, it is now interesting to calculate differences in the relative order of the α - and β-phase at the temperature of the phase separation. A simple computation of the equilibrium constants at the corresponding equilibrium values of y results in the data presented in Table 17.

Table 17. Relative Occupation of the States in the α - and β-Mo_2C-Phase at the Temperature of the Phase Separation ($T = 1748°K$, $w = \frac{\Delta E}{RT} = 2.5$)

Compositions of the Coexisting Phases	Model 1		Model 2		$\frac{1}{K}$
	x_{CA}	x_{CB}	x_{CA}	x_{CB}	
$y = 0.98$ (α-Mo_2C)	0.767	0.213	0.718	0.173	0.082
$y = 1.02$ (β-Mo_2C)	0.787	0.233	0.746	0.194	

At this temperature, the B-states in the α-phase are to about 17% filled, compared to approximately 19% for the β-Mo_2C-phase. Thus, the difference in the degree of order in both phases is small.

Since we may assume ΔE as arising from the volume increase in the disordering process, we expect ΔE to decrease with the temperature. The value of the energy parameter $w = \frac{\Delta E}{RT}$, which controls the relative distribution of the interstitial atoms among the two sites, will therefore decrease (increase) faster with rising (falling) temperature, as would be expected with a constant value for ΔE.

Neglecting this dependence for these discussions, i.e. referring our discussion to the temperatures which would be predicted from the

relationship $w = \frac{\Delta E}{RT}$ with ΔE as constant, we observe that, for example, for a temperature of 2200°K (w = 1.5), approximately 27% of the B-sites are occupied (Figure 71). At room temperature (298°K), the equilibrium constant

$$K = \frac{x_{CA}}{x_{\Delta A}} \cdot \frac{x_{\Delta B}}{x_{CB}} \tag{78}$$

calculated with an energy parameter w = 6.4, takes a value of $K \simeq 1.7 \times 10^{6}$, i.e. less than 1 pro mille of the B-states is occupied ($y \sim 1$). The structure at room temperature can therefore be regarded as completely ordered.

Other data, which are of interest, in this connection, are the heat effects due to the disordering reaction. The excess enthalpies as a function of temperatures and for a series of discrete concentration values y have been computed for model (1) and are shown in Figure 72. In the vicinity of y = 1 the data presented should not differ very much from those calculated for the refined model.

The graph indicates that the observable heat effect is quite large (~ 2000 cal at 1800°K) and therefore is well within the temperature and accuracy range of presently available high temperature calorimeters. Knowing ΔH^{exc} as a function of temperature, the excess heat capacity can be computed from

$$C_p^{exc} = \left[\frac{\partial \Delta H^{exc}}{\partial T}\right]_{p,y} \tag{79}$$

i.e. by measuring experimentally the excess enthalpies as a function of temperature and concentration, the excess free energy as well as ΔE can be computed directly from the measured quantities.

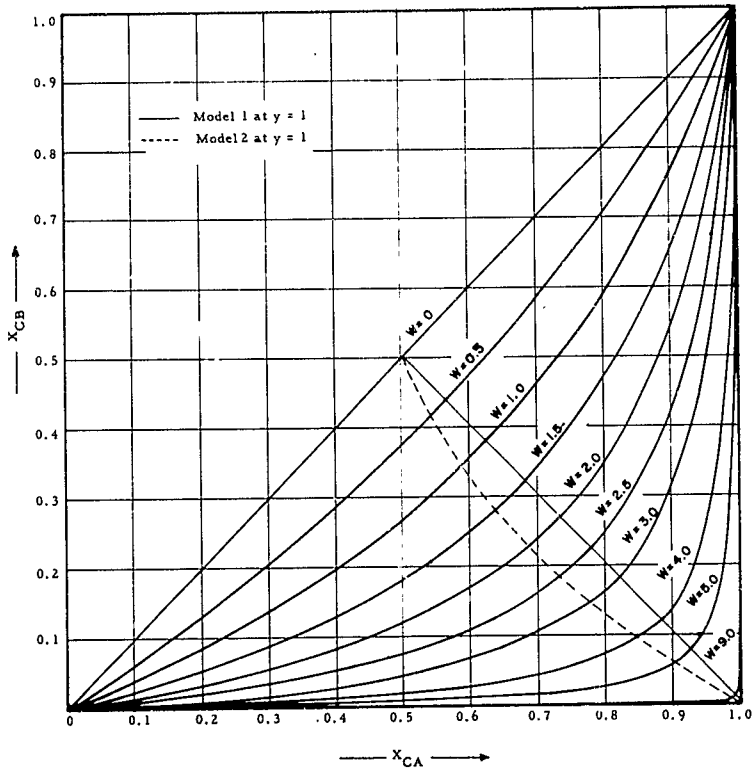

Figure 71. Relative Occupation of Sites A and B as a Function of the Energy Parameter $w = \frac{\Delta E}{RT}$

The high 'zero point' energy of the compound at the hypothetical compositions above y = 1 causes the enthalpy-temperature to curve to assume a very flat shape in the lower temperature range (Figure 72). A related plot but with $\Delta G^{exc}/RT$ as the independent variable is shown in

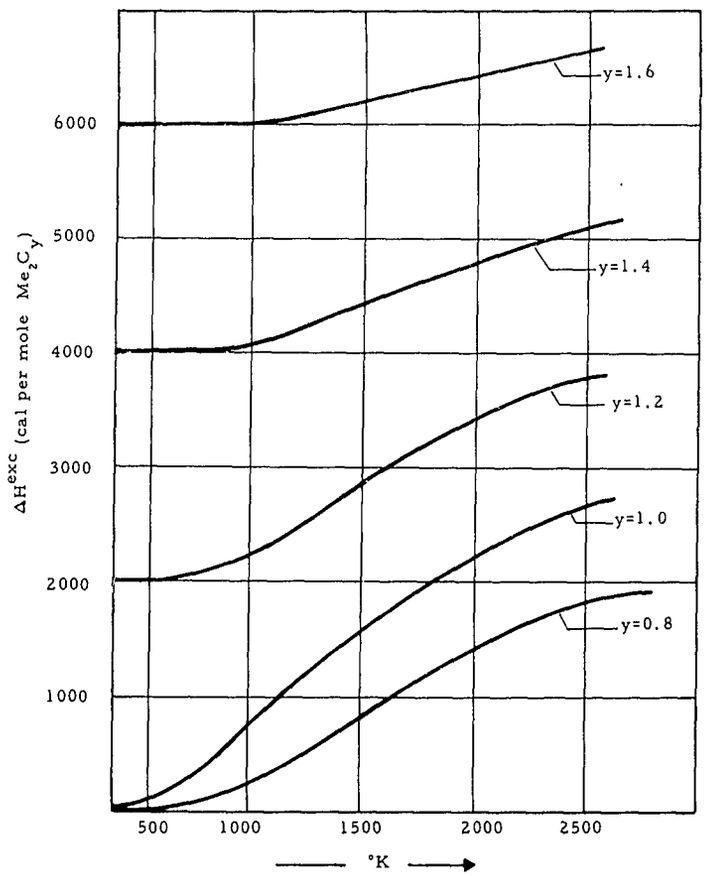

Figure 72. Excess Enthalpy due to the Disordering Reaction in Mo_2C
(Data Calculated with ΔE = 8500 cal per Mole Me_2C_y)

Figure 73 and explains the instability of hyperstoichiometric Mo_2C at low temperatures.

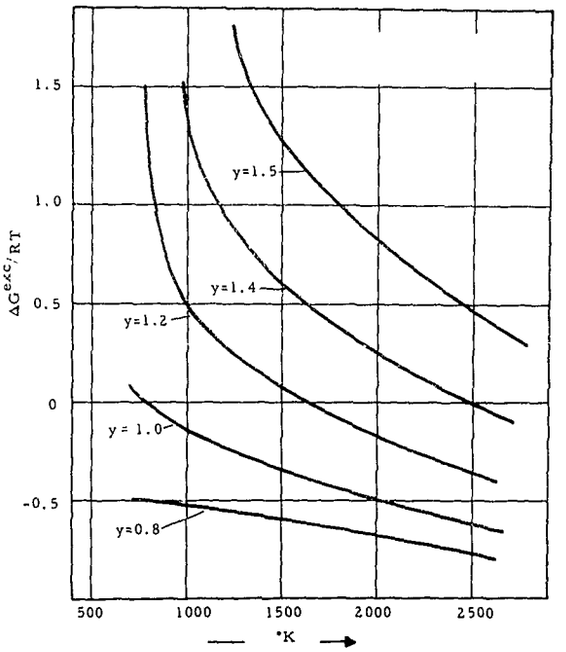

Figure 73. Excess Free Energy due to Sublattice Disorder in Mo_2C.
(Data Calculated with ΔE = 8500 cal per Mole Mo_2C_y)

D. LITERATURE REVIEW AND EVALUATION OF THE THERMODYNAMIC DATA ON MOLYBDENUM CARBIDES

1. Low-Temperature Data

There are no experimental low-temperature heat capacities available for any of the molybdenum-carbon alloys. Krikorian[68] estimated the standard entropy of Mo_2C at 298.15°K to be 17.1 $\pm$ 1.0 cal/°K·mole. Using the entropies of molybdenum and graphite selected by Kelley and King[69], one obtains $\Delta S_{f,\ st} = +2.1\ (\pm\ 1.0)$ cal/°K · mole.

2. High-Temperature Data

There are no experimental high-temperature heat capacities for any of the molybdenum-carbon alloys.

3. Equilibrium Measurements

Gleiser and Chipman[70] studied the equilibrium, $Mo\text{-}Mo_2C\text{-}MoO_2\text{-}CO\text{-}CO_2$ from 1200° - 1340°K. From the known values of the free energies of formation of MoO_2, CO and CO_2, they obtained the free energies of formation of $Mo_{2.23}C$ to be

$$\Delta G_f = -11,710 - 1.83\ T$$

Schenck, Kurzen and Wesselkock[42] studied the equilibrium; $Mo\text{-}Mo_2C\text{-}CH_4\text{-}H_2$ at 973° and 1123°K. However, their results are doubtful due to the thermal segregation of the static gas mixtures present in their experiment as pointed out originally by Richardson[71]. Also, the values for the free energy of formation of CH_4 determined by Schenck et.al. from an equilibrium study of $CH_4\text{-}H_2\text{-}C$, using the same technique, do not agree with the presently accepted values for CH_4.

Browning and Emmett[73] claimed to have studied the equilibria $Mo\text{-}Mo_2C\text{-}CH_4\text{-}H_2$ from 820° - 952°K and $Mo_2C\text{-}CH_4\text{-}MoC\text{-}H_2$ from 936° - 1098°K, using a dynamic technique. According to Gleiser and Chipman[70], the first equilibrium yielded an impossibly large entropy change of 26 e.u. for the reaction $2\ Mo_{(s)} + C_{(gr)} = Mo_2C_{(s)}$. The second equilibrium as written is incorrect according to our presently established phase diagram, since none of the other three intermediate phases, i.e. $\beta\text{-}Mo_2C$, $\eta\text{-}MoC_{1-x}$ and $\alpha\text{-}MoC_{1-x}$ are stable with respect to $\alpha\text{-}Mo_2C$ and C in this temperature interval.

4. Heat of Formation

Mah[72] determined the heat of combustion of $\alpha\text{-}Mo_2C$ calorimetrically. Knowing the heats of formation of MoO_3 and CO_2, the heat of formation of $\alpha\text{-}Mo_2C$ was found to be - 11,000 ± 700 cal/mole. The specimen was prepared by directly reacting molybdenum with graphite powders at 1150°C in an atmosphere of hydrogen. The chemical composition of the sample was 94.09% Mo and 5.89% C.

An attempt was also made to measure the heat of combustion of MoC_{1-x}; however, the results obtained are doubtful because the composition of the sample was not well-defined.

5. Selection of Data

The free energy of formation of $\alpha\text{-}MoC_{0.449}$, the metal-rich boundary of the $\alpha\text{-}Mo_2C$ phase, selected by us is

$$Mo_{(s)} + 0.449\ C_{(gr)} \longrightarrow MoC_{0.449}$$

$$\Delta G_{f,1200\ -\ 1340\ °K} - 5,250 - 0.82\ T$$

The selected value is based on the equilibrium data of Gleiser and Chipman. The heat of formation derived from the equilibrium measurement of Gleiser and Chipman is in good agreement with the value obtained from combustion calorimetry by Mah.

IV. DISCUSSION OF THE RESULTS

A. PHASE DIAGRAM

The newly established phase-diagram deviates appreciably from the previously accepted system. This applies especially to the temperature and concentration ranges of stability of the intermediate phases. The eutectic temperature in the metal-rich part of the system (2200°C) agrees very well with the old measurements by W. P. Sykes, et.al.[16] and the more recent determinations by M. R. Nadler and C. P. Kempter[31]. The mean temperature for the carbon-rich eutectic line reported by T. C. Wallace, et.al.[13], (2580 $\pm$ 5°C), is identical with the value obtained by us (2584 $\pm$ 5°C). Although the measurements of the latter authors appear to be the most accurate determinations made hitherto, agreement in the middle concentration ranges (34 - 39 At% C) with our data is poor; the relatively large error limits attached to their data are certainly too high, in order to reflect the small differences encountered in the melting temperatures of the various carbide phases. The phase separation of the Mo_2C-phase had not been previously reported, although the sudden emissivity changes of carburized molybdenum wires at 1810°K, which has been observed by E. Bas-Taymaz[73], may have been related to this phase-reaction.

B. PHASES AND PHASE EQUILIBRIA

The system shows several interesting features which to a great part have to be attributed to the close structural similarities of the intermediate phases occurring in the system.

The α-β-phase separation of the Mo_2C-phase has been discussed in an earlier section and was attributed to homogeneous disordering reactions occurring in the carbon sublattice.

Related reactions have been meanwhile observed to occur also with W_2C, Ta_2C, and Nb_2C, and there are indications that certain diborides (c.f. TaB_2) show a similar behavior.

The relatively high occupation of additional interstitial lattice sites in the Me_2C-structures, causing the stability maxima of these phases to shift towards higher carbon concentrations, is directly reflected in the observation, that the carbon-rich boundaries of these phases move to higher carbon-concentrations at higher temperatures. While, due to the relatively high energy differences of the two kinds of interstitial lattice sites and the low melting temperatures of the phases, this effect is less pronounced in the molybdenum and tungsten-system, a quasi-continuous transition between the subcarbide and the cubic monocarbide has been found in the tantalum-carbon system at high temperatures[6]. A similar behavior is expected for the system niobium-carbon system.

At low temperatures, the energy parameter $\Delta E/RT$, which controls the relative occupation of the available lattice sites, is large, and the degree of disorder at the concentration of order will be correspondingly small. In the case of strong temperature effects a description of the structure would therefore also have to include a specification of the state of order. As an example, one would suspect that at temperatures close to melting the structure of the Me_2C-phases will correspond closely to the L' 3-type (complete disorder of the carbon sublattice.)

Similar considerations as for the Mo_2C-phase will have to be applied for a thermodynamic description of η-MoC_{1-x}, which in many respects resembles a transition structure between Mo_2C and the cubic (B 1) α-MoC_{1-x} [7]. For this case, the effect of the occupation of two crystallographically unequivalent interstitial lattice positions upon the neighboring sites has to be considered, although, in view of the closer spacing of the carbon atoms on the point position (4 f), the distribution of the interstitial atoms among these lattice sites (2 A-sites, 2 B-sites, according to the previously used notation) may possibly take account of the greatest part of the ordering effect.

Accurate and detailed experimental data on the individual phases would be highly desirable for the theoretical interpretation of observed phase-phenomena. In some instances, relations between the free energy formation of the various phases in the system can be obtained from an analysis of the observed phase-equilibria, but heat capacity data are needed for the calculation of their temperature dependence.

As an example, the following relations between the free energies of formation of the phases occurring in the system molybdenum-carbon can be formulated from the observed non-variant (p = const) equilibria:

(a) $Mo_2C_{1.02}$ (β) $\longrightarrow$ $Mo_2C_{0.98}$ (α) + 0.04C ..... ΔG_R

$$\Delta G_R = G_f(MoC_{0.49}) - \Delta G_f(MoC_{0.51}) = 0 \text{ at } T = 1748\,^\circ K$$

(b) $MoC_{0.64}\ (\eta) \longrightarrow MoC_{0.51}\ (\beta) + 0.13\ C \quad \ldots \Delta G_R^{'}$

$\Delta G_R^{'} = \Delta G_f(MoC_{0.51}) - \Delta G_f(MoC_{0.64}) = 0$ at $T = 1928\,^{\circ}K$

(c) $MoC_{0.68}\ (\alpha) \longrightarrow MoC_{0.66}\ (\eta) + 0.02\ C \quad \ldots \Delta G_R^{''}$

$\Delta G_R^{''} = \Delta G_f(MoC_{0.66}) - \Delta G_f(MoC_{0.68}) = 0$ at $T = 2233\,^{\circ}K$

Of further importance would be data of the strain energies envolved in the formation of the phases, in order to obtain data for the true semimetal metal bonds[74], and an evaluation of the stabilities of the parent metals in lattice arrangements equivalent to those of the intermediate phases. However, in concurrence with the views of L. Kaufman [75], we believe that the energies associated with changes in the crystal modification, at least among the most common types (bcc, fcc, and hcp) are fairly small quantities, and should therefore be of influence only in the metal-rich part of the systems.

As an example, an evaluation of the phase-equilibria of molybdenum and tungsten with the platinum metals yields transformation energies for Mo (bcc) $\longrightarrow$ Mo (hcp), and W(bcc) $\longrightarrow$ W (hcp) values of + 1500 and + 2800 cal. per gramatom metal respectively, and for the corresponding face-centered cubic modifications, these values are only insignificantly higher.

A knowledge of these parameters would allow the establishment of generalized free-energy concentration relationships between the component and intermediate phases and facilitate significantly the interpretation and precalculation of the phase-reactions in combined (higher order) systems.

REFERENCES

(1) M. G. Bowman: Paper presented at the V. Plansee Seminar in June 1964 in Reutte, Tirol, Austria. (Plansee Proc. 1964, in print).

(2) F. Skaupy: Z. Elektrochem. 33 (1927), 487

(3) K. Becker: Z. Elektrochem. 34 (1928), 640
Z. Physik 51 (1828), 481
Z. Metallkde 20 (1928), 437

(4) W. G. Burgers and J.C.M. Basart: Z. anorg. allg. chemie, 216 (1934), 209

(5) E. Rudy and St. Windisch: Technical Documentary Report, Part I, Vol II, under AF 33(615)-1249 (in preparation).

(6) E. Rudy, C.E. Brukl, and D.H. Harmon: Technical Documentary Report, Part I, Vol. III, under AF 33(615)-1249 (in preparation).

(7) H. Nowotny, E. Parthé, R. Kieffer, and F. Benesovsky: Mh. Chem. 85 (1954), 255.

(8) R. Kieffer, and F. Benesovsky: Hartstoffe (Wein, Springer 1963)

(9) A. Westgren, and G. Phragmen: Z. angor. allg. chemie, 156 (1926), 27

(10) E. Parthé and V. Sadagopan: Mh. Chem. 93 (1962), 263

(11) E. Rudy, F. Benesovsky and K. Sedlatschek: Mh. Chem. 92 (1961), 841.

(12) E. Rudy, El. Rudy, and F. Benesovsky: Planseeber, Pulvermet. 10 (1962), 42.

(13) T. C. Wallace, C. P. Guitierrez, and P.L. Stone: J. Phys. Chem. 67 (1963), 796

(14) E. V. Clougherty, K. H. Lothrop, and J. A. Kafalas: Nature, 191 (1961), 1194

References (continued)

(15) T. Takei: Sci. Rep. Tohoku Univ. 17 (1928), 939

(16) W. P. Sykes, K. R. van Horn, and C. M. Tucker: Trans. Am. Inst. Min. Met. Eng. 117 (1935), 173

(17) W. E. Few and G. K. Manning: J. Metals 4 (1952), 271

(18) R. Speiser, J. W. Spretnak, W. E. Few and R. M. Parke: J. Metals 4 (1952), 275

(19) H. Moissan: Compt. Rend. 116 (1893), 1225
ibid. 120 (1895), 1320
ibid. 125 (1897), 839

(20) H. Moissan and M. K. Hoffmann: Compt. Rend. 138 (1904), 1358; Ber. dtsch. chem. Ges. 37 (1904), 3324

(21) J. N. Pring and W. Fielding: J. Chem. Soc. 95, (1909), 1497

(22) S. Hilpert and M. Ornstein: Ber. dtsch. chem. Ges. 46 (1913), 1669

(23) H. Tutiya: Sci. Pap. Inst. Phys. Chem. Res. Tokyo, 19 (1932), 384

(24) E. Friedrich and L. Sittig: Z. anorg. allg. chemie. 144 (1925), 169

(25) C. Agte and H. Alterthum: Z. techn. Physik, 11 (1930), 182

(26) G. Weiss: Ann. Chim. 1 (1946), 446

(27) J. L. Andrieux and G. Weiss: Bull. Soc. Chim. France 15 (1948), 598

(28) I. E. Campbell, C. F. Powell, D. H. Nowicki, and B. W. Gonser: J. Electrochem. Soc. 96 (1949), 318

(29) J. L. Lander and L. H. Germer: Am Inst.Min. Met. Eng. Techn. Pub. Nr. 2259 (1947)

(30) I. F. Ferguson, J. B. Ainscough, D. Morse, and A. W. Miller: Nature, 202 (1964), 1327.

References (continued)

(31) M. R. Nadler and C. P. Kempter: J. Phys. Chem. 64 (1960), 1468

(32) G. A. Geach and F. O. Jones: Plansee Proc. 1955, 80

(33) Compare also M. Hansen: Constitution of Binary Alloys (McGraw-Hill, 1958)

(34) H. Nowotny and R. Kieffer: Z. anorg. allg. chemie. 267 (1952), 261.

(35) J. L. Engelke, F. A. Halden and E. P. Farley: WADC-TR-59-654 (1960)

(36) E. K. Storms: LAMS-2674 (1962)

(37) A. E. Kovalskii and S. V. Semenovskaja: Kristallografia, 4 (1959), 923

(38) K. Kuo and G. Hägg: Nature 170 (1952), 245.

(39) L. C. Browning and P. H. Emmett: J. Am. Chem. Soc. 74 (1952), 4773

(40) L. Kaufman and E. V. Clougherty: Progr. Rep. AF 33(657)-9826 (1963)

(41) A. A. Ravdel: J. russ phys. chem. Ges. 62 (1930), 515

(42) R. Schenck, F. Kurzen, and H. Wesselkock: Z. anorg. allg. chemie. 203 (1932) 159

(43) W. B. Pearson: Lattice Spacings and Structures of Metals and Alloys (Pergamon, 1958)

(44) H. Heetderks and E. Rudy (to be published)

(45) Dr. S. Langer, General Atomic, San Diego: Private Communication 1961 and 1963

(46) R. T. Doloff and R. V. Sara: WADD TR 60-143 (1962), Part II

(47) A. Taylor, N. J. Doyle, and B. Kagle: WADD TR 80-132 (1962) Part II, 77.

References (continued)

(48) B. Riley: J. Sci. Instr. 41 (1964), 504

(49) R. F. Mehl and C. S. Barrett: Trans. Am. Inst. Min. Met. Eng. 93 (1931), 93

(50) H. Nowotny and R. Kieffer: Metallforschung 2 (1947), 257

(51) R. J. Fries and C. P. Kempter: Analyt. Chem. 32 (1960), 1898

(52) E. Rudy and Y. A. Chang: Paper presented at the V. Plansee Seminar, Reutte, Tirol, June 1964 (Plansee Proc., in print)

(53) J. S. Anderson, "The Physical Chemistry of Metallic Solutions and Intermetallic Compounds" (Chemical Publishing Co., New York 1960), 234

(54) G. Brauer: Naturwiss, 28 (1940), 30

(55) G. Brauer: Z. anorg. chem. 248 (1941), 1

(56) G. Brauer: III Plansee Seminar, Reutte, Tirol, 1958 (Plansee Proc., Springer, Wien, 1959)

(57) L. Kaufman, H. Bernstein, and A. Sarney: ASD-TR-61-445 Part II (1963)

(58) W. Schottky and C. Wagner: Z. Phys. Chem. B 11 (1930), 163

(59) Compare the compilation of references in C. Wagner, Thermodynamics of Alloys (Addison Wesley, Reading, Mass., 1952)

(60) R. H. Fowler and E. A. Guggenheim: Statistical Thermodynamics (Cambr. Univ. Press. 1939)

(61) J. R. Lacher: Proc. Roy. Soc. A 161 (1937), 525

(62) J. S. Anderson: Proc. Roy. Soc. A 185 (1946), 69

(63) A. L. G. Rees: Trans. Faraday Soc. 50 (1954), 335

(64) S. L. H. Martin and A. L. G. Rees: Trans. Farad. Soc. 50 (1954) 343

(65) A. L. G. Rees: Chemistry of the Defect Solid State (Methuen, London, 1955)

References (continued)

(66) R. Smoluchovsky: Discussion to the paper by R. Siegel in Phase Transformations in Solids (R. Smoluchovsky, J. E. May, W.A. Weyl editors, John Wiley and Sons, 1957)

(67) E. Rudy: Z. Metallkde, 54 (1963), 112

(68) O. Krikorian: High-Temperature Studies, UCRL 2888 (1955)

(69) K.K. Kelley and E. G. King: "Contribution to the Data on Theoretica Metallurgy", XIV, U. S. Bur. Min. Bull. 592 (1961)

(70) M. Gleiser and J. Chipman: J. Phys. Chem. 66, 1539-40 (1962)

(71) F. D. Richardson: J. Iron Steel Inst. 175 , 33 (1953)

(72) A. D. Mah: U.S. Bureau of Mines RI 6337 (1963)

(73) E. Bas-Taymaz: Z. Angew. Math. Phys. 2 (1951), 49

(74) L. Brewer: Private Communication, Dec. 1964

(75) L. Kaufman: Private Communication, Dec. 1964

DISTRIBUTION LIST

Aeronutronic
Division of Ford Motor Company
Ford Road
ATTN: Dr. W.M. Fassell, Jr.
Newport Beach, California

Stanford Research Institute
ATTN: Dr. A.E. Gorum
Menlo Park, California

Arthur D. Little, Incorporated
15 Acorn Park
ATTN: Dr. Berkowitz - Mattuck
Cambridge 40, Massachusetts

I I T R I
Technology Center
ATTN: Dr. S. Blum
10 West 35th Street
Chicago 16, Illinois

Spindletop Research Center
2224 Young Drive
ATTN: Dr. W. Lambertson
Lexington, Kentucky

Scientific & Technical Info. Facility
P. O. Box 5700
ATTN: NASA Representative (SAK/DL)
Bethesda, Maryland 20014

Westinghouse Electric Company
Astronuclear Laboratory
ATTN: Dr. D. Goldberg
Pittsburg, Pennsylvania

North American Aviation, Inc.
Rocketdyne Division
6633 Canoga Avenue
ATTN: Dr. R. P. Frohmberg, Chief
Materials Research
Canoga Park, California

Atomics International
P. O. Box 309
ATTN: S. C. Carniglia
Canoga Park, California

General Electric Company
P. O. Box 84
ATTN: Dr. A.N. Holden
Pleasanton, California

Melpar, Incorporated
3000 Arlington Boulevard
ATTN: Dr. J. Pentecost
Falls Church, Virginia

Materials Research Corporation
ATTN: V. E. Adler
Orangeburg, New York

California Institute of Technology
Jet Propulsion Laboratory
4800 Oak Grove Drive
ATTN: Martin H. Leipold
Pasadena 2, California

U. S. Department of Interior
Bureau of Mines Region
Metallurgy Research Station
P. O. Box 492
ATTN: Dr. J. L. Henry
Albany, Oregon

AVCO Corporation
201 Lowell Street
ATTN: Dr. T. Vasilos
Wilmington, Massachusetts

General Technologies Corporation
708 North West Street
ATTN: J. C. Withers, Manager
Materials Division
Alexandria, Virginia

General Electric Company
Space Sciences Laboratory
P. O. Box 8555
ATTN: L. R. McCreight
King of Prussia, Pennsylvania

Norton Company
Research & Development Depart.
1 New Bond Street
ATTN: Dr. N. N. Ault
Worcester 6, Massachusetts

Boeing Airplane Company
P. O. Box 3707
ATTN: Technical Library
Seattle 24, Washington

General Electric Company
FPD Technical Information Center
Building 100
Cincinnati 15, Ohio

Texas Instruments, Incorporated
P. O. Box 5474
ATTN: J. McCrary
Dallas 22, Texas

Convair Division
General Dynamics Corporation
ATTN: P. R. de Tonnacour
Chief Librarian
Fort Worth, Texas

Cornell University
Material Sciences Center
ATTN: Professor E. Scala
Ithaca, New York

Battelle Memorial Institute
ATTN: H. R. Ogden
Nonferrous Metallurgy Div.
ATTN: W. Duckworth
Ceramics Division
505 King Avenue
Columbus 1, Ohio

The Carborundum Company
Research & Development Division
ATTN: Dr. J. E. Niesse
ATTN: Librarian
Niagara Falls, New York

Ling-Temo-Vought, Incorporated
P. O. Box 5907
ATTN: W. Aves
Dallas 22, Texas

United Technology Corporation
P. O. Box 358
ATTN: M. A. Schwartz
ATTN: Library
Sunnyvale, California

American Lava Corporation
Cherokee Blvd. & Manufacturers Rd.
ATTN; Director of Research
Research Department
Chattanooga 5, Tennessee

Raytheon Company
Missile Systems Division
ATTN: Library
Bedford, Massachusetts

General Dynamics/Convair
Mail Zone 6-157
ATTN: Engineering Library
San Diego, California

General Atomic
Division of General Dynamics Corp.
P. O. Box 608
ATTN: Technical Library
San Diego 12, California

Speer Carbon Company
Research Department
ATTN: Dr. W. E. Parker
Packard Road
Niagara Falls, New York

DISTRIBUTION LIST (continued)

Thompson Ramo Wooldridge, Inc.
TAPCO Division
ATTN: R. A. Jefferys
23555 Euclid Avenue
Cleveland 17, Ohio

McDonnell Aircraft Corporation
Mat'ls & Processes Develop. Department
ATTN: D. Kummer
P. O. Box 516
St. Louis 66, Missouri

University of Michigan
Department of Chemistry
ATTN: Prof. E.F. Westrum, Jr.
Ann Arbor, Michigan

Massachusetts Institute of Technology
Department of Metallurgy
ATTN: Dr. W. D. Kingery
Cambridge 39, Massachusetts

Dr. Hans Thurnauer
1690 Bohland Avenue
St. Paul 16, Minnesota

Pfaudler Company
Research Laboratory
ATTN: B. Payne
1000 West Avenue
Rochester 3, New York

USAEC
Division of Reactor Development
ATTN: J. Simmons
Washington 25, D. C.

Los Alamos Scientific Laboratory
ATTN: Report Librarian
P. O. Box 1663
Los Alamos, New Mexico

Value Engineering Company
ATTN: H. P. Weinberg
2320 Jefferson Davis Highway

Lockheed Aircraft Corporation
Missiles and Space Division
Metallurgy & Ceramics Research Dept
ATTN: R. A. Perkins
Stanford Industrial Park
Palo Alto, California

Solar Aircraft Company
Research Laboratories
ATTN: A. R. Stetson
Pacific Highway
San Diego 12, California

Aerospace Corporation
ATTN: W. C. Riley
2400 East El Segundo Blvd.
El Segundo, California

University of Illinois
ATTN: Prof. A. L. Freedberg
Urbana, Illinois

DMIC
Battelle Memorial Institute
ATTN: R. J. Runck
505 King Avenue
Columbus 1, Ohio

University of California,
Radiation Laboratory
Information Division
ATTN: Clovis G. Craig
P. O. Box 808
Livermore, California

AF Office of Aerospace Research
ATTN: Solid State Division
Washington 25, D. C.

Watertown Arsenal
ATTN: A. Levitt
Watertown, Massachusetts.

NASA
Langley Research Center
ATTN: Technical Library
Langley Field, Virginia

DISTRIBUTION LIST (continued)

NASA
Lewis Research Center
ATTN: Dr. H. B. Probst
21000 Brookpark Road
Cleveland 35, Ohio

Department of the Navy
Bureau of Weapons
ATTN: I. Machlin, Code 232
Washington 25, D. C.

Army Missile Command
ATTN: Library
Redstone Arsenal, Alabama

General Electric Research Labs.
Metallurgy & Ceramics Res. Dept.
ATTN: Dr. J.E. Burke
Manager of Ceramics Studies
Schenectady, New York

Union Carbide Research Institute
ATTN: Dr. S. R. Aspinall
Tarrytown, New York

Professor Leo Brewer
Department of Chemistry
University of California
Berkeley, California

Dr. R. J. Thorne
Argonne National Laboratory
Argonne, Illinois

Dr. M. Steinberg
Lockheed Aircraft Corporation
Missiles and Space Division
Palo Alto, California

NASA
Marshall Space Flight Center
Redstone Arsenal
ATTN: Technical Library
Huntsville, Alabama

Aerospace Corporation Library
Technical Reports
2400 El Segundo Blvd.
El Segundo, California

Department of the Navy
Special Projects Office
ATTN: SP-2722
Washington 25, D. C.

USAEC
Technical Information Service
P. O. Box 62
Oak Ridge, Tennessee

General Telephone and Electronics
Laboratories
ATTN: Dr. Robert Steinitz
Bayside 60, New York

Professor Margrave
Department of Chemistry
Rice University
Houston, Texas

Professor A. W. Searcy
Department of Mineral Technology
University of California
Berkeley, California

Professor R. Schuhmann
Department of Metallurgy
Purdue University
Lafayette, Indiana

Dr. D. R. Stull
Thermal Laboratory
574 Building
Dow Chemical Corporation
Midland, Michigan

Dr. R. Coble
Lexington Laboratories
35 Cambridge Parkway
Cambridge, Massachusetts

DISTRIBUTION LIST (continued)

Advanced Research Projects Agency
Washington 25,
D. C.

The Marquardt Corporation
ATTN: Mr. Sam Sklarew
Materials & Processes Section
16555 Saticoy Street
Van Nuys, California

Commanding Officer
U. S. Army Signal Research and
Development Laboratory
ATTN: Mr. G.K. Gauli
Code XE
Fort Monmouth, New Jersey

Professor Rustum Roy
Pennsylvania State University
221 Mineral Science Building
University Park, Pennsylvania

Dr. Melvin Bowman
Los Alamos Scientific Laboratory
Los Alamos, New Mexico

Dr. Milton Linensky
General Electric Company
Philadelphia, Pennsylvania

Dr. Michael Humenick
Manager
Ceramics and Glass Department
Ford Scientific Laboratory
20000 Rotunda Drive
Dearborn, Michigan

Professor Michael Hoch
Department of Material Science
University of Cincinnati
Cincinnati, Ohio

Kaiser Aluminum and Chemical Corp.
ATTN: A. C. Byrns
1924 Broadway
Oakland 12, California

Texaco Experiment, Incorporated
Exploratory Research Laboratory
ATTN: Dr. L.E. Line, Jr.
Richmond 2, Virginia

Director
U. S. Naval Research Laboratory
ATTN: Code 2027, Documents Sec.
Washington 25, D. C.

NASA
1520 H. Street, N. W.
ATTN: J. S. Gangler
Washington 25, D. C.

Dr. T. F. Lyon
General Electric Company
Evandale, Ohio

Man Labs, Incorporated
21 Erie Street
ATTN: Dr. L. Kaufmann
Cambridge 39, Massachusetts

Union Carbide Corporation
Carbon Products Division
P. O. Box 6116
Cleveland 1, Ohio
ATTN: Dr. J. C. Bowman

Los Alamos Scientific Laboratory
P. O. Box 1663
Los Alamos, New Mexico
ATTN: Dr. C. P. Kempter

Department of Mineral Technology
University of California
Berkeley, California
ATTN: Prof. R. Hultgren

Department of Mineral Technology
University of California
Berkeley, California
ATTN: Dr. Wayne Worrell

Unclassified
Security Classification

DOCUMENT CONTROL DATA - R&D

(Security classification of title, body of abstract and indexing annotation must be entered when the overall report is classified)

1. ORIGINATING ACTIVITY *(Corporate author)*
Materials Research Laboratory
Aerojet-General Corporation
Sacramento, California

2a. REPORT SECURITY CLASSIFICATION
Unclassified

2b GROUP
N.A.

3. REPORT TITLE
Ternary Phase Equilibria in Transition Metal-Boron-Carbon-Silicon Systems.
Part I. Related Binary Systems Volume I. Mo-C System

4. DESCRIPTIVE NOTES *(Type of report and inclusive dates)*
1 January 1964 to 15 December 1964

5. AUTHOR(S) *(Last name, first name, initial)*
Rudy, Erwin
Windisch, Stefan
Chang, Austin Y.

6. REPORT DATE	7a. TOTAL NO. OF PAGES	7b. NO. OF REFS
January 1965	164	77

8a. CONTRACT OR GRANT NO. AF 33(615)-1249
b. PROJECT NO. 7350
c. Task No. 735001
d.

9a. ORIGINATOR'S REPORT NUMBER(S)
AFML-TR-65-2
Part I, Vol I

9b. OTHER REPORT NO(S) *(Any other numbers that may be assigned this report)*
N.A.

10. AVAILABILITY/LIMITATION NOTICES
Qualified requesters may obtain copies of this report from DDC.

11. SUPPLEMENTARY NOTES

12. SPONSORING MILITARY ACTIVITY
AFML (MAMC)
Wright-Patterson AFB, Ohio 45433

13. ABSTRACT

A complete phase diagram of the system molybdenum-carbon is presented. A thermodynamic model for the description of the phase separations of the Me_2C phases in transition metal-carbon systemshas been developed and was semiquantitatively applied to Mo_2C. Literature data on thermodynamic properties of molybdenum carbides have been critically evaluated and data were selected.

Apparative techniques for the precise study of phase reactions at high temperatures are described.

DD FORM 1 JAN 64 1473

Unclassified
Security Classification

14. KEY WORDS	LINK A		LINK B		LINK C	
	ROLE	WT	ROLE	WT	ROLE	WT
Carbide High Temperature Phase Equilibria Thermodynamic Properties Theoretical Thermodynamics						

INSTRUCTIONS

1. ORIGINATING ACTIVITY: Enter the name and address of the contractor, subcontractor, grantee, Department of Defense activity or other organization *(corporate author)* issuing the report.

2a. REPORT SECURITY CLASSIFICATION: Enter the overall security classification of the report. Indicate whether "Restricted Data" is included. Marking is to be in accordance with appropriate security regulations.

2b. GROUP: Automatic downgrading is specified in DoD Directive 5200.10 and Armed Forces Industrial Manual. Enter the group number. Also, when applicable, show that optional markings have been used for Group 3 and Group 4 as authorized.

3. REPORT TITLE: Enter the complete report title in all capital letters. Titles in all cases should be unclassified. If a meaningful title cannot be selected without classification, show title classification in all capitals in parenthesis immediately following the title.

4. DESCRIPTIVE NOTES: If appropriate, enter the type of report, e.g., interim, progress, summary, annual, or final. Give the inclusive dates when a specific reporting period is covered.

5. AUTHOR(S): Enter the name(s) of author(s) as shown on or in the report. Enter last name, first name, middle initial. If military, show rank and branch of service. The name of the principal author is an absolute minimum requirement.

6. REPORT DATE: Enter the date of the report as day, month, year; or month, year. If more than one date appears on the report, use date of publication.

7a. TOTAL NUMBER OF PAGES: The total page count should follow normal pagination procedures, i.e., enter the number of pages containing information.

7b. NUMBER OF REFERENCES: Enter the total number of references cited in the report.

8a. CONTRACT OR GRANT NUMBER: If appropriate, enter the applicable number of the contract or grant under which the report was written.

8b, &c, & 8d. PROJECT NUMBER: Enter the appropriate military department identification, such as project number, subproject number, system numbers, task number, etc.

9a. ORIGINATOR'S REPORT NUMBER(S): Enter the official report number by which the document will be identified and controlled by the originating activity. This number must be unique to this report.

9b. OTHER REPORT NUMBER(S): If the report has been assigned any other report numbers *(either by the originator or by the sponsor)*, also enter this number(s).

10. AVAILABILITY/LIMITATION NOTICES: Enter any limitations on further dissemination of the report, other than those imposed by security classification, using standard statements such as:

(1) "Qualified requesters may obtain copies of this report from DDC."

(2) "Foreign announcement and dissemination of this report by DDC is not authorized."

(3) "U. S. Government agencies may obtain copies of this report directly from DDC. Other qualified DDC users shall request through _____."

(4) "U. S. military agencies may obtain copies of this report directly from DDC. Other qualified users shall request through _____."

(5) "All distribution of this report is controlled. Qualified DDC users shall request through _____."

If the report has been furnished to the Office of Technical Services, Department of Commerce, for sale to the public, indicate this fact and enter the price, if known.

11. SUPPLEMENTARY NOTES: Use for additional explanatory notes.

12. SPONSORING MILITARY ACTIVITY: Enter the name of the departmental project office or laboratory sponsoring *(paying for)* the research and development. Include address.

13. ABSTRACT: Enter an abstract giving a brief and factual summary of the document indicative of the report, even though it may also appear elsewhere in the body of the technical report. If additional space is required, a continuation sheet shall be attached.

It is highly desirable that the abstract of classified reports be unclassified. Each paragraph of the abstract shall end with an indication of the military security classification of the information in the paragraph, represented as *(TS), (S), (C), or (U)*.

There is no limitation on the length of the abstract. However, the suggested length is from 150 to 225 words.

14. KEY WORDS: Key words are technically meaningful terms or short phrases that characterize a report and may be used as index entries for cataloging the report. Key words must be selected so that no security classification is required. Identifiers, such as equipment model designation, trade name, military project code name, geographic location, may be used as key words but will be followed by an indication of technical context. The assignment of links, rules, and weights is optional.